THE

LONDON, EDINBURGH, AND DUBLIN

PHILOSOPHICAL MAGAZINE

AND

JOURNAL OF SCIENCE.

[SEVENTH SERIES.]

NOVEMBER 1933.

LXXIV. *The Theory of Electrocapillarity.*—Part I. *Capillarity. By* S. R. CRAXFORD, O. GATTY, *and* J. ST. L. PHILPOT *.

GENERAL INTRODUCTION.

IN recent years attention has been concentrated once more on the electro-chemistry of the interphase between mercury and an aqueous solution containing electrolytes, and especially on changes of the properties of this interphase with changing electrical potential difference across it, because an exact knowledge of such effects would give a means of obtaining information about the details of the arrangement and properties of ions and molecules that may be present in the interphase under various conditions. Such a knowledge would be of the utmost importance in dealing with the outstanding electrochemical problems encountered in a study of muscular and nervous action and in general cytology; but at the moment there is so little agreement on the elementary physics of the simple mercury-aqueous solution interphase that any useful application to more complicated problems is impossible. Thus, for example, one of the more important difficulties consists of the fact that the electrostatic capacity of the interphase

* Communicated by Sir Harold Hartley, F.R.S.

as measured by finding the charge required to produce a unit change in the potential difference between the two phases is of the order of 5 micro-farads cm.$^{-2}$ [1], while a similar quantity, measured by finding the charge that has to flow on to an expanding interphase in order to maintain a constant unit potential difference between the two phases, is of the order of 25 micro-farads cm.$^{-2}$ [2]. Another difficulty concerns the so-called interfacial charge. Not only is the definition of such a quantity necessarily arbitrary, but attempts to measure the potential at which it is zero—that is, the so-called absolute zero of potential—have given consistently one or other of two sets of values. A value near $-0{\cdot}25$ volt on the normal hydrogen scale can be obtained from methods involving a dropping mercury electrode [3], electrocapillary curves [4], and electrophoresis [5]; but all these methods are capable of giving values near $\epsilon_H = +0{\cdot}5$ volt if used under other conditions (see Billiter [6] and Bennewitz and Küchler [7]), as also does the scraped electrode method of Bennewitz [8]. Further, it has long been known that a study of electrocapillary curves could be made to give much information about the problem; but here again there is little agreement about the underlying theory and the interpretation of results. These examples are sufficient to show that it is necessary thoroughly to review, and where necessary to extend or correct, the existing theories of these simple phenomena before physical arguments can be applied with certainty to the more interesting problems of physiology mentioned above. The present paper gives an exposition of the theory of capillarity as a foundation for an exact thermodynamic treatment of capillarity and of electrocapillarity, which is given in the next two papers of this series.

Capillarity.

1. *Surface Tension and Internal Pressure.*

The fundamental fact about capillarity is that the surface separating two immiscible phases tends to contract so as to assume a minimum area, and in so doing can be made to do work. The amount of external work required per unit increase of surface area is called the surface tension because it has the dimensions of force per unit length. Physically the work that has to be done to increase the surface area is required to transfer molecules

from the bulk phases to the interphase in equilibrium with them. so that it is evident that on a time average molecules in the interphase have energies that differ from their energies while in the bulk phases.

A qualitative explanation of this phenomenon is easy. The field of force acting between collisions on a given particle in a homogeneous phase of finite bulk is zero on a time average, if the effects of gravity and other externally applied fields of force are assumed to be zero. This is so, since all intermolecular forces, even including the electrostatic ones, are of comparatively short range, and therefore the interaction of the particle with matter situated outside its own phase may be assumed to be zero, unless the particle is closer to the phase boundary than a few molecular diameters. In that case its interaction with molecules across the boundary has to be considered, and as this interaction is in general different from that with particles of its own phase the particle considered will be subjected to a field of force which in general is normal to the phase boundary at that point. Particles in the interphase are kept in equilibrium by balancing this steady field of force by a difference in collision number or internal pressure.

2. *The inadequacy of the concept of Internal Pressure, which is analogous to the inadequacy of the Concept of Electrostatic Potential in Material Media. Surface Tension as Surface Energy.*

The simple picture of the previous paragraph will not be investigated further here, since it involves an arbitrary splitting of the forces acting on a molecule into those acting during collisions and those acting at other times, and this must necessarily depend on an arbitrary definition of what constitutes a collision. A similar difficulty arises if an attempt is made to measure an internal pressure directly, because a piston or wall has to be introduced somewhere in the bulk phase if a pressure is to be observed. Since walls and pistons must be material, their introduction means another phase and pair of interphases through which a pressure is measured, but it is no longer an internal pressure. The number of particles crossing an immaterial or an idealized boundary in a given direction, together with their momenta, cannot be observed directly. If all the matter on one side of the boundary is removed it is

possible, in theory at any rate, to observe the rate of evaporation into a vacuum. This figure, however, does not give values for the internal pressure, since the existence of a vacuum on one side of the boundary alters the field of force acting on particles near the interphase, even when they are not in collision. All differences of pressure observed should therefore refer ultimately to two surfaces in the same phase, whether the pressure difference is applied mechanically or by gravity. The use of the weight of a column of fluid as a source of pressure difference may be compared to the use of a potentiometer wire as a source of potential difference. The difference in pressure between two points in the column of liquid is a quantity that is readily ascertained, as is also the potential difference between two points in a potentiometer wire. The theoretical and experimental difficulties of attaching a meaning to the difference in electrical potential between two points in two different media have already been pointed out by Guggenheim [9].

Clearly the simpler picture to take of surface tension is that particles in an interphase possess energies that differ from those they possess when in the bulk phases that are in equilibrium with the interphase. This is shown to be the case, since work has to be done in order to increase the surface area. Such a picture is independent of any arbitrary interpretation in terms of hypothetical internal pressures, and will be taken as the basis for the logical development of the theory.

3. *How Surface Work is done. A hypothetical Apparatus is described.*

Owing to its tendency to assume a minimum area an interphase behaves like a membrane with a tension in it. For instance, there is a difference of pressure on the two sides of a curved membrane in a state of tension, and the same is true for a curved interphase. Direct observation of the tension itself is difficult, and in the majority of cases impossible, but a direct determination of the difference of external hydrostatic pressure of two phases is always possible. Similarly the direct control of surface area is difficult.

In all methods for the determination of surface tension the forces caused by the surface tension are balanced by measured mechanical forces or hydrostatic pressure,

and from this the value of the surface tension may be calculated if the geometry of the system is known. A generalized machine which in principle embraces all the common practical methods is shown in the figure. The area of the interphase is controlled by the pressures

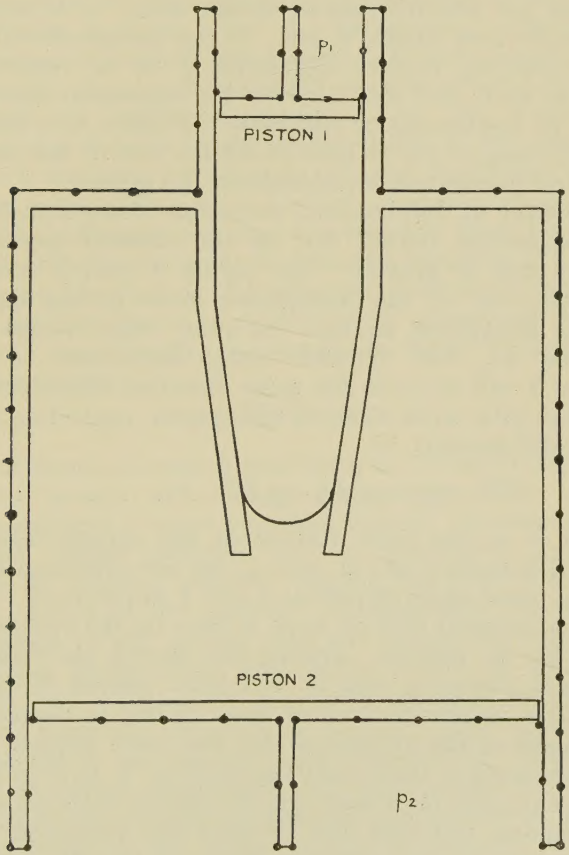

applied to the pistons and by the mechanical constraints due to the geometry of the system.

In any apparatus of this sort a third phase has to be introduced in order to apply the pressure, and this means the existence of three interphases rather than of one, and the elimination of a third phase seems impossible in all cases of measurement of surface tension, even

including the method of the height of a flat drop. Furthermore, changes in surface area will be accompanied by compressional changes in the bulk phases, and by transference of matter from the homogeneous bulk phases to the interphase, which also causes a volume change. If a precise meaning is to be attached to the phrase "work per unit increase of surface area," it is necessary to decide how much, if any, of the compressional work accompanying surface expansion is to be regarded as surface work, and also whether the expansion considered is to be isothermal or adiabatic. Finally, it is desirable to eliminate as far as possible effects due to the presence of other phases and interphases in the system.

Consider an infinitesimal reversible change made with the apparatus shown, and for the moment neglect any effects due to gravity. Let piston 1, which is on the concave side of the interphase, move in the direction of the interphase, so that its outer edge sweeps out a volume dv_1, the cylinder being considered as fixed, Piston 2 will move in the same direction simultaneously. and the total work done on the system, neglecting second order differentials, is

$$\delta W = (p_1 - p_2)dv_1 - p_2 dV, \quad . \quad . \quad . \quad . \quad . \quad . \quad . \quad . \quad (1)$$

where V is the total volume of the system inside the dotted boundary and p_1 and p_2 are the pressures applied to the outer edges of pistons 1 and 2 respectively.

It is assumed that no work is done on the system other than by the pistons. During this change the interphase between phases I. and II. will have altered its position and area, while the area of these phases in contact with the walls of the apparatus will also have altered. Thus surface work is done, and the problem is how to extract from equation (1) a term for the surface work at a single interphase, and also how to treat the remainder of the work done by the pistons. This can be solved, and the first step is a discussion of the number of degrees of freedom possessed by the system under consideration.

4. *Degrees of Freedom in Systems with no Capillary Effects. An alternative statement of the Phase Rule.*

In stating the phase rule Gibbs [10] only considered independently variable quantities whose values were

independent of the bulk of the system, so that his degrees of freedom refer to intensive factors only. In the development of the theory of capillarity it is essential on occasion to know the total possible number of degrees of freedom of a system when the numbers of molecules of the various components are allowed to vary. This is necessary for deriving the generalization of the Gibbs adsorption equation and for generalizing Butler's [11] discussion of surface free energy. A little consideration shows that there must be at least one extensive independent variable for every phase present in the system, for unless this is so it would be impossible to determine the relative amounts, for example, of solid, liquid and vapour at the triple point. Any number of variables above the required minimum can also be extensive, since the excess can readily be converted to intensive variables.

Thus in the absence of gravitational, electrical, magnetic, and capillary forces, a system of P phases and C components may readily be shown to have F degrees of freedom, where

$$F = C + 2,$$

and of these at least P *must* refer to extensive properties or the system will not be determinate. The method is to consider a more complete system, containing more phases, where particles can be transferred from one phase to another without varying the total number of each species in the system. Provided that the number of phases in the system does not exceed the number of chemical components, this device avoids all difficulties about the number of extensive degrees of freedom. In the following papers only systems where the number of phases is not greater than the number of chemical components are considered. In cases where the number of phases exceeds the number of components, in addition to maintaining the total number of particles of all the components constant it will be necessary to have at least (P—C) additional extensive degrees of freedom. Gibbs's phase rule shows that $P - C = 2 - F$, where F refers to intensive degrees of freedom, and since F cannot be less than zero, (P — C) can never be greater than 2. At first sight it might appear that one of the necessary P—C additional extensive degrees of freedom would have to refer to each phase, and that it would be necessary

to define the exact positions of all the phase boundaries in all the non-homogeneous regions or interphases in the system. Fortunately this is not so, since it is possible in all cases to find extensive variables summed over all the phases which do equally well. It is well known from Gibbs's statement of the phase rule that it is never possible to have more than $C+2$ phases coexisting in equilibrium. For a system with $C+2$ such phases, the total volume, the total heat content, and the number of molecules of each chemical component throughout the whole system form a possible set of $C+2$ extensive variables, so that there is no need to consider the exact position of the phase boundaries.

In illustration consider a one-component system. For one phase there is one equation connecting the four quantities, pressure, temperature, volume, and number of particles, making $1+2=3$ degrees of freedom in all. For two phases in equilibrium the pressure and temperature as predicted by Gibbs's phase rule are no longer independently variable. Complete specification of such a system is obtained when the temperature, the volume, and the number of particles are known. Here also there are three degrees of freedom, but *two* are extensive. At the triple point the pressure and temperature are fixed, and the relative bulks of the three phases are given by the total volume, the total entropy, and the total number of particles. In this case also there are three degrees of freedom, and all of them are extensive.

5. *Degrees of Freedom in a System of the type shown in the figure when the number of Particles between the Pistons is allowed to vary.*

Similar arguments apply to this system, but, in addition, it presents special features. The two pistons and the walls must be regarded as forming three extra phases and an uncertain number of extra components. As far as the extensive degrees of freedom are concerned there are three additional ones, namely, the number of molecules in each of these phases. Assuming these phases to be completely immiscible with phases I. and II., they may be regarded as forming three independent components, and their total quantities are kept constant. These three restraints on the extensive degrees of freedom exactly cancel the effect of the three extra components

formed by the three extra phases. In fact, the degrees of freedom of the phases I. and II. in contact with each other are unaffected by the walls and pistons.

The degrees of freedom are therefore similar to those of other two-phase systems, except that (i.) the position of the meniscus is variable at will, (ii.) the two phases are no longer at the same pressure, as they would be in the absence of capillary effects. Experimental evidence shows that for an apparatus of the type described the pressure difference can be altered at will, since the capillary is conical, and that to each pressure difference there corresponds a definite curvature of the interphase. It also shows that for each position of the meniscus the latter takes up a definite shape, so that fixing the position of the meniscus determines both the curvature and the pressure difference between the phases. Conversely for a definite difference of pressure the meniscus takes up a definite position. Should the cone degenerate into a cylinder it is still possible to alter the position of the meniscus at will, but its curvature is independent of its position, and therefore the pressure difference between the phases is a constant, provided that the change in composition of the two phases, due to surface adsorption as the meniscus is moved, is so small as to have no appreciable effect on the surface tension. Whether this concentration effect is negligible or not, it is evident that in the case of a cylindrical capillary, as with a conical capillary, the system has one additional degree of freedom corresponding to the variable position of the interphase. It is only in the case of a conical capillary that this extra degree of freedom is non-trivial, because it then allows variations in the pressure difference between the phases. In the next section theoretical reasons based on the first two laws of thermodynamics are advanced, showing why a meniscus in a definite position tends to contract its surface to the shape which reduces the total surface free energy to a minimum.

In systems of this type therefore, the introduction of a surface whose area may be independently altered leads to the introduction of an extra degree of freedom into the system whose degrees of freedom (neglecting those that are ankylosed because they belong to the container of the system) are therefore given by

$$F = C + 3 \text{ [P extensive]},$$

or more generally by

$$F=C+2+S \text{ [P extensive]}, \quad . \quad . \quad . \quad . \quad (2)$$

where S is the number of independently controllable surface areas in the system. This equation refers to interphases of a homogeneous type throughout, and does not refer to the type of " fields " considered recently by Langmuir[12]. It is necessary to emphasize that this result only applies to a system of the special type considered. With other apparatus the conceivable possibility of altering surface area at constant curvature would give a second additional independent variable; yet others would be the alteration at constant curvature of the actual values of the principal curvatures of the interphase and the planes in which they lie. Before extending this result, so as to allow for alterations in the shape of the surface at constant surface area, it is necessary to separate out any effects that result from altering the area of the liquid-liquid interphase from the resultant effects due to alteration in the area of the two phases in contact with the walls of the vessel. This will be done in the sequel, but at this point it is sufficient to note that in all ordinary cases equation (2) will still be valid, since for each position of the meniscus, the interphase will take up a definite area and shape controlled by the mechanical constraints of the apparatus, and by other factors subsequently to be discussed.

6. *Surface Work done during an Expansion with an Apparatus of the type shown in the figure.*

If surface energy were non-existent expression (1) would be simplified, since p_1 would equal p_2, and it would become

$$\delta W=p_2 dV.$$

Thus the total change in the properties of the system due to work done on the surfaces is presumably given by $(p_1-p_2)dv_1$. Although this is said to equal the work done on the surfaces this term will include work for any compressional changes that accompany changes in the surface area. This includes both bulk phase compressions owing to changes in the pressure p_1 and also work for volume changes at the interphase itself. This term for surface work has, however, to be split up between the various

interphases. The system has an interphase between phases 1 and 2, another between phases 2 and 3, a third between phases 3 and 1, and, lastly, a small region where these three phases meet in which the properties of any one interphase are presumably affected somewhat by the proximity of the other two. The total work due to the expansion of these three surfaces by amounts ds_{12}, ds_{23}, ds_{31} respectively, accompanied by expansions $ds_{12\Delta}$, $ds_{23\Delta}$, $ds_{31\Delta}$ near the point of intersection of the three interphases may be represented in terms of

$$\gamma'_{12},\ \gamma'_{23},\ \gamma'_{31},\ \gamma'_{12\Delta},\ \gamma'_{23\Delta},\ \text{and}\ \gamma'_{31\Delta}$$

respectively by

$$(p_1-p_2)dv_1=\gamma'_{12}ds_{12}+\gamma'_{23}ds_{23}+\gamma'_{31}ds_{31}$$
$$+\gamma'_{12\Delta}ds_{12\Delta}+\gamma'_{23\Delta}ds_{23\Delta}+\gamma'_{31\Delta}ds_{31\Delta}. \quad . \quad . \quad (3)$$

This equation is to be taken as defining the γ''s. Thus $\gamma'_{12}=(p_1-p_2)\left(\frac{\partial v_1}{\partial s_{12}}\right)$ subject to the condition that all the other s's remain constant.

It is possible to attach a meaning to the γ''s if the following conditions are fulfilled, namely, if the total number of particles of the various chemical components of the system are kept constant, and also the pressure p_2, the temperature T, and the position of piston 1, so that $dv_1=0$, and if no other work is done on the system by any other means; for then, since $dv_1=0$, $\Sigma\gamma' ds=0$. Furthermore, the system is completely determined except for increases of the area of one interphase with corresponding decreases in the area of another.

No actual work is done on the system at all, so that it is possible to identify the γ''s with a definite type of energy per unit surface area in the different interphases, such that the condition $\Sigma\gamma' ds=0$ merely becomes the type of equilibrium predicted by the equations of virtual work. The various surfaces adjust their relative areas at p_2, v_1, T constant, so that the total surface energy is a minimum.

Thus

$$\gamma'_{12}=(p_1-p_2)\left(\frac{\partial v_1}{\partial s_{12}}\right)_{s_k,\,p_2,\,\mathrm{T},\,\mathrm{W}',\,\mathrm{N},}$$

where the suffix s_k denotes that all the surface areas

other than s_{12} are kept constant, W′ that work done on the system other than by the pistons 1 and 2 is kept constant, and N that the total numbers of particles of all chemical components in the system are kept constant.

In actual fact the process of altering s_{12} while the other interfacial areas are kept constant is *not* possible. The position of piston 1 is an independent variable of the system under consideration, but the respective surface areas are not. The actual values of the γ''s refer to a special type of surface energy determined by the independently variable properties of the system, and the relative changes in the various surface areas are given by equation (3) together with the geometry of the system.

Though it is difficult to attach a meaning to

$$\left(\frac{\partial v_1}{\partial s_{12}}\right)_{s_k,\, p_2,\, \mathrm{T},\, \mathrm{W}',\, \mathrm{N}}$$

directly, the introduction of this quantity allows attention to be concentrated on a single interphase rather than on six. For instance, surface work $(p_1 - p_2)dv_1$ can be done on the system at p_2, T, W′, N constant, and it may be assumed in the *first* instance to have occurred at s_k constant as well, and then that a subsequent shift involving no work being done is allowed to follow. An observer actually observes the initial and final states of the system, but would work mathematically with the energy changes of the first half of the process, which are equal to those for the whole change. This simplification allows us to define the surface tension of a single interphase in the next section.

7. *Surface Tension, defined in such a manner as to be applicable to a Boundary of Finite Thickness.*

The difficulty about assigning a value to the term $\left(\frac{\partial v_1}{\partial s_{12}}\right)_{s_k \ldots}$ lies in the fact that the surface to which s_{12} refers is not situated on the outside of piston 1. But if in expanding from s_{12} to $s_{12} + ds_{12}$, surface s_{12} sweeps out a volume dv_{12} in the same direction as dv_1 the expression $\left(\frac{\partial v_{12}}{\partial s_{12}}\right)_{s_k,\, p_2,\, \mathrm{T},\, \mathrm{W}',\, \mathrm{N},}$ refers to the expansion of the isolated surface s_{12}, while the other s's are all kept constant.

This expression will therefore refer to a normal expansion, and is equal to the reciprocal of the sum of the principal curvatures of the surface s_{12}, which is here assumed to be so small a portion of the surface as to have constant curvature all over.

The quantity $\left(\frac{\partial v_{12}}{\partial s_{12}}\right)_{s_k,\ p_2,\ \mathrm{T},\ \mathrm{W}',\ \mathrm{N},}$ unlike $\left(\frac{\partial v_1}{\partial s_{12}}\right)_{s_k,\ p_2,\ \mathrm{T},\ \mathrm{W}',\ \mathrm{N},}$

depends only on changes that occur actually *at* the interphase separating phases 1 and 2. It seems likely that the true surface energy residing in the interphase itself is better defined, not as γ'_{12}, but by

$$\gamma_{12}=(p_1-p_2)\left(\frac{\partial v_{12}}{\partial s_{12}}\right)_{s_k,\ p_2,\ \mathrm{T},\ \mathrm{W}',\ \mathrm{N},} \quad . \quad . \quad . \quad (4)$$

or

$$\gamma_{12}=\frac{p_1-p_2}{\mathrm{C}_1+\mathrm{C}_2}, \quad . \quad . \quad . \quad . \quad . \quad . \quad . \quad (5)$$

where C_1 and C_2 are the two principal curvatures of the surface s_{12}.

This definition, which defines the surface tension at any point, is in agreement with the previous work of Laplace, Young, and others on surface tension. In the case of an interphase of finite thickness a surface tension could be defined by equation (4) for any appropriate boundary in the non-homogeneous region between the two phases, and γ_{12} could be regarded as the surface tension in that particular boundary to which dv_{12} and ds_{12} both refer. It is essential in this case that they refer to the same arbitrary boundary.

Now let some arbitrary boundary separating phases 1 and 2 be described in the non-homogeneous interphase, and this boundary be produced, but so as to separate phases 1 and 3, and be produced back further so as to separate the piston from the walls of the containing vessel and on till it finally intersects the outer edge of piston 1. Let the total volume enclosed by this boundary and the outer edge of piston 1 be V_1.

Then $$[dv_{12}-dv_1=d\mathrm{V}_1]_{p_2,\ \mathrm{T},\ \mathrm{W}',\ \mathrm{N},\ s_k}.$$

This is so because the condition s_k constant, which means that $ds_k=0$, implies that these particular parts of the surface have undergone no increase of area, and therefore have had no work done on them, and so sweep out zero volume.

8. *The Redistribution of Work done in an Infinitesimal Expansion in an Apparatus of the sort described in the figure.*

If V_2 is put equal to $V - V_1$ equation (1) can now be written

$$[\delta W = -p_1 dV_1 - p_2 dV_2 + (p_1 - p_2) dv_{12}]_{s_k}, \quad . \quad . \quad . \quad (6)$$

or $$[\delta W = -p_1 dV_1 - p_2 dV_2 + \gamma_{12} ds_{12}]_{p_2,\, T,\, w',\, N,\, s_k}. \quad . \quad (7)$$

This expression *defines* the surface tension of the interphase separating phases 1 and 2. It also shows that the total work done by piston 1 and the external pressure p_2 on the system can be split to 3 terms :

The first, $-p_1 dV_1$, which is the compressional work done on phase 1 and piston 1, together with the product of any volume changes that occur during increase of the surface s_{12}, with a pressure p_1.

The second, a similar term, $-p_2 dV_2$, which applies to volume changes in phase 2, the vessel containing the system, and piston 2.

The third term represents surface work, and by supposing it to occur at s_k constant this is set equal to $\gamma_{12} ds_{12}$.

Expression (7) for δW is so constrained, however, that the system has only *two* degrees of freedom, so that the terms on the right-hand of expressions (6) and (7) are not all independently variable.

9. *The Stability of a Meniscus.*

The observed pressure difference $(p_1 - p_2)$ may be regarded as being in equilibrium with an opposing pressure $\gamma\left(\frac{ds_{12}}{dv_{12}}\right)$ due to tension in the interphase. Towards any virtual change the equilibrium is stable, neutral, or unstable according to whether for that change $(p_1 - p_2)$ is less, equal, or greater than $\gamma\left(\frac{ds_{12}}{dv_{12}}\right)$, because the restoring pressure is equal to $\gamma\left(\frac{ds_{12}}{dv_{12}}\right) - (p_1 - p_2)$. For virtual changes in which $(p_1 - p_2)$ and γ are kept constant the type of equilibrium is determined by the sign of

$\frac{d^2s_{12}}{dv^2_{12}}$, being stable if it is positive—that is, if the capillary tapers towards phase 2. An important special case is that of a cylindrical capillary where $\frac{d^2s}{dv^2}=0$ and the equilibrium is neutral. This means that for a given value of γ and of (p_1-p_2) either there is no equilibrium or, if there is equilibrium, s can have any value. If (p_1-p_2) is made to depend upon s, as can be done by a variety of devices—as, for example, by using an apparatus of varied shape and when (p_1-p_2) depends on the height of a column of liquid—any shape of capillary can be made to yield any type of equilibrium.

10. *The Introduction of a Gravitational Field.*

The introduction of a gravitational field affects the system both at the interphase and in the bulk phases. The former effect has been neglected because we are of the opinion that it would not sensibly affect the form of our final equation. The latter effect would convert expressions (6) and (7) into

$$[\delta W=-p_1dV_1-p_2dV_2+(p_1-p_2)dv_{12}+Mgd\bar{h}]_{p_2,\,T,\,W'',\,N,\,s_k},$$

where W'' shows that all work done on the system other than gravitational work and compressional work is kept constant, M is the total mass of the system, g the acceleration due to gravity, and $d\bar{h}$ an infinitesimal change in the height of the centre of gravity of the complete system.

In this case a quantity γ^* defined by $\gamma^*ds_{12}=(p_1-p_2)dv_{12}$ would still obey the final equations given in papers II. and II. of this series, since $Mg\bar{h}$ is a complete differential. But for finite bulk phases γ^* will have no direct relationship to the properties of the interphase, since p_1 and p_2 refer to external pressures which in practice are measured against the atmosphere. Thus (p_1-p_2) would correspond only to the weight of unit cross-section of a short column of air, and γ^* would be nearly zero. Denoting the actual pressures just at the interphase by p_1^* and p_2^*, it is clear that

$$\gamma_{12}=(p_1^*-p_2^*)\left(\frac{\partial v_{12}}{\partial s_{12}}\right)_{p_2^*,\,T,\,W'',\,N,\,s_k},$$

In actual fact it is γ_{12} and not γ^* that is measured when a capillary rise method for finding the surface tension is used. The interesting point to observe is that γ_{12} only obeys our final equations if p_1 is sensibly equal to p_1^*, and p_2 is sensibly equal to p_2^* — that is to say, if the total volume of phases 1 and 2 is supposed to be confined to a very narrow layer on either side of the interphase.

Summary.

1. The surface tension of a liquid-liquid interphase is defined in such a way as to be applicable to any desired boundary in an interphase of finite thickness.

2. A generalized apparatus for doing surface work is discussed, and also the degrees of freedom of systems containing interphases of variable area.

3. This discussion involves extensive degrees of freedom, and so leads to a restatement of the phase rule.

4. It is shown that measurements of surface tension in reality involve several interphases and also volume changes in the bulk phases.

One of us (S. R. C.) wishes to express his thanks to the Department of Scientific and Industrial Research for a grant which enabled this work to be carried out.

References.

(1) Bowden and Rideal, Proc. Roy. Soc. A, cxx. p. 59 (1928); Erdey-Grúz and Kromrey, *Zeit. phys. Chem.* A, clvii. p. 213 (1931).
(2) Philpot, Phil. Mag. (7) xiii. p. 775 (1932); Frumkin, *Zeit. phys. Chem.* ciii. p. 55 (1923).
(3) Paschen, *Ann. Phys.* xliii. p. 568 (1891).
(4) Gouy, *Ann. Chim. Phys.* (7) xxix. p. 145 (1903).
(5) Frumkin, J. Russ. Proc. Chem. Soc. xlix. (1) p. 207 (1917); Bodforss, *Z. Elektrochem.* xxxix. p. 121 (1923).
(6) Billiter, *Ann. Phys.* xi. pp. 902 & 937 (1903); *Zeit. phys. Chem.* xlviii. p. 513 (1904).
(7) Bennewitz and Delijannis, *Zeit. phys. Chem.* A, cxxv. p. 144 (1927); Bennewitz and Küchler, *ibid.* A, cliii. p. 443 (1931).
(8) Bennewitz and Schulz, *ibid.* A, cxxiv. p. 115 (1926); Bennewitz and Bigalke, *ibid.* A, cliv. p. 113 (1931).
(9) Guggenheim, *J. Phys. Chem.* xxxiii. p. 842 (1929); *ibid.* xxxiv. p. 1540 (1930).
(10) Gibbs, 'Scientific Papers,' i.
(11) Butler, Proc. Roy. Soc. A, cxxxv. p. 348 (1932).
(12) Langmuir, J. Chem. Phys. i. p. 3 (1932).

Physical Chemistry Laboratory, Balliol & Trinity Colleges, Oxford, and the National Institute for Medical Research, Hampstead.

LXXV. *Induction Coil Discharges.* *By* WALTER MCFARLANE, *M.A., B.Sc.* (*Lecturer in Natural Philosophy in the University of Glasgow*)*.

[Plates XXIV.–XXVII.]

1. INTRODUCTION.

THE following investigation was undertaken for the purpose of determining the precise nature of the discharge produced by an induction coil across an air-gap, under any conditions of primary current and secondary capacity, and to find what influence the constants of the coil may have on the characteristics of that discharge.

It is well known that the discharge may take several different forms, the principal features of which have been observed and described by Prof. E. Taylor Jones [1]. Few attempts have been made, however, to obtain the precise variation of potential and current as the discharge is passing, possibly because the mirror oscillographs employed necessarily possessed inertia, and were, therefore, incapable of recording faithfully abrupt changes or high-frequency oscillations. The cathode-ray oscillograph does not possess this disadvantage, and, in addition, permits the combination of two variables, such as current and potential, thus widening considerably the scope of experiment.

While this work was in progress, a paper appeared by G. I. Finch and R. W. Sutton [2], in which they describe the variations of potential and current with time during the discharge produced by an ignition coil, and offer an approximate theory of its action which is shown to be adequate for the coil used. Many features of importance, however, both in theory and experiment, were concealed because of the smallness of the coil.

It has been shown that the power of an induction-coil discharge to produce ignition of an explosive mixture varies widely with the form of the discharge. It is, therefore, of considerable practical importance to know what type of discharge will take place under any given conditions.

* Communicated by Prof. E. Taylor Jones, D.Sc., F.Inst.P.

2. Experimental Arrangements.

The induction coil used was a fairly large one, capable of giving a 12-inch spark. The electromotive force applied to the primary was usually 18 volts, the circuit being broken by a hand-operated mercury dipper interrupter of the type described by J. Meiklejohn [3]. The primary condenser had a capacity of 2·67 μF. The potential across the spark-gap, and the current passing through the discharge, were measured by an Ardenne cathode-ray oscillograph, the circuit being indicated in fig. 1 (*a*). R_1, R_2, R_3 were non-inductive liquid resistances R_1 usually between 10 and 20 megohms and R_2

Fig. 1.

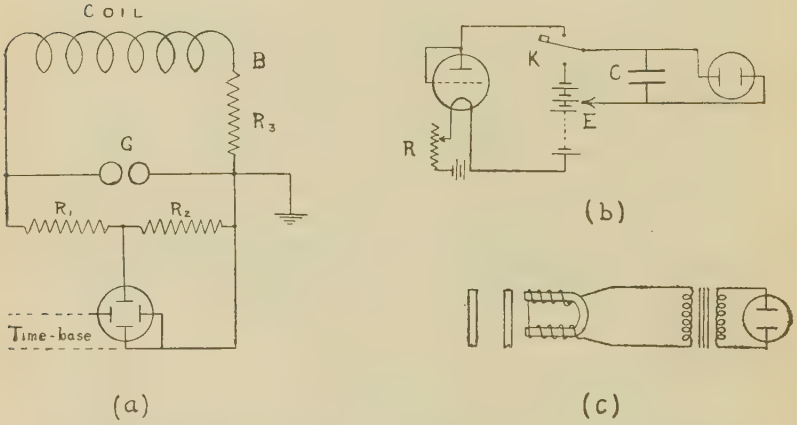

varied according to the sensitivity desired on the oscillograph. The current was measured by the potential difference developed across R_3, which could also be varied, but usually had a value of about 4000 ohms. An accurate knowledge of these resistances was unnecessary, since the sensitivity of the oscillograph during any experiment could be found simply and quickly by connecting a known potential across the spark-gap G, the current flowing through the secondary being directly measured by a milliammeter and the resulting potential and current deflexions on the oscillograph by a travelling microscope. Several methods of potential division were tried before finally adopting a division by means of resistances. For some other experiments made by the

author condensers were employed, but this proved unsuitable for the present case. Many of the discharges here investigated were of relatively long duration, and spurious effects were produced by the fact that the gas between the deflecting plates of the oscillograph possesses a certain conductivity. It was found inadvisable also simply to use the resistance between the plates as R_2, since the gas does not obey Ohm's law. The connexion of even high resistances across the terminals of an induction coil is known to affect appreciably the maximum potential produced and the wave-form of the potential, if no other discharge is passing between the terminals. When, however, a spark-discharge takes place, the effective resistance of the gap becomes small compared with the measuring resistances, and no spurious effects can be introduced.

Fig. 1 (*a*) shows the connexions to the oscillograph when the potential-time oscillograms were investigated, one terminal of the gap and one plate of each pair of deflecting plates being connected to the anode of the oscillograph and earthed. The alterations required to give current-time and potential-current curves were thus made simple, a single lead from the point B giving the current.

The time-base circuit employed is shown in fig. 1 (*b*). A condenser C, of capacity $\cdot 2\ \mu$F., was charged and discharged by operation of a double-pole key K through a saturated diode valve. The valve was a bright emitter (Cossor P. I.), with grid and anode connected. A uniform sweep of the spot was thus obtained, the filament rheostat R providing a smooth control over the speed. Adjustment of the connexion E to the battery (total E.M.F. 240 volts) brought that part of the sweep desired to the centre of the oscillograph-screen. Calibration of the time-base was effected by means of the arrangement in fig. 1 (*c*). A tuning-fork of known frequency was caused to vibrate with one prong in close proximity to a small electromagnet (a telephone earpiece with the diaphragm removed). The oscillatory current induced in the windings passed through the primary of a transformer of the wireless low-frequency type, the secondary terminals of which could be switched on to the plates of the oscillograph. When time-measurement of a discharge was required, a trace of the wave produced by the tuning-fork was superposed on the same photographic plate immediately

after the discharge-oscillogram was obtained. The key K was mounted alongside, but insulated from, the dipper interrupter, and was operated by the same lever. This lever was raised by the action of a strong spring, and the contacts of K, which were adjustable by screws, could be arranged so that the sweep of the spot commenced at a suitable interval before the dipper left the mercury and broke the primary circuit. In this way, by simple operation of the interrupter-lever, oscillograms corresponding to single discharges were obtained. The photographs were taken with an Ernemann F/2 focal-plane camera.

For visual observation of some of the phenomena the dipper interrupter was replaced by a mercury-jet interrupter, which was modified to produce only one "break" per revolution, the primary circuit being open for three-quarters of a revolution. The key K was replaced by a rotating arm mounted on the motor spindle and making spring contact with the inside of a cylinder. Metal linings on the cylinder permitted contact with the valve anode and the battery alternately, the connexion to the valve occupying most of the time of revolution. By adjustment of the moving arm on the spindle the "break" could be made to take place at any part of the sweep of the spot. This arrangement was set up in the first instance in an attempt to obtain a stationary repetition of the fainter oscillograms, and thus facilitate photography, but it was found that that the instant of "break" varied slightly and produced irregular small displacements of the pattern. This difficulty could not be overcome, since its cause lay in the unavoidable production of an arc at "break." Even for visual observation the method was limited in application to discharges which lasted for a shorter time than the interval between "break" and "make" permitted by the interrupter working at its lowest speed.

The appearance of the discharge was observed and photographed by means of a rotating plane mirror and a lens. A magnified image was produced in order that discharges through small gaps could be investigated.

3. Discharges with a Large Primary Current.

It will facilitate an understanding of the processes at work if the experiments made on the most usual type of induction coil discharge are described first, *i. e.*, a discharge

which is produced by the interruption of a primary current much larger than the minimum necessary to produce a discharge. Under these circumstances it is well known that the discharge consists of two distinct parts, usually described as the capacity and inductance components. The former consists of a single bright spark which represents the breakdown of the air-gap and the discharge of static electricity from the capacity of the electrodes and the coil. This is followed by the inductance component, which is a much fainter and more prolonged discharge. It has been shown that the current flowing during this part of the discharge is unidirectional but pulsating, and can, in turn, be divided into two parts, viz., a decaying aperiodic component, superposed on which is a decaying oscillatory component, the period of oscillation being approximately given by

$$2\pi\sqrt{\{L_1C_1(1-k^2)\}}, \text{ where } k^2=\frac{M^2}{L_1L_2},$$

L_1, L_2 being the self-inductances of the primary and secondary circuits, M the mutual inductance, and C_1 the primary capacity.

The inductance component has usually been described as taking the form of a "pulsating arc," but inquiry into the appearance of the discharge, and the potential at which it takes place, leads to a different view. The experiments to be described show that, in most cases, it has all the characteristics of a "glow" discharge at atmospheric pressure. Only under special circumstances is the true "arc" produced, and it then only forms part of the inductance component.

The word "spark" is often used to describe the whole discharge produced by an induction coil, but in what follows it will only be used to denote the oscillatory discharge of a capacity. On this understanding the capacity component only will be called a "spark."

The variation of potential between the electrodes during a discharge of the above type through a small gap, when observed with a low sensitivity on the oscillograph, is of the form shown in fig. 2. At the break of the primary current the potential rises rapidly from A to B, the sparking potential of the gap. The rate of rise is governed by the constants of the coil and the magnitude of the primary current. It increases with the latter. The

capacity spark now passes between the electrodes, the high frequency of the oscillating potential rendering the oscillograph-trace invisible. A break in the curve therefore appears, and the spot becomes visible again at C, where the inductance component commences. CD represents the potential during the inductance component. It has a relatively low value which, when observed on this scale, appears practically constant. When the discharge ceases at D the energy remaining in the coil produces oscillations of potential (DE) which are controlled entirely by the coil constants. The above is the type of oscillogram obtained by Finch and Sutton, and they based their theory of the inductance component on the assumption

Fig. 2.

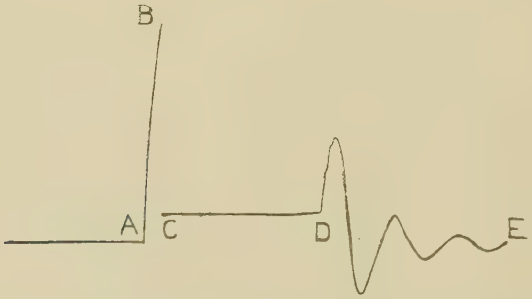

that the potential (CD) remained constant, irrespective of the current passing through the discharge.

When the sensitivity of the oscillograph is considerably increased two new features of the portion CD appear. Fig. 3 (Pl. XXIV.) shows the variation of potential during the inductance component for a discharge between zinc spheres 2 cm. in diameter, 4 mm. apart, the primary current being 4 amperes. On this scale the other variations are too rapid to be photographed *. Firstly, it is shown clearly that the potential increases quite considerably with the time, *i. e.*, with diminishing current; and, moreover, that the rate of increase of potential increases with time. Secondly, the pulsations in current produce corresponding pulsations in potential, but with the coil used these pulsations are of a period small compared with

* In all oscillograms involving time the time-axis is horizontal and from left to right.

the duration of the discharge, and are rapidly damped, so that they only appear faintly at the beginning of the curve. Their presence is shown more clearly in fig. 15 (*b*) (Pl. XXV.), which will be described later. The pulsations play a very important part in determining the nature of the discharge when the primary current is small, and their effect will be discussed separately. Meantime our attention will be confined to the effect of the aperiodic component of the current through the discharge. The amount by which the potential rises is a function of the gap-length, being greater as the gap-length is increased. This explains the result obtained by Finch and Sutton, who used very small gaps (of the order of ·008 inch). With such a gap, and a low sensitivity on their oscillograph, the increase would be very small, and would easily escape observation. In order to verify that no spurious effect was being introduced by the method of potential division, the leads from the gap were taken direct to the oscillograph and a magnetic bias applied to the spot by means of a current through deflecting coils. By adjustment of this current the curve CD could be brought near the centre of the screen. Its appearance agreed exactly with that described above, the variation, of course, being much magnified.

The condition governing the cessation of the discharge is revealed when the current flowing through it is considered. The variation of current with time is shown in fig. 4 (Pl. XXIV.). It is there evident that when the current falls to a certain value the discharge ceases. The oscillatory current flowing through the initial spark is of large amplitude and high frequency, and is not shown on the screen. Again, the pulsations appear only faintly at the beginning of the discharge. The aperiodic current appears almost linear, but shows a slight convexity towards the time-axis, suggesting the presence of an exponential term. This curvature depends on the length of the gap, being more pronounced the smaller the gap.

Fig. 5 (Pl. XXIV.) shows the potential-current characteristic of the inductance component, voltage being vertical and current horizontal. The axes were superposed after the characteristic was photographed by connecting the leads from the time-base circuit to each pair of deflector plates in turn. This oscillogram shows clearly the increase in potential with decrease in current and the fact that

the discharge ceases when the current reaches a certain minimum value. A point of some importance is that the pulsations in current trace the same curve, or, in other words, the relation between the potential and current is independent of the manner in which the current is varied.

The appearance of the whole discharge as it appeared in the rotating mirror is shown in fig. 6 (Pl. XXIV.). The initial spark appears as a bright line (accompanied by fainter multiple reflexions at the mirror). The inductance component gives all the characteristic appearance of the "glow" discharge. On the cathode (the lower electrode in fig. 6 (Pl. XXIV.)) appears a bright blue glow which is not confined to a point but occupies a considerable area of the electrode. This area diminishes with the current. Just outside this cathode glow appears a Crookes's dark space, which has a width in this case of about ·3 mm. It is noticed that the width does not vary with the current. It was found, also, that the width did not increase with the gap-length, but remained practically constant. It appeared to diminish, however, when the gap became very small, of the order of ·5 mm., *i. e.*, when the dark space became comparable in width with the whole length of the gap. The dark space is succeeded by a reddish glow which is brightest at the border of the dark space and at the anode, where it terminates in a bright red spot. The brightness of the whole anode glow also diminishes with the current. The band of light above the anode spot is simply an optical reflexion of the cathode glow from the opposite electrode. In fig. 6 (Pl. XXIV.) the discharge is terminated by three sparks in rapid succession. This phenomenon occurred very frequently when observing these discharges. They were indicated in the potential curves by a number of almost vertical straight lines indicating the rising potential between the sparks. These, of course, occurred at the point D in fig. 2. They are explained by the fact that there is still current flowing into the capacity of the secondary coil, insufficient to maintain the glow, but sufficient to raise the gap to sparking potential several times. Owing to the condition of ionization in the gap, and possibly, also, the condition of the electrode surfaces, after the passage of the glow, the sparking potential is lower than in the initial spark. This, however, seems inadequate as an explanation of the

great difference in intensity from the initial spark, in the case of fig. 6 (Pl. XXIV.). It is probable that, whereas in the initial spark we have the discharge of static electricity from the self-capacity of the coil, in these rapid and much less intense sparks only the much smaller capacity of the electrodes and leads is involved. Instances will be given later which show that whenever an abrupt change of potential occurs between the electrodes of the gap there is a great tendency for these high-frequency low-intensity sparks to appear. It should be pointed out, however, that the case of fig. 6 (Pl. XXIV.) was not general, and that in many discharges the terminal sparks were comparable in intensity with the initial spark. This was particularly the case with large gaps, where either no terminal sparks appeared at all or a single bright spark took place.

Formation of the Arc.

When the primary current is increased beyond a certain limit for a given gap-length, a very sudden break appears in the potential curve for the inductance component. Fig. 7 (Pl. XXIV.) shows the curve obtained for a gap of 4 mm. between 2 cm. zinc spheres (the same gap as for fig. 3 (Pl. XXIV.)), but here the primary current was 6 amperes. The inductance component commences at a much lower potential than usual, and then, after some time, breaks and assumes the potential associated with the above described glow discharge. The corresponding potential-current characteristic is shown in fig. 8 (Pl. XXIV.). It is there noticeable that, although the potential is discontinuous, the current passing through the discharge remains continuous. This was, of course, also shown by the current-time curve, which remained rather similar to the type shown in fig. 3 (Pl. XXIV.), except for a sudden slight change in gradient where the potential altered. When the potential jumped to the higher value the gradient of the current-curve became slightly greater, with the result that a kink appeared. The value of the primary current at which this new phenomenon set in was not absolutely constant for a given gap. For example, frequently with the above conditions only the usual discharge was observed. In many instances, also, the discharge jumped backward and forward from the one potential to the other during a single discharge.

Neither was any constancy associated with the value of the secondary current at which the change took place. In the example shown in fig. 8 (Pl. XXIV.) the current at the break was 36·7 milliamp. Occasionally it was observed that the whole inductance component took place at the lower potential. When this occurred, the whole curve presented the same appearance as the glow-curve, *i.e.*, the potential increased with the time and diminishing current, or, in other words, this new type of discharge also had a negative dynamic characteristic. Here again it was observed that the sudden change of potential was accompanied often by one or more rapid low intensity sparks. A clue to the nature of this lower potential discharge was sought in the rotating mirror. A photograph of the whole discharge is shown in fig. 9 (Pl. XXV.). A distinct difference exists between the two parts. For the lower potential no diffuse cathode glow and no dark space appear. The anode glow stretches right across the gap, and only a small bright spot appears on the cathode. When the jump in potential takes place, the discharge assumes the usual glow form, the change being accompanied by two sparks in this case.

Many writers have investigated the glow and arc discharges in air at atmospheric pressure, and have obtained their static potential-current characteristics. Thus V. L. Chrisler[4] has described the two types of discharge and investigated the transition between them. The above observations agree exactly with his description in respect of the absence of diffuse cathode glow and dark space in the arc, and also the much lower potential associated with it. Chrisler showed that the difference in potential necessary to maintain the two discharges arises from the fact that the cathode fall of potential in the case of the arc is very much smaller than in the glow, the anode fall remaining the same. The increase in potential, then, in figs. 7 and 8 (Pl. XXIV.) is to be interpreted as the sudden change in cathode fall as the discharge changes from arc to glow. This change, as measured by figs. 7 and 8 (Pl. XXIV.), is for this case about 340 volts. The interpretation of figs. 7 and 8 (Pl. XXIV.) and fig. 9 (Pl. XXV.) is, therefore, the following:—When the primary current broken is large enough, *i. e.*, when the current supplied to the gap is large enough, a true arc discharge is formed immediately

on the cessation of the initial spark. The current, however, diminishes with time and reaches a value which is unable to sustain the arc form. The discharge then suddenly takes the form of a glow, and this continues until the current reaches a value at which the glow must cease.

It was found that this formation of an arc took place more readily with zinc electrodes than any other metal tried (copper, brass, iron, and aluminium) under the same conditions. Also, zinc electrodes which had been in use for some time, and were coated with a film of oxide, showed a greater tendency to form an arc than when clean.

Glow and Arc Discharge with Condenser.

Similar types of discharge to those described above are formed when a condenser is connected across the terminals of the coil in parallel with the gap, only in this case a much larger primary current is necessary. (The nature of the condenser discharge with small primary current will be described later.) It was found that the potentials at which the arc and glow passed were unaltered by the inclusion of a condenser. Fig. 10 (Pl. XXV.) shows a direct comparison of the potential oscillograms for a gap of 2·5 mm., the primary current being 7·4 amperes. (*a*) is the result with no capacity (other than the coil self-capacity), and (*b*) that for a condenser of ·00087 μF. It is observed that (*b*) shows a small arc, while (*a*) shows only the glow. Under the conditions of gap and primary current above it was found that with no condenser a short arc appeared in about half the number of observations. When the condenser was inserted, however, the arc appeared more frequently. The larger the capacity associated with the discharge, the more easily is the arc discharge formed (*i. e.*, in preference to the glow), even although the current supplied to the gap is approximately the same. The explanation of this no doubt lies in the fact that the amplitude of the oscillatory current flowing in the spark increases as the square root of the capacity. The larger this current is, the greater will be the heating effect on the cathode in the time occupied by the spark, and, therefore, conditions will be more favourable for the formation of an arc by the secondary-coil current.

The Glow Characteristic.

Curves of the type shown in figs. 3, 4, and 5 (Pl. XXIV.) (*i. e.*, for the glow-discharge) were investigated under different conditions of gap-length and primary current, using the same electrodes, viz., zinc spheres 2 cm. in diameter. Maintaining the length of the gap constant, an increase of primary current, of course, produced an increase in the current flowing in the secondary coil, *i. e.*, in the current passing through the discharge. The initial value of the aperiodic component of the current was, indeed, almost exactly proportional to the primary current. The gradient of the current-curve remaining roughly the same, this resulted in a discharge of longer duration. On the other hand, the potential curve commenced at a slightly lower value as the primary current was increased, but ended at approximately the same value. The terminal potential corresponds to the current at which the glow is extinguished, and this is approximately constant for a given spark-length.

With variation of the gap-length, maintaining a constant primary current, the aperiodic component of the current commenced always at approximately the same value. The gradient of the curve, however, increased with the gap, as also did the current at which the discharge ceased. As a consequence of these the discharge lasted for a shorter time. This latter current, while in general increasing in value as the gap was increased, showed slight variations for any given gap. This could probably be traced to changes in the surfaces of the electrodes, viz., the formation of a coating of oxide by previous discharges. The potential-time curve commenced at a higher value as the gap was increased, and the increase in potential as the current diminished became more prominent. These results can all be illustrated by considering the potential-current characteristics. Fig 11 shows these for gaps of 1, 2, 3, and 4 mm., the primary current being the same (5 amperes) in all cases. An increase of primary current merely elongates these curves in the direction of the current-axis. (When, however, the current was great enough to maintain the arc-discharge the transition shown in fig. 8 (Pl. XXIV.) occurred.) These curves were obtained by means of a travelling microscope focussed on the oscillograph-screen, the coordinates of the centre of the line being taken. Slight variations in the position

of the line occurred, the position taken being the mean of many discharges. Fig. 12 shows the product of current and potential plotted against the current in the four cases. The observations lie closely on straight lines, showing that the power supplied to the gap is a linear function of the current. The relation may be written $iV=ai+b$, where i and V are the current and potential and a and b are constants depending only on the length

Fig. 11.

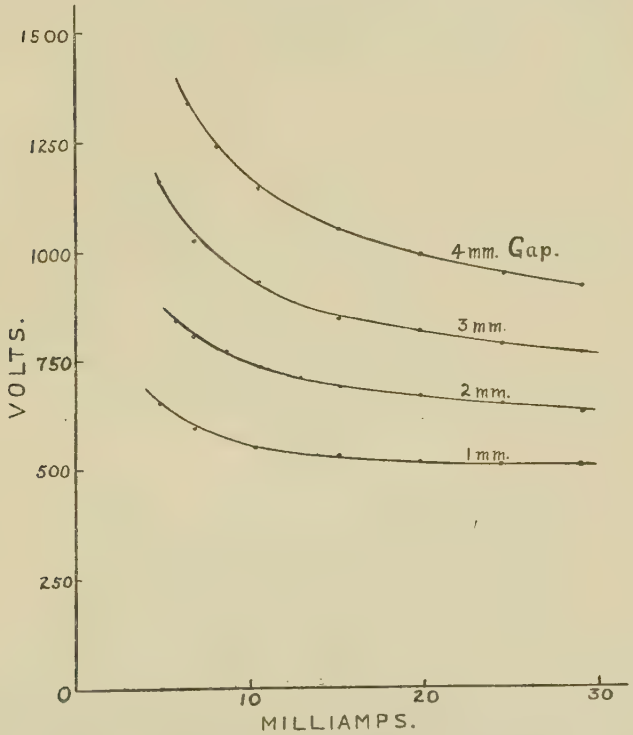

of the gap and, possibly, the material of the electrodes. The above relation is, of course, the usual Ayrton formula for the *arc* characteristic, but, within the range of the present experiments, it seems to apply also to the glow at atmospheric pressure. It was found, as in the case of the Ayrton formula, that the constants a and b are approximately linear functions of the gap-length, the relations most closely fitting the present case being

$$a=380+108l, \qquad b=\cdot 8l,$$

if V is measured in volts, i in amperes, and l in mm. These values were found simply from the lines in fig. 12, so that no great accuracy can be claimed, particularly for the value of b, which is simply the intercept of these lines on the iV axis. The 380 volts in the above expression for a no doubt represent the cathode fall of potential, which is independent of gap-length or current. It is of interest to note that the jump of 340 volts which accompanied the transition from arc to glow in fig. 8 (Pl. XXIV.) represents the difference in value between the

Fig. 12.

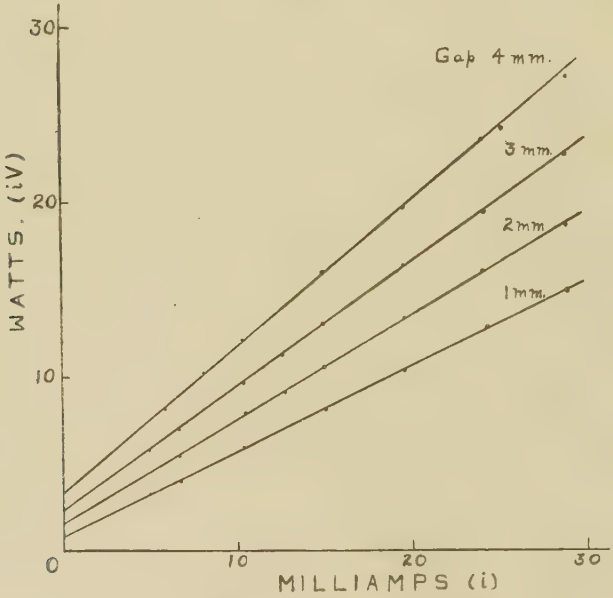

cathode falls in the two types of discharge. According to the curves given by Chrisler, the cathode fall for the arc between zinc electrodes is about 40 volts. It is natural, then, that the principal change in the appearance of the two discharges should occur at the cathode.

4. Theory of the Inductance Component.

The full circuit equations for an induction coil producing a discharge of any type may be written

$$L_1 \frac{di_1}{dt} + L_{12} \frac{di_2}{dt} + R_1 i_1 + V_1 = 0, \quad . \quad . \quad . \quad (1)$$

$$L_2\frac{di_2}{dt}+L_{21}\frac{di_1}{dt}+R_2i_2+V_2=0, \quad . \quad . \quad . \quad (2)$$

$$i_1=C_1\frac{dV_1}{dt}, \quad . \quad . \quad . \quad . \quad . \quad . \quad . \quad (3)$$

$$i_2-i=C_2\frac{dV_2}{dt}, \quad . \quad . \quad . \quad . \quad . \quad . \quad . \quad (4)$$

$$V_2=f(i), \quad . \quad . \quad . \quad . \quad . \quad . \quad . \quad . \quad (5)$$

where L, R, V, i, and C denote inductance, resistance, potential, current, and capacity respectively, the suffixes 1 and 2 referring to the primary and secondary circuits *. R_2 will include any resistance in series with the secondary which is used for measurement of current. L_{12}, L_{21} are the inductances of the secondary on the primary, and the primary on the secondary, respectively. i is the current flowing through the discharge, and equation (4) states simply that the difference between i and i_2, the current flowing in the secondary coil, is the current flowing into the secondary self-capacity. Equation (5) represents the characteristic equation of the discharge.

Eliminating i_1, V_2, i_2, by means of (3) and (4), and writing $k^2=\frac{L_{12}L_{21}}{L_1L_2}$ (the coupling of the coils) and D for $\frac{d}{dt}$, we obtain

$$\begin{aligned}C_1L_1L_2(1-k^2)D^3i+C_1(L_1R_2+L_2R_1)D^2i+(C_1R_1R_2+L_2)Di\\ +R_2i+C_1C_2L_1L_2(1-k^2)D^4V_2+C_1C_2(L_1R_2+L_2R_1)D^3V_2\\ +(C_1C_2R_1R_2+C_2L_2+C_1L_1)D^2V_2\\ +(R_2C_2+R_1C_1)DV_2+V_2=0 \quad . \quad . \quad . \quad . \quad . \quad . \quad (6)\end{aligned}$$

A knowledge of equation (5) would, theoretically, enable the solution of this equation to be found.

The substitution of the relation

$$V_2=a+\frac{b}{i}, \quad . \quad . \quad . \quad . \quad . \quad . \quad . \quad (7)$$

which most closely fits the experimental curves for the glow, gives a non-linear differential equation which cannot be solved by ordinary methods. However, the dimensions of the quantities involved permit close approximations to be made. It has been shown that b is small

* V_1 is, more precisely, the excess of the potential across the primary condenser over the battery E. M. F

compared with a, and the term b/i becomes important only for small currents. The current, also, cannot have a value below the minimum necessary for maintenance of the glow. We shall assume, therefore, as a first approximation, that $V_2=a$, a constant, during the glow-discharge. This is the basis of the theory put forward by Finch and Sutton, but they also neglected the secondary resistance.

The above considerations will also apply to the case where the true arc is formed, if the appropriate lower value of a is substituted.

If V_2 is constant, then by (4) $i_2=i$, i. e., the secondary capacity is inoperative. Under these conditions

$$L_{12}=L_{21}=M,$$

the mutual inductance. Equation (6) reduces to

$$C_1L_1L_2(1-k^2)D^3i+C_1(L_1R_2+L_2R_1)D^2i \\ +(L_2+C_1R_1R_2)Di+R_2i=-a. \quad (8)$$

Let $n^2=\dfrac{1}{L_1C_1(1-k^2)}$ and $S=C_1(L_1R_2+L_2R_1)$.

$C_1R_1R_2$ is negligibly small in comparison with L_2. With these changes (8) becomes

$$\frac{L_2}{n^2}D^3i+SD^2i+L_2Di+R_2i=-a. \quad . \quad . \quad (9)$$

It is necessary to consider later the relative magnitudes of the coefficients in this equation, so that their approximate values are stated here. For the coil used,

$L_2 \doteqdot 1500$ henries. $\qquad n^2=3{\cdot}13.10^7$.

$S=\cdot 023$. $\qquad R_2 \doteqdot 28{,}000$ ohms.

The solution of (9) is of the form

$$i=-\frac{a}{R_2}+A_1e^{\lambda_1 t}+A_2e^{\lambda_2 t}+A_3e^{\lambda_3 t}, \quad . \quad . \quad (10)$$

where λ_1, λ_2, λ_3 are the roots of the cubic equation

$$\frac{L_2}{n^2}\lambda^3+S\lambda^2+L_2\lambda+R_2=0. \quad . \quad . \quad (11)$$

The substitution of

$$\lambda=x-\frac{Sn^2}{3L_2} \quad . \quad . \quad . \quad . \quad . \quad . \quad (12)$$

transforms (11) into the soluble form

$$x^3+px+q=0, \quad \ldots\ldots \quad (13)$$

where

$$\left.\begin{aligned} p&=n^2-\frac{S^2n^4}{3L_2^2}, \\ q&=\frac{2}{27}\frac{S^3n^6}{L_2^3}-\frac{Sn^4}{3L_2}+\frac{R_2}{L_2}n^2. \end{aligned}\right\} \quad \ldots\ldots \quad (14)$$

The solutions to (13) are

$$x_1=-(\xi+\eta);$$

$$x_2, x_3=\tfrac{1}{2}(\xi+\eta)\pm\sqrt{-1}\,\frac{\sqrt{3}}{2}(\xi-\eta),$$

where

$$\xi^3=\frac{q}{2}+\sqrt{\left(\frac{q^2}{4}+\frac{p^3}{27}\right)};$$

$$\eta^3=\frac{q}{2}-\sqrt{\left(\frac{q^2}{4}+\frac{p^3}{27}\right)}.$$

Since

$$\frac{q^2}{4}\left(\doteqdot 5{\cdot}3.10^{18}\right)$$

is small compared with

$$\frac{p^3}{27}\left(\doteqdot 1{\cdot}1.10^{21}\right),$$

ξ and η may be found by a double application of the binomial theorem. After omitting all small terms, it is found that ξ and η reduce simply to

$$\xi=\frac{n}{\sqrt{3}}+\frac{q}{2n^2}; \qquad \eta=-\frac{n}{\sqrt{3}}+\frac{q}{2n^2}.$$

Hence

$$x_1=-\frac{q}{n^2}; \qquad x_2, x_3=\frac{q}{2n^2}\pm n\sqrt{-1}.$$

Thus from (12) and (14) the approximate solutions of (11) are

$$\left.\begin{aligned} &\lambda_1=-\frac{R_2}{L_2}; \quad \lambda_2=-\mu+\sqrt{-1}n; \quad \lambda_3=-\mu-\sqrt{-1}n, \\ &\text{where} \\ &\mu\doteqdot-\frac{Sn^2}{2L_2}+\frac{R_2}{L_2}=-\frac{R_1}{2L_1(1-k^2)}-\frac{R_2k^2}{2L_2(1-k^2)}. \end{aligned}\right\} \quad (15)$$

The solution (10) may thus be put in the form

$$i=-\frac{a}{R_2}+A_1e^{-\frac{R_2}{L_2}t}+Pe^{-\mu t}\cos nt+Qe^{-\mu t}\sin nt, \quad (16)$$

where $P=A_2+A_3$, $Q=\sqrt{-1}(A_2-A_3)$.

For the determination of the constants of integration the form (10) of the solution is more convenient. The solution for V_1 is, of course, of similar type. We have

$$\left.\begin{aligned} i&=-\frac{a}{R_2}+A_1e^{\lambda_1 t}+A_2e^{\lambda_2 t}+A_3e^{\lambda_3 t};\\ V_1&=B_1e^{\lambda_1 t}+B_2e^{\lambda_2 t}+B_3e^{\lambda_3 t}. \end{aligned}\right\} \quad . \quad . \quad . \quad (17)$$

If i_0 is the primary current, and E the battery E.M.F. at "break" of the primary circuit, the initial conditions are

$$\left.\begin{aligned} i_1=i_0&=C_1\frac{dV_1}{dt};\\ V_1&=-E;\\ i&=0. \end{aligned}\right\} \quad . \quad . \quad . \quad . \quad . \quad . \quad (18)$$

The last condition requires some explanation. The solutions (17) are based on the assumption that $V_2=a$, but this condition only applies when the inductance component has commenced, that is, when current above a certain value is flowing. It is the initial spark which really makes the conditions of the gap suitable for the initiation of the inductance component. The interval of time between "break" and the commencement of the inductance component is occupied by the charging of C_2 and the spark itself. The latter has an exceedingly short duration, and so, also, has the former if the primary current is well above the minimum, as it is in the case under consideration. During this interval the secondary current is absorbed by C_2, and will have grown to some value greater than zero by the time the capacity discharge has ceased. The energy associated with this current is dissipated in the spark. This energy is in the present circumstances, however, only a very small part of the total energy given to the coil. A primary current of 5 amperes provides energy of amount $\frac{1}{2}L_1i_0^2 \doteqdot 1{\cdot}3$ joules, while if the gap-length were 2 mm. the energy in the initial spark is only of the order of $\frac{1}{2}C_2V_2^2 \doteqdot {\cdot}0034$ joule.

This was also confirmed experimentally by comparing the secondary currents which passed with the same primary current when the coil was shorted and when it was producing a discharge across a small gap. It was found that the initial value of the aperiodic component of the current was practically the same in both cases, as also was the initial amplitude of the pulsations. As the gap-length was increased, however, the initial aperiodic current became slightly less than that for the shorted coil. This is only as expected, of course, since the spark-energy increases as V_2^2. It is unlikely, then, that for gaps of a few mm. in length, the assumption that $i=0$ initially will lead to any appreciable error.

Using the conditions (18), and substituting the solutions (17) in equations (1) and (2), the following equations are obtained for determination of the A's :—

$$A_1+A_2+A_3=\frac{a}{R_2}=G_1;$$

$$\frac{A_1}{\lambda_1}+\frac{A_2}{\lambda_2}+\frac{A_3}{\lambda_3}=-\frac{L_2}{R_2}\left(\frac{Mi_0}{L_2}+\frac{a}{R_2}\right)=G_2;$$

$$\frac{A_1}{\lambda_1^2}+\frac{A_2}{\lambda_2^2}+\frac{A_3}{\lambda_3^2}=\frac{L_2^2}{R_2^2}\left(\frac{Mi_0}{L_2}+\frac{a}{R_2}\right)+\frac{MEC_1}{R_2}=G_3.$$

From these

$$A_1=\lambda_1^2\frac{G_1-G_2(\lambda_2+\lambda_3)+G_3\lambda_2\lambda_3}{(\lambda_1-\lambda_2)(\lambda_1-\lambda_3)},$$

with similar expressions for A_2 and A_3.

On substitution of the values of the λ's and the G's, and neglecting $\lambda_1^2(\fallingdotseq 360)$ and $\mu^2(\fallingdotseq 5{\cdot}8.10^4)$ in comparison with $n^2(\fallingdotseq 3.10^7)$, it is found that

$$A_1\fallingdotseq\frac{Mi_0}{L_2}+\frac{a}{R_2};$$

$$A_2\fallingdotseq-\frac{Mi_0}{2L_2}-\frac{\sqrt{-1}}{2}\left(\frac{Mi_0}{L_2}\frac{\mu-\lambda_1}{n}+\frac{MEC_1}{R_2}\lambda_1 n\right),$$

and A_3 is a similar expression to A_2 with a positive sign before the imaginary part. Hence P and Q of (16) are given by

$$P=-\frac{Mi_0}{L_2};\qquad Q=\frac{Mi_0}{L_2}\frac{\mu-\lambda_1}{n}-\frac{MEC_1 n}{L_2}.$$

Under working conditions the quantity Q is small compared with P, so that a good approximation to the current flowing through the discharge is given by

$$i=-\frac{a}{R_2}+\left(\frac{Mi_0}{L_2}+\frac{a}{R_2}\right)e^{-\frac{R_2}{L_2}t}-\frac{Mi_0}{L_2}e^{-\mu t}\cos nt. \quad (19)$$

If the secondary is shorted the expression for the current may be found simply by putting $a=0$, *i. e.*,

$$i=\frac{Mi_0}{L_2}\left(e^{-\frac{R_2}{L_2}t}-e^{-\mu t}\cos nt\right). \quad . \quad . \quad . \quad (20)$$

5. Experimental Verification of Theory.

The above solutions (19) and (20) become similar to the solutions given by Finch and Sutton if R_2 tends to zero. The main difference lies, therefore, in the expression for the aperiodic component of the current and it will suffice to show here that the consideration of R_2 is necessary in the case of an induction coil of any size.

It has already been stated that the initial values of the aperiodic components of the current in the two cases were observed to be approximately equal. These by (19) and (20) are both given by Mi_0/L_2. It should be pointed out that this value is what would be obtained from consideration of energy. The magnetic flux through the secondary coil when i_0 is flowing in the primary is Mi_0, and when I′ is flowing in the secondary is L_2I'. If there is no magnetic leakage these two would be equal. From actual experiment the mean value of the ratio I'/i_0, with the coil shorted, for a range of 1–8 amps. was 7·15 milliamps. per ampere. The ratio increased slightly for the larger values of i_0 because of the change in values of the inductances. The expression M/L_2, calculated from the constants of the coil for a current of 2 amperes, gives $\frac{11\cdot2}{1500}=\cdot0075$, or 7·5 milliamps. per ampere.

Fig. 13 shows a drawing obtained by measurements on photographs of the secondary current (aperiodic component, as in fig. 4 (Pl. XXIV.)) in the cases of coil shorted and discharge through gaps of 1, 2, and 3 mm., when the primary current was 4·05 amps. Curve A is accurately

exponential, and gives for the exponent a value 18·5, while

$$\frac{R_2}{L_2}=\frac{28{,}500}{1500}=19{\cdot}0.$$

If R_2 were taken as zero the theory would give for A a straight line parallel to the time-axis, and an error of the same order would be shown in the other cases.

By comparison of expressions (19) and (20) it is seen that the current through a discharge at any instant can

Fig. 13.

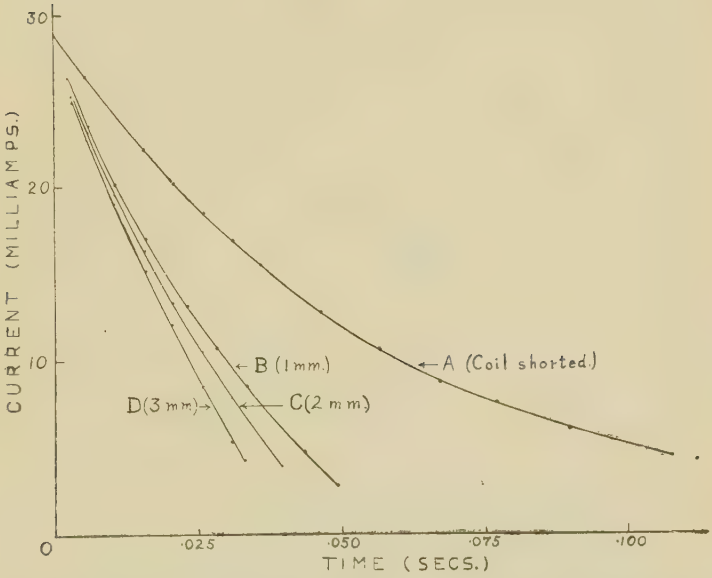

be derived from that of the shorted coil, with the same primary current, by subtracting the expression

$$\frac{a}{R_2}\left(1-e^{-\frac{R_2}{L_2}t}\right).$$

This increases with a, and hence gives a steeper curve as the gap is increased.

As the gap is opened there is a considerable drop from curve A, no matter how small the gap is. This is explained by the fact that a has a minimum value of 380 volts, the cathode fall.

The curves B, C, D fit very closely to those derived from (19) if, instead of using the calculated value, Mi_0/L_2, of the initial amplitude of the aperiodic component, the experimental value ($7{\cdot}15\ i_0$ milliamps.) is taken. Fig. 14 shows a comparison of the aperiodic component for the case of the 3 mm. gap and the curve from (19), using the value of a obtained from

$$a = 380 + 108\,l = 704 \text{ volts.}$$

Fig. 14.

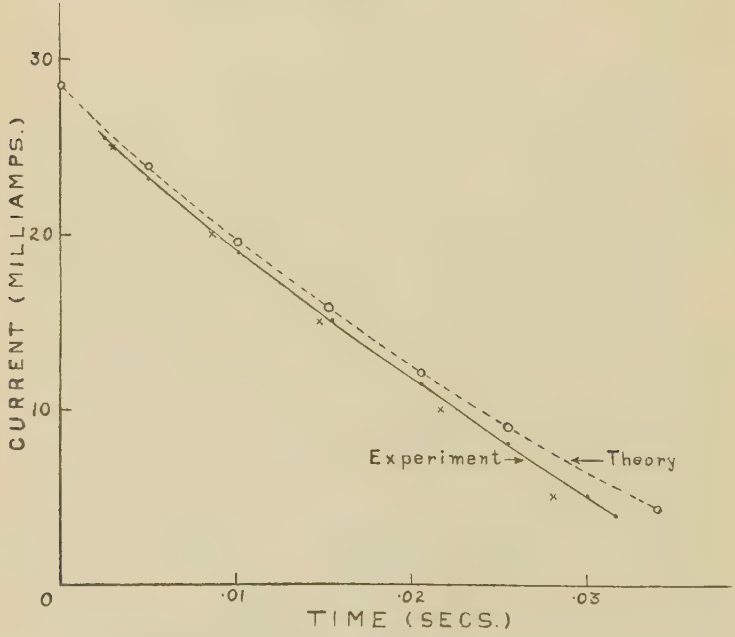

The theoretical curve lies a little above the experimental. The difference may be attributed to the various approximations made, including the neglect of the energy dissipated in the initial spark, The greatest deviation occurs at the small values of the current, as would be expected from the assumption made in the above theory that V_2 is constant. The term b/i increases in value as i diminishes, and produces the same effect as an increase in the value of a. As a result the curve should become a little more steep than the theoretical curve.

A sudden change from arc to glow, as exemplified in fig. 7 (Pl. XXIV.), means a sudden increase in the value of a. As a consequence of this the current-curve would show an increase of gradient at the point of transition. This agrees with observation.

Duration of the Discharge.

From (19) an aproximate value of the duration of the discharge may be obtained if the initial and final values of the aperiodic component of the current are known and if the oscillatory component has attained a negligible amplitude when the discharge ceases. If I and I′ are the initial and final currents, then the duration T is given by

$$I' = -\frac{a}{R_2} + \left(I + \frac{a}{R_2}\right) e^{-\frac{R_2}{L_2} T} \quad \text{or} \quad T = \frac{L_2}{R_2} \log \cdot \frac{IR_2 + a}{I'R_2 + a}.$$

TABLE I.

I = 28·6 milliamps.

Gap-length (mm.).	I′ (milliamps.).	Duration (secs.).	
		Experiment.	Theory.
1.....	2·4	·049	·0517
2.....	3·5	·038	·0382
3.....	4·0	·032	·0340

Table I. shows a comparison of theory and experiment for the cases of fig. 13, using the experimental value of I in the calculation.

The agreement between the theoretical and experimental values shows that for small gaps of a few mm. in length the neglect of the term b/i in the expression V_2 does not lead to serious discrepancy.

In order to facilitate the qualitative study of the pulsations an iron-core inductance was connected in series with the primary of the coil. The resultant increase in L_1 increases the period of oscillation ($2\pi\sqrt{L_1C_1(1-k^2)}$), and also diminishes the damping factor μ. For both reasons

the pulsations are rendered more prominent. Fig. 15 (*a*) (Pl. XXV.) shows a typical current oscillogram.

The second approximation for V_2 will be given by $V_2=a+b/i$, where the expression (19) is substituted for i. Fig. 15 (*b*) (Pl. XXV.) is the potential oscillogram of the same discharge as (*a*). It is clearly shown that the potential pulsations are not sinusoidal, but represent precisely what is obtained from the above relation between V_2 and i. The maxima are more sharply pointed than the minima, and rise to a greater distance above the aperiodic potential component than the minima fall below it. It may be observed that the first minimum of the current in (*a*) approaches closely to the extinguishing current for the gap. This corresponds to the first maximum of the potential in (*b*), which almost reaches the terminal potential.

Fig. 15 (*c*) (Pl. XXV.) is a photograph of a similar discharge in the rotating mirror, illustrating how the pulsations in current produce pulsations in intensity of the glow.

An interesting feature is illustrated in the potential oscillogram of fig. 16 (Pl. XXV.), ($l=4$ mm., $i_0=5$ amps.). In this case the first few maxima of the current have been sufficiently high to cause the true arc to flow, the potential dropping to the lower value. Since, however, the current must fall to a low value between the maxima, the arc must change to a glow. In fig. 16 (Pl. XXV.) two oscillations have taken place showing this transition. These are followed by two and a half oscillations of unstable arc, during which the fall in current has not been sufficient to produce the change. Thereafter a sudden change to a continuous glow takes place.

Second Approximation to the Aperiodic Current.

From the form of equation (19) it may be observed that the aperiodic current flowing in the inductance component, viz.,

$$i=-\frac{a}{R_2}+\left(\frac{Mi_0}{L_2}+\frac{a}{R_2}\right)e^{-\frac{R_2}{L_2}t},$$

is precisely what would have been obtained from consideration of the secondary circuit alone if, by some means, a current of amount Mi_0/L_2 is set flowing initially

and is then left to itself. In other words, the presence of the primary circuit produces a negligible effect on this component once the current is started. The pulsations are, of course, due entirely to the current oscillations in the primary circuit.

If it is assumed that the primary circuit produces no effect, and also that the secondary capacity is too small to produce an appreciable difference between i_2 and i, there is no necessity to neglect the term b/i in the value of V_2. The circuit equations are simply

$$L_2 \frac{di}{dt} + R_2 i + V_2 = 0 ;$$

$$V_2 = a + \frac{b}{i} .$$

The solution for i is, since $a^2/4R_2 > b$,

$$[(i+\alpha)^2 - \beta^2]^{\frac{1}{2}} \left[\frac{i+\alpha+\beta}{i+\alpha-\beta}\right]^{\frac{\alpha}{2\beta}} = Fe^{-\frac{R_2}{L_2}t},$$

where $\alpha = a/2R_2$, $\beta^2 = \alpha^2 - b/R_2$, and F may be found if the initial current is known.

The current cannot be found from this equation as an explicit function of t, but the relationship gives a good agreement with experiment. It shows the effect on the current of the increase in V_2 at small currents. The values of i for given values of t calculated from the above equation are indicated in fig. 14 by crosses.

6. Variation of the Discharge as the Primary Current is increased from the Minimum.

The type of discharge considered so far is only obtained with a primary current considerably in excess of the minimum. With intermediate values the discharge takes several forms, which are described below. Observations were taken both with the coil alone and with condensers connected across the secondary in parallel with the spark-gap. It was found that the various types of discharge observed in the case of the coil alone could always be reproduced for the case of the condensed discharge by suitable increase of the primary current. In other words, more energy had to be supplied to the coil to provide for the greater dissipation of energy in the sparks. Since

the frequencies of oscillation of the coil-circuits are diminished by addition of a condenser, photographs are more easily obtained. For this reason the earlier stages of the discharge are best illustrated by the condensed discharge.

The types of discharge may be classified as under, the succeeding types corresponding to increasing primary current :—

(a) *Single Spark.*—When the primary current is just sufficient to produce a discharge, the variation of potential is of the form shown in fig. 17 (*a*) (Pl. XXVI.). The potential rises to the maximum, which in this case coincides with the sparking potential of the gap. The spot becomes visible again after the passage of the spark, either at the zero line or at the height usually associated with the glow discharge, and then performs oscillations governed by the coil constants. These oscillations are produced by the current which is still flowing in the secondary. On the occasions when the spot rises from the glow-value, which become more frequent if the primary current is slightly increased above the absolute minimum, a very brief curve appears just at the point at which it commences to rise. This could only be observed when the time-sweep was made very fast. It suggests that a glow sets in for a very short time after the spark. It should be mentioned that in some cases, particularly with large capacities, that the spot rose from the arc-potential, suggesting in this case the formation of a brief arc.

When the electrodes of the gap are carefully cleaned, the potential at which the first spark commences does not coincide with the first maximum of the coil-oscillation, but takes place a little later, when the potential has fallen a little below the maximum. This, of course, is the well-known effect of sparking time-lag. After a few discharges have passed this effect disappears.

The variation of the potential across the gap with current during an oscillatory capacity discharge has been investigated by Prof. Milner [5] and J. Thomson [6]. These writers have shown that after the initial breakdown of the gap the discharge takes the form of an alternating arc, each half-oscillation of the current in the spark-circuit producing a little arc, the discharge being extinguished as the current passes through zero. This was

verified in the present case by lowering the frequency of oscillation by inclusion of an inductance in series with the gap in the condenser-gap circuit. Fig. 17 (*b*) (Pl. XXVI.) is a typical potential-time oscillogram for a single "spark," which, however, only shows the traces of the potential minima of the little arcs, the minima rising as the current amplitude diminishes. This result, and the shape of the arc-curves, which appeared on the screen convex to the time-axis, are what one would expect from a negative arc characteristic. The potential variation across the condenser (or the coil) corresponding to this discharge was approximately of decaying sinusoidal form, the cessation of the discharge occurring at a potential peak.

(b) *Multiple Spark.*—As the primary current is increased slowly, the amplitude of the coil oscillations succeeding the spark increases, the sparking potential remaining constant. Ultimately a second spark occurs at the peak immediately following the spark. This usually occurs at a slightly lower potential than that of the initial spark, because of the effect produced by the latter on the electrode surfaces and on the gas between the electrodes. Further increase in primary current merely produces a succession of sparks, an example of such a multiple-spark discharge being shown in fig. 18 (*a*) (Pl. XXVI.). The time-interval between two successive sparks is not constant, but increases gradually. The explanation of this lies in the fact that the time-interval depends on the rate of rise of the potential from zero, or near zero, to the sparking potential, and this is governed by the slow oscillation of the coil. Each of the lines seen in fig. 18 (*a*) (Pl. XXVI.) is really part of a sine-curve, but, since each spark removes some of the energy in the coil, the amplitude of this sine-curve diminishes. It follows that the sparks succeed each other more rapidly and more frequently as the secondary capacity, or the gap-length, is reduced. When there is a large number of sparks the increasing time-interval between them permits the gap conditions to approximate more closely to the conditions pertaining to the initial spark. Consequently the sparking potential tends to increase towards the end of the discharge, and the last spark may be as bright as the initial spark.

With the inductance mentioned above in the spark-circuit each separate spark contained only one complete

oscillation of current or potential, so that one positive and one negative arc was formed for each. The resulting oscillogram is shown in fig. 18 (*b*) (Pl. XXVI.).

In the case of the condensed discharge this multiple-sparking stage covers a wide range of primary current (and for this reason is usually described as the typical induction coil condensed discharge), but with no condenser the discharge passes quickly into phase (*c*).

Generally the value of the primary current at which the discharge leaves this stage increases with the gap-length. The behaviour, however, of very small gaps is exceptional. With zinc electrodes this multiple-sparking stage covered a very wide range of primary current when the gap-length was less than ·5 mm., even with no condenser across the gap. At first the oscillogram was similar to fig. 18 (*a*) (Pl. XXVI.), but an increase in primary current produced a long series of separate discharges occurring at a very high frequency, instead of passing into the phases (*c*) and (*d*), as normally occurs. The smallness of the gap seems to militate against the formation of a continuous glow. With a condenser across a small gap this prolonged multiple-sparking phase gives a potential variation like fig. 19 (Pl. XXVII.) (C_2=·0016 μF, i_0=7 amps., l=·2 mm.). The potential minima (at extinction of the sparks) trace two distinct lines, which slope downwards with time. These heavier traces are due to little curves, convex to the zero line, preceding each potential rise, and no doubt indicate the formation of brief arcs and glows. The slope downward suggests an increasing current through these low potential discharges. It is probable that what is observed here is the formation of arcs and glows *during* the spark oscillations. The current would then be proportional to the sparking potential, which is seen to increase with time. If this interpretation of the oscillogram is correct, it suggests that the effective resistance of very small gaps is sufficiently large to render the oscillations slow enough to be observed. This anomalous behaviour was not found to the same extent with small gaps between copper and iron electrodes, but was evident even up to a gap of 2 mm., in the case of aluminium.

(c) *Spark-glow or Spark-arc Groups.*—A further increase in primary current produces the form of discharge corresponding to fig. 20 (Pl. XXVI.), which was for an

uncondensed discharge across a 2 mm. gap, $i_0 = 2{\cdot}3$ amps.* When the current flowing into the secondary capacity, immediately after the initial spark has passed, is great enough to sustain the glow discharge, the glow is formed,

Fig. 21.

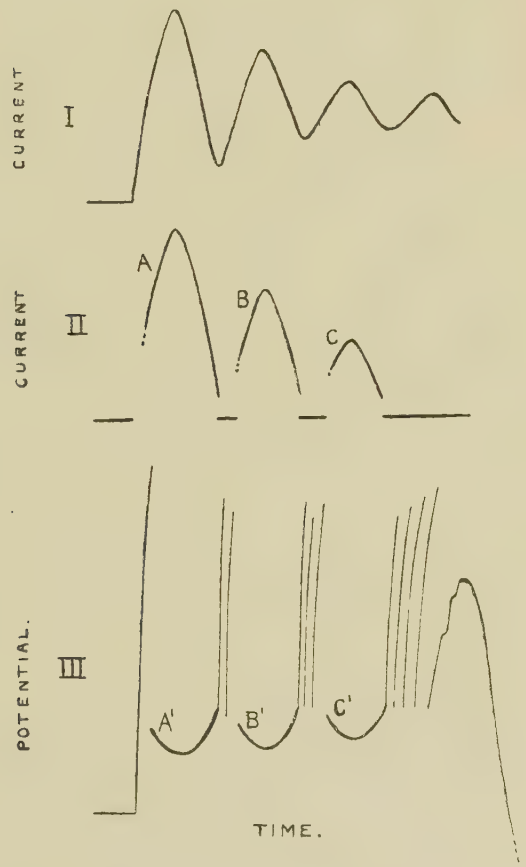

and lasts as long as the current exceeds the minimum corresponding to the gap-length. For purposes of comparison, and to make the details more clear, the oscillograms of fig. 20 (*a*) and (*b*) (Pl. XXVI.) are sketched in fig. 21

* Figs. 20, 22, 23, and 24 were taken with the iron-cored inductance mentioned in § 5 in series with the primary of the coil. This facilitated the study of the effect of the pulsations.

(curves II. and III.), in which, also, the current oscillogram for the gap shorted is inserted (I.). Corresponding to the current pulsation A in II. there appears a short glow represented by a potential curve A′ in III. The glow commences at a current greater than the minimum, so that the little curve A′ is not symmetrical, but is obtained from A by applying the relation $V=a+b/i$. When the current reaches the minimum for the gap, the discharge ceases, and the secondary current now serves only to raise the potential of the secondary capacity. The sparking potential is again reached, and several sparks take place, until the current has again attained a value necessary for the maintenance of the glow. The glow represented by B and B′ is then formed. This process is repeated until, on the cessation of one of the sparks, the potential fails to reach sparking potential, and the whole discharge then ceases. There is a succession of spark-glow groups, the periodicity being that of the pulsations. Fig. 20 (*c*) (Pl. XXVI.) is a photograph of this type of discharge with the above gap, but a primary current of 2·7 amps. Four spark-glow groups are produced, the glows being represented principally by the traces of cathode glow.

Precisely the same phenomena are found with a condenser across the gap, only here the sparks are much more intense and form the most conspicuous feature of the discharge. Frequently the low-potential discharge between the spark-groups in this case takes the form of the arc, particularly if the capacity be large. Fig. 22 (*a*) and (*b*) (Pl. XXVII.) are the current and potential oscillograms of a discharge when a leyden jar (·00087 μF) was connected across the gap ($l=1$ mm., $i_0=6$ amps.) They each indicate six spark-arc groups. The potential sensitivity of the oscillograph was made small in this case in an attempt to reproduce the rising potential between the sparks. As a result, the arcing potential practically coincides with zero. Fig. 22 (*c*) (Pl. XXVII.) is a photograph of such a discharge showing some of the groups of sparks. The arc is relatively faint and does not reproduce well, but in this case the third pulsation has taken the form of a glow, as shown by the bright cathode glow.

This grouping of sparks in the condensed discharge has already been observed and described by Prof. Taylor Jones,

although the low-potential discharge between the groups has not been noticed. Prof. Taylor Jones found that for a given primary current the number of sparks in a group increases as the gap-length or capacity is diminished. A simple explanation of this now offers itself. The time during which the current is below that suitable for a glow is controlled mainly by the period of the pulsations, which is independent of the above variables. As the gap-length, or capacity, is diminished, less time is necessary for the sparking potential to be reached, and it can, therefore, be reached more often in the time available.

The number of spark-glow or spark-arc groups increases with primary current until the current minima rise above the glow minimum. The glow then becomes continuous, and the little potential curves *a*, *b*, *c* coalesce. A glance at fig. 15(*a*) (Pl. XXV.) shows that the earlier minima will be the last to attain the necessary value, and thus, by adjustment of the primary current, it is possible to obtain a few spark-glow or spark-arc groups followed by a continuous pulsating glow. Fig. 23 (Pl. XXVII.) illustrates a discharge where sparks have occurred only after the first pulsation, and fig. 24 (Pl. XXVII.) shows a condenser discharge in which three spark-arc groups are followed by a continuous glow, the whole discharge being terminated by a number of sparks:

(d) *Spark followed by Continuous Glow or Arc.*—When the primary current is still further increased the discharge now passes into the forms previously described in § 3 or § 5.

7. Review of Types of Discharge.

Table II. summarizes the types of discharge produced as the primary current is increased from the minimum. Two examples of actual cases are given, both with a gap 1 mm. long between 1 cm. zinc spheres, in one case with no condenser, and in the other with a leyden jar (·00087 μF) across the gap. The values of the primary current at which the changes in type take place are not accurately defined, owing to slight changes in gap conditions, so that only round figures are given.

The primary current necessary for any type of discharge increases rapidly with the length of the gap and with the secondary capacity. With a condenser made up of two

or three leyden jars in parallel and a gap of even 5 mm. it would require an excessive primary current to produce the later forms of the discharge described above.

TABLE II

Description of discharge.	Primary currents (amps.). Without condenser.	Primary currents (amps.). With condenser.	Type of potential oscillogram.
Single spark	·40	·69	Fig. 17 (*a*) (Pl. XXVI.).
Multiple spark	·5–·9	·7–2·5	Fig. 18 (*a*) (Pl, XXVI.).
One spark-glow group followed by sparks.	·9	2·5	—
Spark-glow groups or spark-arc groups (condenser).	·9–2·5	2·5–4	Figs. 20 (*b*), 22 (*b*) (Pls. XXVI. & XXVII.).
Spark-glow groups or spark-arc groups followed by continuous glow.	2·5–3	4–6	Fig. 24 (Pl. XXVII.).
Spark followed by continuous glow and usually terminated by several sparks.	3 to about 6	Above 6	Figs. 3, 15 (*b*) (Pls. XXIV. & XXV.).
True arc appeared for short time after initial spark, but passed into glow.	Above 6	Above 6	Figs. 7, 16 (Pl. XXIV. & XXV.).

In conclusion, the writer wishes to express his gratitude to Prof. Taylor Jones for his helpful advice and criticism throughout the work.

References.

(1) E. Taylor Jones, 'Induction Coil Theory and Applications' (1932), ch. v.
(2) G. I. Finch and R. W. Sutton, Proc. Phys. Soc. xlv. pt. 2, p. 288 (1933).
(3) J. Meiklejohn, Phil. Mag. xv. p. 146 (1933).
(4) V. L. Chrisler, Astrophysical Journ. liv. p. 273 (1921).
(5) S. R. Milner, Phil. Mag. ser. 6, xxiv. p. 709 (1912).
(6) J. Thomson, Phil. Mag. xv. p. 682 (1933).

May 1933.

LXXVI. *Turbulent Flow through Fine Eccentric Clearances.*

By R. J. Cornish, *M.Sc.**

List of Symbols.

r_1=radius of outer cylinder.

r_2=radius of inner cylinder.

$a=r_1-r_2$.

m=hydraulic mean depth of annulus=$\frac{1}{2}a$.

e=eccentricity.

$\frac{dp}{dz}$=pressure gradient parallel to the axis.

Q=total quantity per second.

A=area of annulus.

S=mean velocity of flow parallel to the axis.

Q_c=quantity passed through concentric annulus.

Q_e=quantity passed through eccentric annulus under corresponding conditions.

ρ=density of fluid.

μ=absolute viscosity of fluid.

ν=kinematic viscosity of fluid.

(1) *Introduction.*

THE type of annular clearance to be considered is that formed by a cylindrical core inside a hollow cylinder, the axes of the two cylinders being parallel and the difference of their radii being small compared with the radii themselves.

Fig. 1 illustrates a section through such an annulus, the difference in radii being exaggerated for clearness. It is evident that under suitable conditions the flow through the annulus may be either laminar or turbulent, but there must also be an intermediate condition when the flow is laminar in the narrower portions and turbulent in the wider portions.

* Communicated by Prof. A. H. Gibson, D.Sc., M.Inst.C.E., M.I.Mech.E.

(2) *General Formula.*

A general formula will first be deduced connecting the pressure gradient and the Reynolds number.

In fig. 1, A, B are the centres of the two circles, O is the mid-point of AB. OFE, OF′E′ are lines making angles of θ, $\theta+d\theta$ with AB. The radii of the larger and smaller circles are r_1, r_2 respectively and the eccentricity $=AB=e$.

Fig. 1.

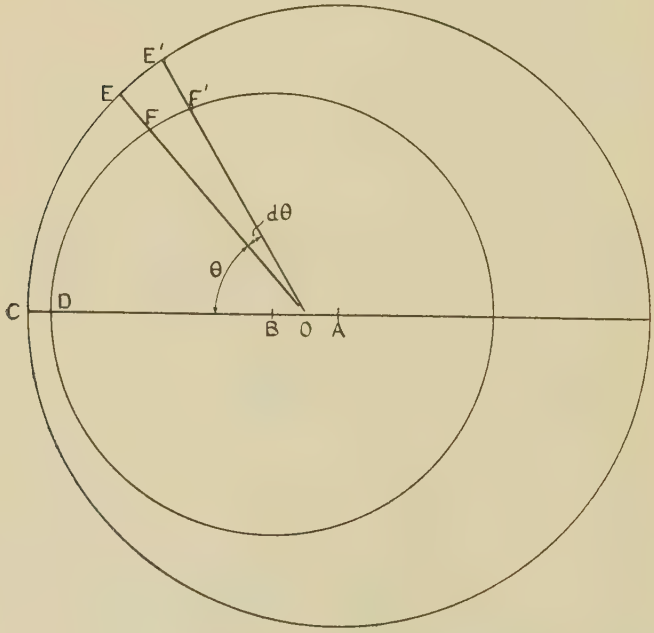

The hydraulic mean depth of the annulus

$$=m=\frac{\pi(r_1^2-r_2^2)}{2\pi(r_1-r_2)}=\frac{r_1-r_2}{2}=\frac{a}{2}$$

and is independent of the eccentricity. It can easily be shown that, with fine clearances, $EF=2m(1-\frac{e}{a}\cos\theta)$, and the area of the part CDFE of the annulus

$$=A_\theta=m(r_1+r_2)\,(\theta-\frac{e}{a}\sin\theta).$$

The flow through the portion EE′F′F is approximately the same as that between two parallel plates whose distance apart is EF. The hydraulic mean depth of this portion is denoted by m_θ and the area by dA.

Then

$$m_\theta = \tfrac{1}{2}\text{EF} = m\left(1 - \frac{e}{a}\cos\theta\right),$$

and

$$\begin{aligned} d\text{A} &= \frac{d}{d\theta}(\text{A}_\theta).d\theta \\ &= m(r_1+r_2)\left(1-\frac{e}{a}\cos\theta\right)d\theta \\ &= (r_1+r_2)m_\theta d\theta. \end{aligned}$$

The formula for the flow in this portion may be written

$$\frac{m_\theta \text{S}_\theta}{\nu} = \phi\left(\frac{m_\theta^3}{\rho\nu^2}\cdot\frac{dp}{dz}\right), \quad . \quad . \quad . \quad . \quad (1)$$

this form being adopted because S_θ occurs on only one side of the equation. The quantity passing through EE′F′F will then be given by

$$\begin{aligned} d\text{Q} &= \text{S}_\theta.d\text{A}, \\ &= \frac{\nu}{m_\theta}\cdot\phi\left(\frac{m_\theta^3}{\rho\nu^2}\cdot\frac{dp}{dz}\right)\cdot(r_1+r_2)m_\theta d\theta, \\ &= \nu(r_1+r_2).\phi\left(\frac{m_\theta^3}{\rho\nu^2}\cdot\frac{dp}{dz}\right).d\theta. \end{aligned}$$

In the whole annulus

$$\begin{aligned} \frac{m\text{S}}{\nu} &= \frac{\text{A}}{2\pi(r_1+r_2)}\cdot\frac{\text{Q}}{\text{A}}\cdot\frac{1}{\nu} \\ &= \frac{1}{2\pi}\int_0^{2\pi}\phi\left(\frac{m_\theta^3}{\rho\nu^2}\cdot\frac{dp}{dz}\right).d\theta \\ &= \frac{1}{\pi}\int_0^{\pi}\phi\left\{\frac{m^3}{\rho\nu^2}\cdot\frac{dp}{dz}\cdot\left(1-\frac{e}{a}\cos\theta\right)^3\right\}.d\theta. \quad . \quad (2) \end{aligned}$$

The three conditions of flow mentioned in Section (1) will now be considered.

(3) *Laminar Flow.*

Laminar flow through pipes with eccentric cores has been dealt with by Caldwell * and Piercy, Hooper and Winny † ; these authors investigated the case when the clearance is not small compared with the radius. The equations for laminar flow to be derived below are the simple ones for fine eccentric clearances ; they are included for the sake of completeness.

Fig. 2.

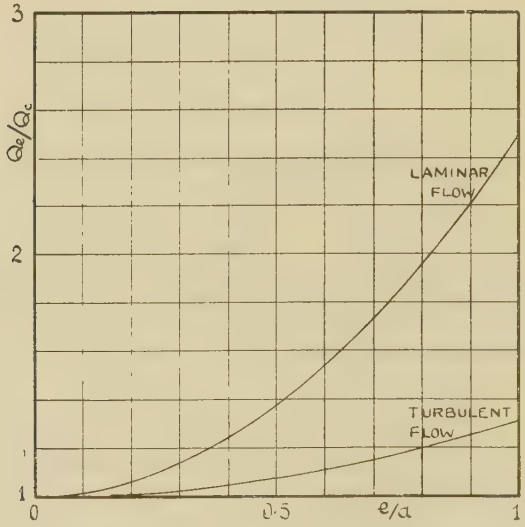

Under stream-line flow conditions equation (1) becomes

$$\frac{m_\theta S_\theta}{\nu} = \frac{1}{3} \cdot \frac{m_\theta^3}{\rho \nu^2} \cdot \frac{dp}{dz},$$

and therefore, from (2),

$$\frac{mS}{\nu} = \frac{m^3}{3\pi\rho\nu^2} \cdot \frac{dp}{dz} \cdot \int_0^\pi \left(1 - \frac{e}{a}\cos\theta\right)^3 . d\theta$$

$$= \frac{m}{3\rho\nu^2} \cdot \frac{dp}{dz}\left(1 + \frac{3e^2}{2a^2}\right).$$

* 'Journal of the Royal Technical College, Glasgow,' vol. ii. p. 203 (1930).

† Phil. Mag. vol. xv. p. 647 (1933).

Then, since m is independent of the eccentricity,

$$\frac{Q_e}{Q_c} = 1 + \frac{3e^2}{2a^2}.$$

This relationship is plotted in fig. 2.

(4) *Turbulent Flow.*

The equation for turbulent flow through a fine concentric clearance or between parallel plates depends on the nature of the surfaces. The evidence of many experimenters * leads to the conclusion that, for smooth surfaces, it is of the form

$$\frac{m^3}{\rho\nu^2} \cdot \frac{dp}{dz} = k\left(\frac{mS}{\nu}\right)^{7/4} \quad . \quad . \quad . \quad . \quad . \quad . \quad (3)$$

Equation (2) then becomes

$$\frac{mS}{\nu} = \frac{1}{\pi}\left(\frac{m^3}{k\rho\nu^2} \cdot \frac{dp}{dz}\right)^{4/7} \cdot \int_0^{\pi}\left(1 - \frac{e}{a}\cos\theta\right)^{12/7} . d\theta.$$

TABLE I.

$\frac{e}{a}$	0·1	0·2	0·3	0·4	0·5	0·6	0·7	0·8	0·9	1·0
$\frac{Q_e}{Q_c}$	1·003	1·012	1·028	1·049	1·077	1·111	1·152	1·196	1·254	1·315

Hence

$$\frac{Q_e}{Q_c} = \frac{1}{\pi}\int_0^{\pi}\left(1 - \frac{e}{a}\cos\theta\right)^{12/7} . d\theta.$$

This integral can be solved only for definite values of $\frac{e}{a}$ from 0 to 1. The expression has been plotted in fig. 2, and Table I. gives the solution for a number of values of $\frac{e}{a}$.

It is important to use the correct value of the index of $\frac{mS}{\nu}$ in equation (3). If the resistance is assumed

* See, for example, Davies & White, 'Engineering,' vol. cxxviii. p. 71 (1929); Suzuki, Journ. Fac. Eng., Imp. Univ. Tokyo, vol. xviii. p. 88 (1929); Winkel, *Z. ang. math.* vol. iii. p. 251 (1923).

to be proportional to the square of the velocity, the calculated increase in quantity for full eccentricity is only

Fig. 3.

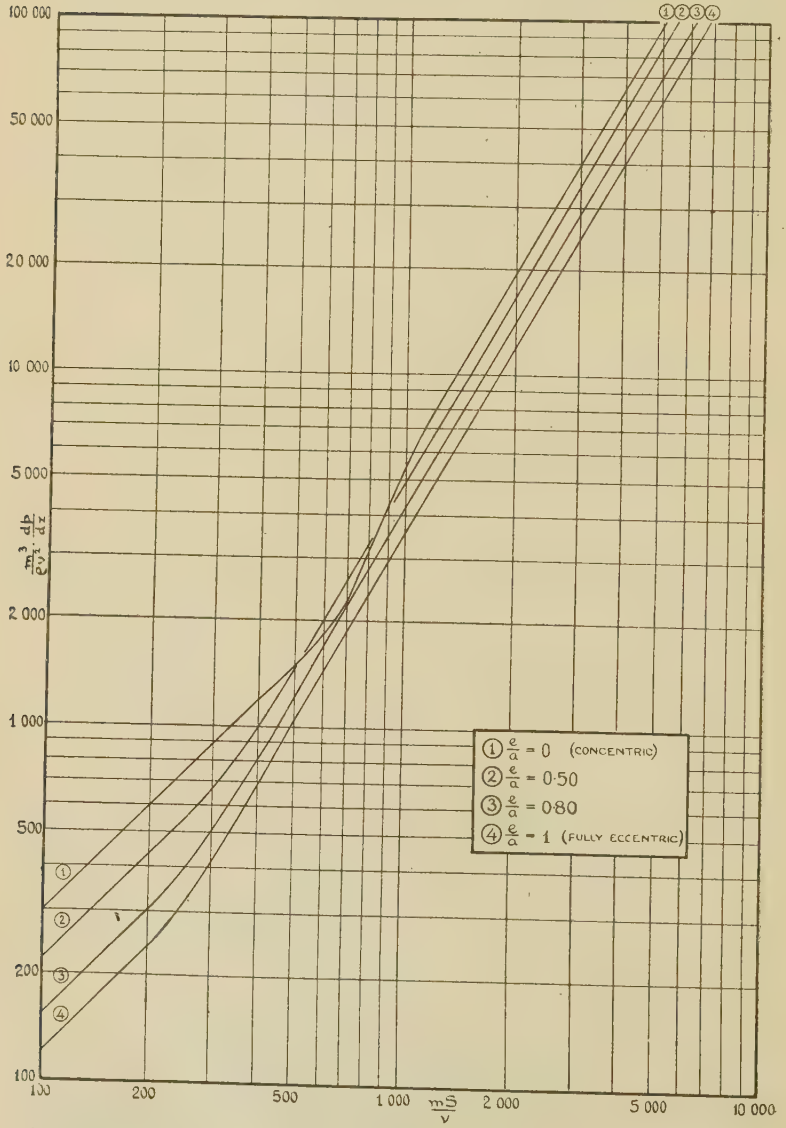

20 per cent., as compared with 31·5 per cent. when the index is taken as 7/4.

(5) *Intermediate Section.*

It is necessary to deal with the case where the flow is partly laminar and partly turbulent by graphical integration, since there is no general equation from which to work. Curve (1), fig. 3, shows the relationship between $\frac{m^3}{\rho\nu^2} \cdot \frac{dp}{dz}$ and $\frac{m\mathrm{S}}{\nu}$ for fine concentric clearances; the actual curve is based on the author's experiments, but the form is common to many investigators. This curve was used for graphical integration, as illustrated in the following example :—

Let it be required to find the value of $\frac{m\mathrm{S}}{\nu}$ corresponding to $\frac{m^3}{\rho\nu^2} \cdot \frac{dp}{dz} = 1000$, when $\frac{e}{a} = 0{\cdot}80$.

The annulus is considered to be divided into sectors subtending equal angles (say 10°) at O (fig. 1), and the value of $(1 - 0{\cdot}80 \cos\theta)^3$ at the centre of each sector is found (*i. e.*, for $\theta = 5°$, 15°, 25°, etc.). These values are each multiplied by 1000, giving in effect a number of values of $\frac{m_\theta^3}{\rho\nu^2} \cdot \frac{dp}{dz}$, and the corresponding values of $m_\theta \mathrm{S}_\theta/\nu$ are read off from curve (1), fig. 3. The average of these values gives the required value of $\frac{m\mathrm{S}}{\nu}$.

In fig. 3 the methods of sections (3), (4) and (5) have been used to draw the curves for $\frac{e}{a} = 0{\cdot}50$, 0·80, and 1·00.

(6) *Experimental Apparatus.*

The author's apparatus has already been described and illustrated in another paper *. It consisted essentially of a brass cylinder of radius 10 cm. and length 28 cm., which was supported inside a hollow cylinder whose radius exceeded that of the core by about 0·0466 cm. Pressures could be measured in the chambers at each end of the clearance (points A and H) and at six equally

* Proc. Roy. Soc. A, vol. cxl. p. 228, fig. 1 (1933).

spaced points (B, C, D, E, F, G) within the clearance, which was thus divided into seven 4 cm. lengths. The

Fig. 4.

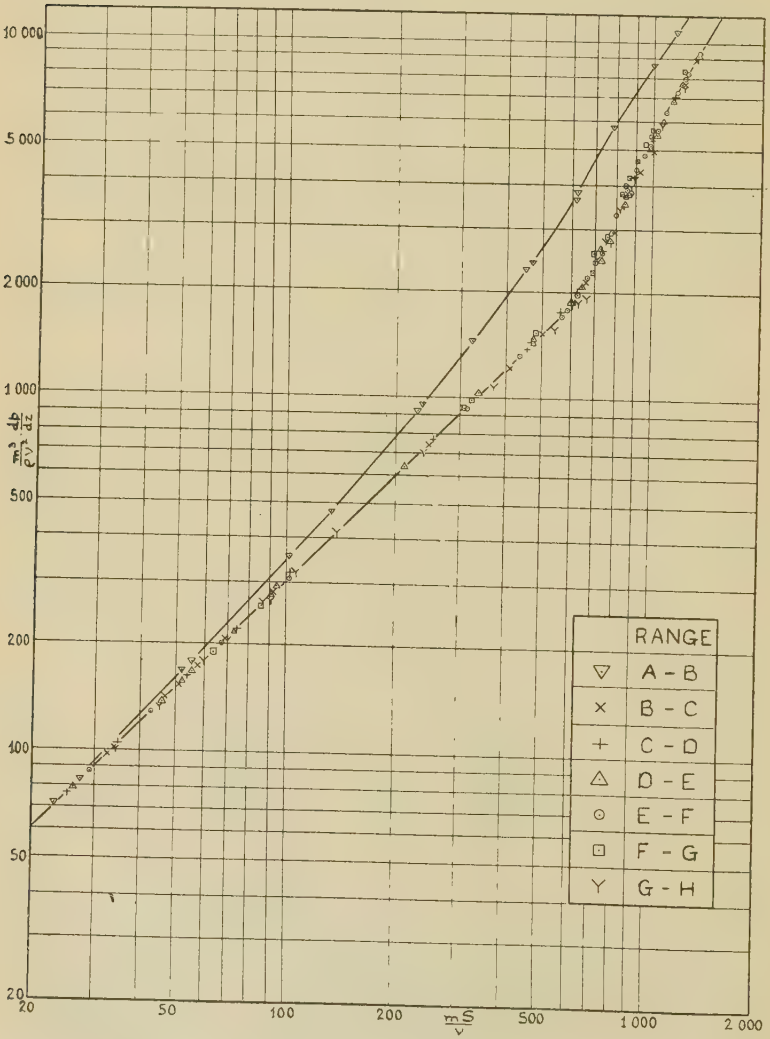

Concentric position.

methods of measuring pressures, temperatures, and quantities were similar to those described in the above-mentioned paper.

(7) *Experiments with Core Concentric.*

The results of these experiments have been plotted in fig. 4, though, owing to the large number of readings taken, it has been necessary to omit many points which almost coincide with others.

The water pressure available limited the maximum value of $\frac{mS}{\nu}$ to about 1300, even with water at 20° C. (water at this temperature was only available under

TABLE II.

Range.	$\frac{mS}{\nu}$.	$\frac{m^3}{\rho\nu^2} \cdot \frac{dp}{dz}$.	k.
D–E	1131	6790	0·0308
E–F	1161	7220	0·0312
C–D	1164	7260	0·0313
E–F	1197	7580	0·0311
D–E	1198	7650	0·0314
E–F	1207	7830	0·0316
E–F	1214	7830	0·0314
E–F	1223	7910	0·0314
E–F	1229	7980	0·0312
E–F	1240	8140	0·0315
C–D	1318	9080	0·0315
D–E	1324	9190	0·0315
E–F	1329	9310	0·0318
E–F	1337	9370	0·0317

exceptional circumstances, and most of the experiments were made at temperatures of from 9° C. to 12° C.); it was therefore necessary to extrapolate the curve into the turbulent flow region to obtain curve (1) of fig. 3. The value of k in equation (3), Section (4) was calculated for all experiments with $\frac{mS}{\nu}$ greater than 1100, and the results are tabulated in Table II. In all subsequent calculations k was taken as 0·0316, the average of the last four values in that table.

The experiments of Davies & White *, Suzuki †, and Winkel †, lead to values of k of respectively 0·0288, 0·0283, and 0·0274. The rather higher value obtained by the author is probably due to the surfaces in his apparatus having been less finely ground.

(8) *Experiments with Core Eccentric.*

The author's experiments were confined to the case of full eccentricity, as the difficulties of setting up in an intermediate position and measuring the eccentricity accurately with such a fine clearance could not be overcome.

Schneckenburg ‡ found that the pressure distribution over a cross-section was not uniform in the case of eccentric annuli, and to test this result the author made experiments with three positions of the line of contact relative to the line of gauge-holes. Positions α, β, and γ correspond to angles of 180°, 90°, and 45° subtended at the central axis by the two lines. The results are plotted in figs. 5, 6, and 7, which show that, provided the gauge-holes are far enough from the entrance and exit, the pressure distribution is sensibly uniform ; this indicates that Schneckenburg's gauge-holes were too near the ends of the annulus. His results were also affected by the fact that his annulus was formed by the space between two cones of very small angle, which were used to give a ready means of varying the clearance. Unfortunately this seems to have introduced complications due to the steadying effect of convergent boundaries, as his " concentric " curve in the neighbourhood of the critical velocity disagrees with those of all other experimenters.

The long " steadying length " required with eccentric annuli is easily explained. In the chambers outside each end of the clearance the water is at a uniform pressure, but inside the clearance S_θ varies from a minimum to a maximum as m_θ varies. The shock losses must therefore also vary, so there cannot be a uniform pressure distribution just inside the ends of the annulus. The tendency is for an excess of water to enter where m_θ is small, and this excess is redistributed by cross-flows until the pressure becomes uniform over a cross-section.

* Proc. Roy. Soc. A, vol. cxix. p. 95 (1928).
† For references see Section (4).
‡ *Z. ang. math.* vol. xi. p. 27 (1931).

(9) *Comparison of Results with Theoretical Investigation.*

Some rough experiments showed the great importance of ensuring that the line of contact should be parallel

Fig. 5.

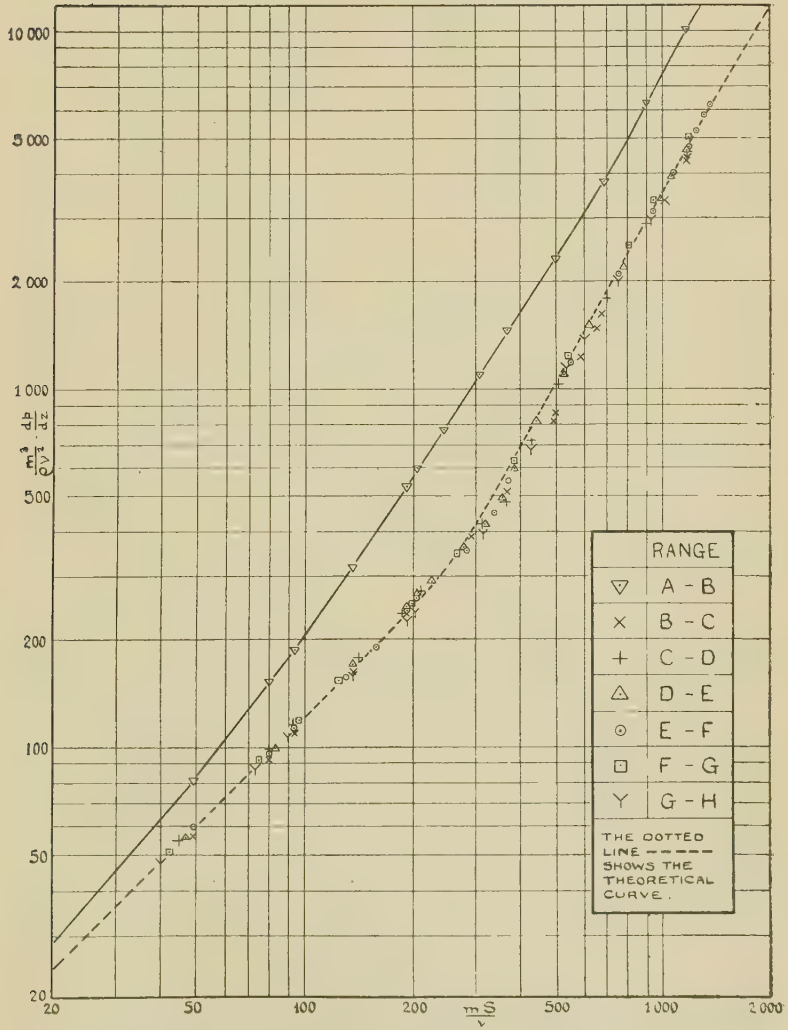

Eccentric position α.

with the axis. The readings of eccentric position α were therefore taken as standard, as a slight error in

Fig. 6.

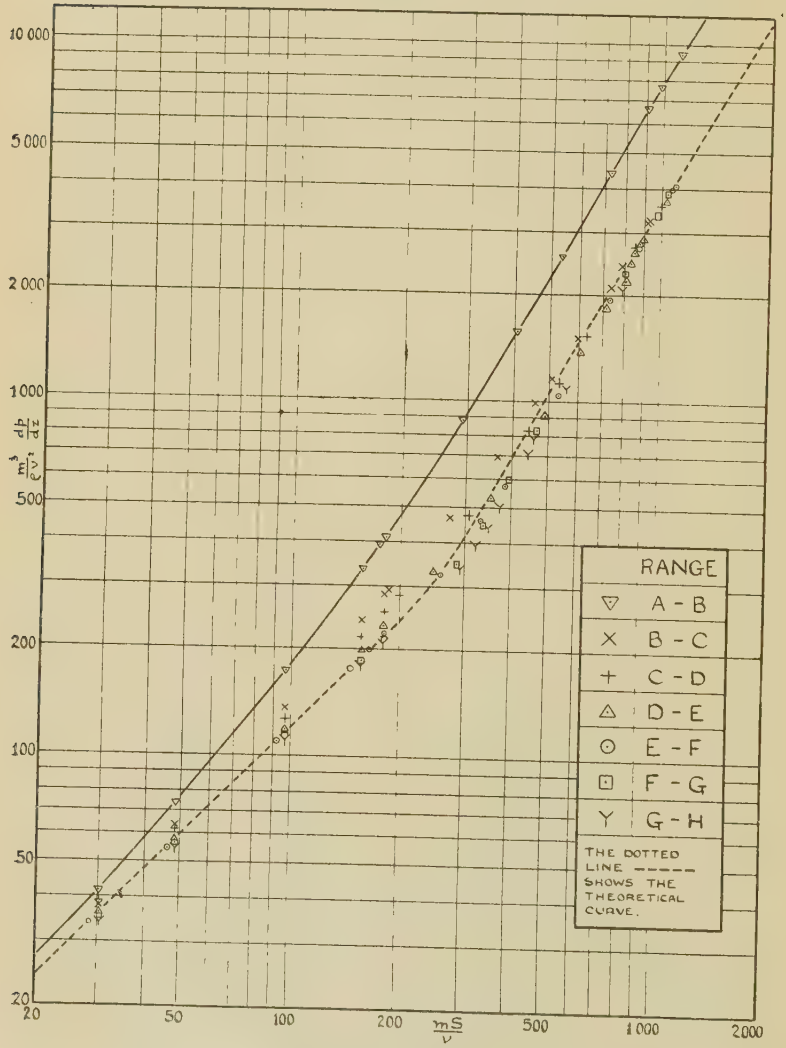

Eccentric position β.

parallelism of the line of contact with the axis seemed likely to have less effect than in any other position.

Actually the apparatus was set up in this position on three separate occasions, with good agreement between

Fig. 7.

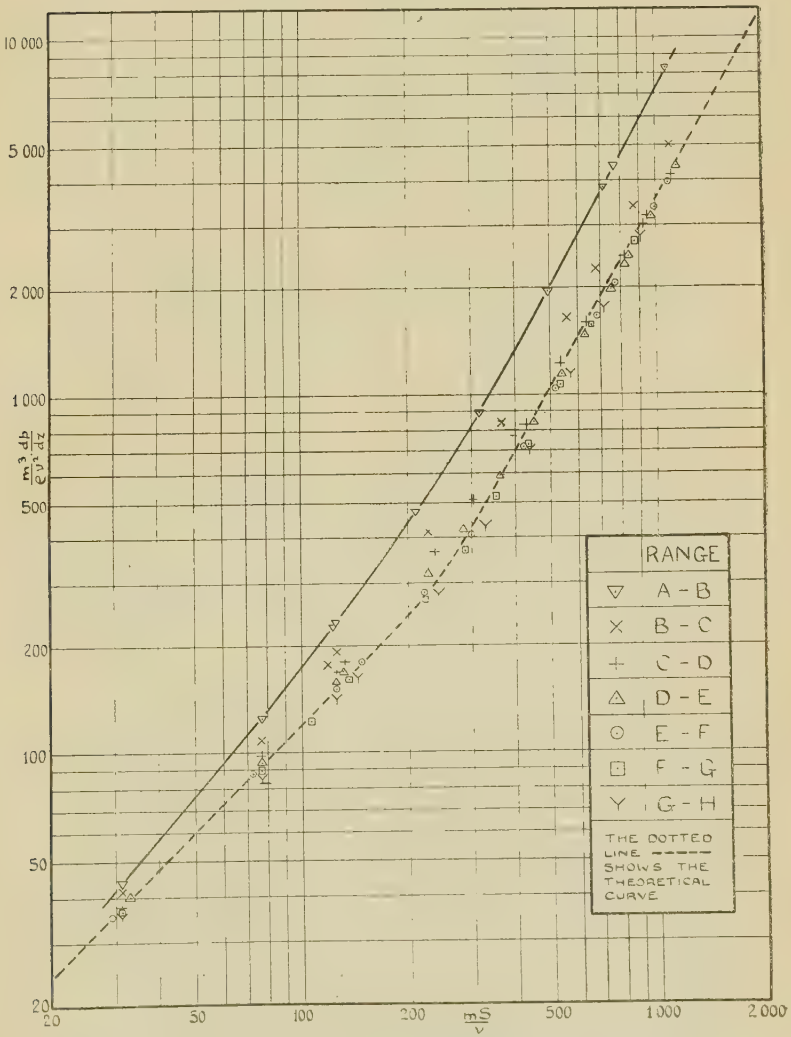

Eccentric position γ.

the results. A useful check on the different settings of the apparatus was obtained by the agreement between

the A–H readings ; the corresponding curve was independent of the relative position of the gauge-holes, but was sensitive to inaccuracies in the setting.

In figs. 5, 6, and 7 curve (4) of fig. 3 is shown dotted. It will be seen that good agreement with the results over the middle gauge ranges is obtained, except in the region of the critical velocity, where the experimental curve is lower than the theoretical. This leads to the deduction that the portions of the annulus where the flow is laminar have a steadying effect on the neighbouring portions, whereas the reverse might have been expected.

(10) *Caldwell's Experiments with Eccentric Annuli.*

Caldwell * carried out his experiments with a core of diameter 0·625 inches in a pipe of diameter 0·740 inches, and in his paper he gives experimental curves with eccentricity ratios $\left(\frac{e}{a}\right)$ of 0, 0·53, 0·80 †, and 1·00. From Caldwell's "concentric" curve the corresponding "eccentric" curves were calculated by the methods of Sections (3), (4), and (5), and in fig. 8 the calculated curves are compared with the experimental ones. It will be seen that, even with such a large clearance, the agreement is very close except in the neighbourhood of the critical velocity.

(11) *Note on the Hydraulic Mean Depth.*

As pointed out by Caldwell, experiments on the resistance to turbulent flow with pipes of such diverse cross-sections as the circle, the ellipse, the rectangle, and the equilateral triangle have all been coordinated to approximately a single curve by using the hydraulic mean depth as the "characteristic length" in the Reynolds number. This coordination breaks down with eccentric annuli, and he suggests that the reason may possibly be that

* Journ. Roy. Tech. Coll. Glasgow, vol. ii. p. 203 (1930).

† The eccentricity ratio given here as 0·80 is given by Caldwell as 0·87. The value 0·80 was obtained by comparing the laminar flow portion of his curve with the theoretical equation, which was satisfied by the curves for the other two eccentricities, and therefore taken as correct.

the latter sections present only one axis of symmetry. The explanation appears to lie, however, in the difference in depth at different parts of the annulus. The following extreme case demonstrates this point :—

Fig. 8.

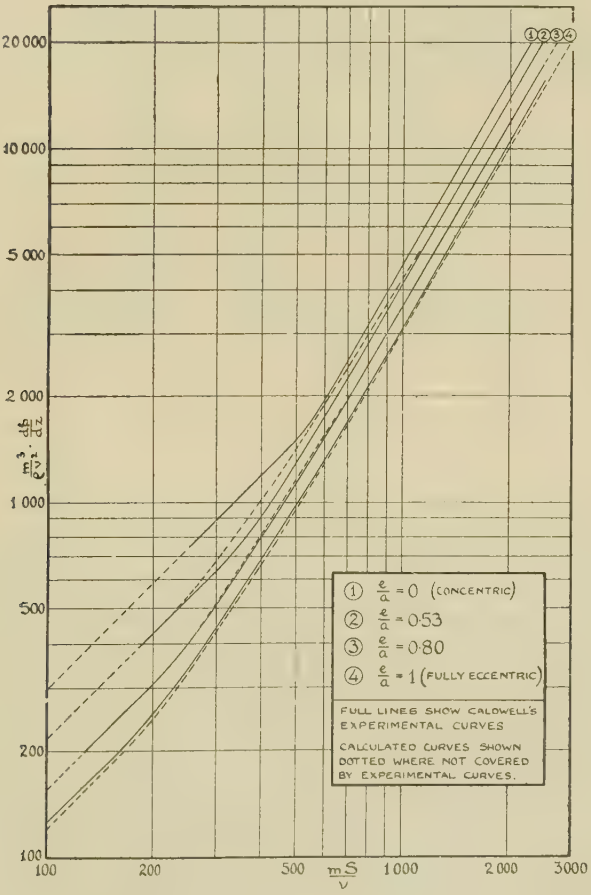

Consider the pipe whose cross-section is shown in fig. 9. The area of the triangular portion could be made negligible compared with that of the circular portion, while the length of the sides of the triangle might be

much greater than the circumference of the circle. The hydraulic mean depth would thus be much less than in the case of the circular portion alone, whereas the quantity flowing through the pipe for a given pressure gradient would evidently be very little affected by the addition of the triangular portion. By lengthening the straight sides one could make the Reynolds number as small as one pleased for any pressure gradient, and there could be no possible correlation of the resistance curves on a hydraulic mean depth basis.

Fig. 9.

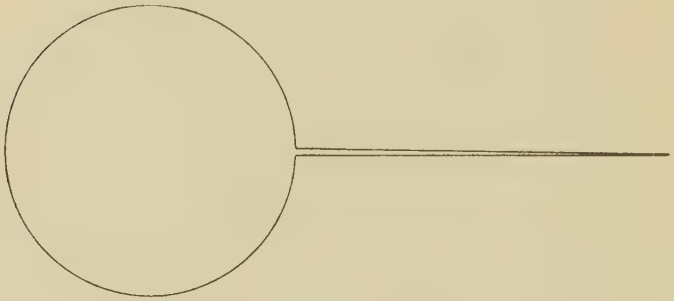

(12) *Summary.*

It is shown that the flow through a fine eccentric clearance may be laminar, turbulent, or laminar in the narrower portions and turbulent in the wider portions. A general formula is developed to cover all three cases, and the increased quantities corresponding to a range of values of the eccentricity ratio are calculated. It is proved that, with smooth boundaries, the maximum increase with turbulent flow is 31·5 per cent. The results of experiments by J. Caldwell and by the author are shown to agree closely with the predicted results. The paper concludes with a note on the use of the hydraulic mean depth in coordinating the resistance curves for turbulent flow through different forms of conduit.

· May 1933.

LXXVII. *A Critical Study of the Hardness Behaviour of Duralumin.*

By Hugh O'Neill, *M.Met.*, *D.Sc.*, J. F. B. Jackson, *B.Sc.*, *and* G. S. Farnham, *B.A.*, *M.Sc.**

[Plate XXVIII.]

Synopsis.

The peculiar hardening and softening changes which occur in heat-treated duralumin have been investigated by means of Meyer (ball-test) analysis. A true "precipitation" process has thus been made evident in certain heat-treatments of duralumin; but, in addition, this alloy is shown to be capable of a different type of behaviour. The hardening at temperatures between 15° C. and approximately 200° C. after quenching is of this latter type, which in some ways resembles a mild strain-hardening process. X-ray and cold-rolling tests have also been made, and the age-hardening process has been discussed.

Introduction.

OWING to geometrical dissimilarity of the indentations, the hardnesses of two different metallic specimens cannot always be properly compared by means of their Brinell ball-numbers. Testing by means of "Meyer analysis" is much more critical, and by making impressions (d) with a ball of diameter D, at different loads L, one can evaluate the required constants of the Meyer expression $L=a_D d^n$, where

n=work-hardening capacity or "*hardenability*";

a="unit hardness," or load to give $d=1$.

Then, $P_u=\frac{4a_D}{\pi}.D^{n-2}$="*ultimate ball-number.*"

If $D=1$, then $P_u=1{\cdot}273\ a_1$.

Hardness values in terms of a or P_u *are* strictly comparable, for they relate to ball impressions having always a constant angle of indentation. The term P_u

* Communicated by Prof. W. L. Bragg, F.R.S.

has the further advantage that it is independent of the grain-size of the specimen.

By having two hardness quantities—a and n—available in place of the usual Brinell number, it was hoped that more light would be thrown upon the duralumin problem. Furthermore, whilst a *high* n value indicates a possible high percentage increase of hardening on cold-working, it also represents a *low* "yield ratio" $\left(e.g. \frac{\text{yield point}}{\text{ultimate stress}}\right)$ and a *high* "extensibility" [1]. Consequently, the results obtained in the present paper may be broadly compared with tensile tests such as those published by Meissner [2] in connexion with his duralumin no. 681 B.

Table I.—Composition of Alloy.

Element.	Percentage by weight.	Atomic volume.	Lattice size (a).	(c).
Cu	4·15	7	3·61 Å.U.	—
Si.....	0·19	12	5·42	—
Mg.....	0·49	14	3·20	5·20
Fe	0·42	7	2·86	—
Mn.....	0·64	7·5	(β) 6·30	—
Al.....	remainder	10	4·04	—

The Age-hardening Process.

A commercial duralumin was used in order to secure results of general interest. Its complex chemical composition does not, of course, make it the most suitable alloy from which to draw theoretical conclusions as to the constitutional processes involved in hardening. The metal was in the form of a rolled plate $\frac{1}{4}$ in. thick, and the analysis, as kindly supplied by Dr. Aitchison, is given in Table I., together with a few particulars of each alloying element.

The process of the age-hardening at room-temperatures of the quenched alloy was first examined. The results

of three normal sets of tests are given in Table II., and may be summarized by saying that a 40 per cent. rise of hardness is accompanied by a fall in the n value of 0·08. It was expected that n would be reduced, but to a much greater extent than this, for such a considerable hardening. The result is, therefore, somewhat exceptional, since a 40 per cent. increase of hardness gives a fall in n of 0·30 for copper and 0·24 for aluminium when the hardening is brought about by cold-rolling. It is, however, quite consistent with the known fact that there is

TABLE II.—Quenching and Ageing of Duralumin.

Treatment.	Hardness Pu, kg./mm.^{2}	n.	Brinell, no. $H_{1/10/30}$.	a_1.
W.Q. 515° C. and aged 5 days.	114	2·25	89	90
W.Q. 490° C. (soaked 30 min.).	108*	2·39	71	85
Aged 4 days—15° C.....	148	2·32	101	116
W.Q. 510° C. (soaked 30 min.).	111*	2·41	71	87
Aged 5 days—15° C.....	155	2·34	106	122
W.Q. 510° C.	111*	2·41	71	87
Aged 6 days—15° C.....	157	2·31	110	123
Summary (mean) :—				
W.Q. 500° C. (30 min.).....	110*	2·40	71	86
Aged 5 days—15° C.....	153	2·32	106	120

* Indentations completed within 10 min. of quenching.

practically no change of the elongation property as a result of age-hardening in duralumin. The conclusion is to be drawn that *this ageing is somewhat analagous to the strain-hardening of a metal* as distinct from the quench-hardening of a pearlitic steel, for n falls during the first operation but rises during the second [3].

Reheating of Aged Duralumin.

Experiments were then made to study the effects of reheating by introducing specimens of fully-aged alloy

into oil baths maintained at 100° C., 150° C., 200° C., 250° C., 300 C., and 360° C. for different periods of time.

TABLE III.—The Reheating of Age-hardened Duralumin.

Treatment.	*n.*	Hardness Pu, kg./mm.²	Brinell, no. $H_{1/10/30}$.	After subsequent cold-rolling—84 % reduction.	
				Hardness, Pu kg./mm.²	*n.*
Quenched 500° C. Aged 5 days ..	2·32	153	106	177	2·07
Do., do. Reheated 100° C.— 4 hr.	2·33	143	98	—	—
„ „ „ „ 100 „*	2·26	157	112	(216)	(2·19)
„ „ „ „ 145 „	2·27	154	112	—	—
„ „ „ „ 257 „	2·27	155	112	—	—
„ „ „ 150° C.—20 min.	2·35	138	95	—	—
(Then aged 3 months.	2·32	142	95)	—	—
„ „ „ 150° C.— 4 hr.	2·25	136	102	—	—
„ „ „ „ 40 „	2·18	149	120	192	2·08
„ „ „ „ 100 „	2·12	139	117	—	—
„ „ „ 200° C.—20 min.	2·40	135	87	—	—
„ „ „ „ 4 hr.	2·22	133	102	—	—
„ „ „ „ 40 „	2·10	110	96	132	2·05
„ „ „ 250° C.—20 min.	2·20	116	91	—	—
„ „ „ 250° C.†—20 „	2·25	126	94	—	—
„ „ „ 300° C. —20 „	2·33	108	76	—	—
(Then aged 24 days.	2·25	106	80)	—	—
„ „ „ 360° C.—20 min.	2·37	89	62	120	2·09

* Tested 18 hours after reheating.
† Specimen previously treated at 200° for 20 min.

A basic heating period of 20 minutes was used in nearly all cases, and more prolonged treatments were also given

at certain temperatures. The results obtained within an hour or so of the conclusion of reheating are given in Table III., and the hardness and n values are recorded graphically in fig. 1.

Fig. 1.

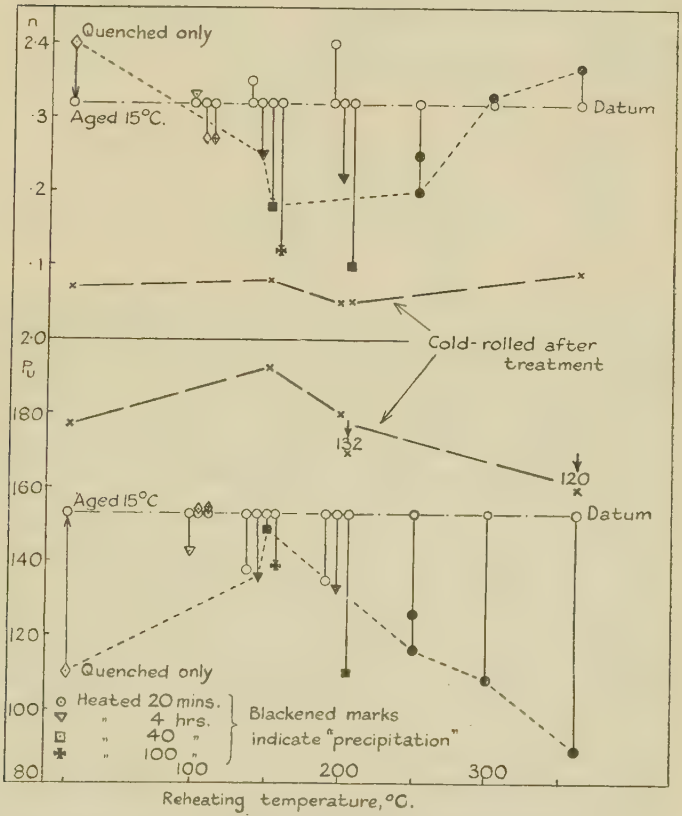

The effect upon the hardness properties of reheating fully-aged Duralumin.

The first point to be noticed is that practically all the treatments given cause a relative softening (P_u value) of the age-hardened duralumin, whereas in some cases the Brinell number indicates either practically no change or else an actual hardening. Our results do not necessarily mean that a hardening of age-hardened duralumin cannot be induced by heat-treatment, for only

certain arbitrary periods of heating have been employed in the present work. There may be optimum times of treatment which will give higher P_u values than that of the ordinary aged alloy. The results do show, however, that the Brinell value may be quantitatively misleading. Very broadly, then, our experiments indicate that the reheating of *aged* Duralumin is a tempering or softening treatment.

Further examination of these results reveals that they may be divided into two divisions :

Group (*a*). Those which cause a rise of n value on reheating.

Group (*b*). Those which cause an initial fall of n value on reheating.

Group (*a*) is represented by the treatments 4 hr.—100° C., 20 min.—150° C., and 20 min.—200° C., the last of which gives the greatest rise of n and the greatest fall of hardness. Such a type of behaviour is also given by a cold-worked metal when it is annealed : n rises, hardness falls, internal stress is reduced. *Meyer analysis consequently leads again to the inference that age-hardened duralumin in some ways resembles a slightly cold-worked alloy* whose (distortion) hardening can be reduced by a Group (*a*) heat-treatment.

The form of the hardness curve (fig. 1) after cold-working certain of the specimens reminded us of that for heat-treated and cold-worked Standard silver—an alloy whose " precipitation hardening " we have studied in detail [4]. We have thus come to the conclusion that Group (*b*) treatments are true " precipitation " treatments. In fig. 1 certain n and P_u results have been joined together by fine dotted lines, whence it appears that the reheatings first cause n to fall and pass through a minimum value corresponding with a maximum in the hardness property. After this maximum, coarsening or " pearlitization " takes place and n steadily rises. Both the factors of time and temperature are involved in this precipitation of duralumin, whereas the time was constant in our experiments with Standard silver. Fraenkel [5] has shown, however, that the time-factor affects the behaviour in quite the same general way during the reheating of the quenched silver alloy.

TABLE IV.—The effect of reheating Quenched Duralumin without R.T. Ageing, followed by Ageing (and Rolling).

Treatment.	*n.*	Hardness P_u, kg./mm.²	Brinell no. $H_{1/10/30}$.	After subsequent cold-rolling—83 % reduction.	Hardness Pu, kg./mm.²	*n.*
W.Q. 500° C. and tested immediately	2·40	110	71	Immediately rolled after quenching	175	2·17
				Aged after rolling	166	2·07
W.Q. 500° C. Aged 5 days—15° C.	2·32	153	106		177	2·07
				54 % reduc.	186	2·13
				92 % „	191	2·18
W.Q. 500° C. Reheated 100° C.—20 min...	2·35	123	84		—	—
„ (20+40)*=60 min.	2·36	127	86		—	—
Then aged 32 days	2·29	138	99		188	2·08
W.Q. 500° C. Reheated 150° C.—20 min...	2·31	120	85		—	—
„ (20+60)†=80 min.	2·32	125	87		—	—
Then aged 36 days	2·34	129	88		160	2·02
W.Q. 500° C. Reheated 200° C.—20 min...	2·24	125	93		—	—
Then aged 11 days	2·24	118	90		—	—
„ „ 18 days	2·24	125	93		—	—
W.Q. 500° C. Reheated 200° C.—2 hr. ...	2·22	112	88		—	—
Then aged 35 days	2·27	130	93		—	—
W.Q. 500° C. Reheated 200° C.—3 hr. ...	2·21	134	102		—	—
Then aged 5 days	2·24	141	105		190	2·09
W.Q. 500° C. Reheated 250° C.—20 min...	2·15	112	95		—	—
Then aged 7 days	2·15	115	96		—	—

* No ageing in between these two treatments.
† 2 hours ageing in between treatments.

Reheating Quenched Duralumin before Ageing.

The effect of heat upon the actual ageing process was examined by a series of experiments in which quenched specimens of duralumin were immediately transferred to hot-oil baths for measured periods of time. On removal from these baths they were cooled in air and rapidly indented, and further tests were made after subsequent ageing at room-temperature for several days. The

Fig. 2.

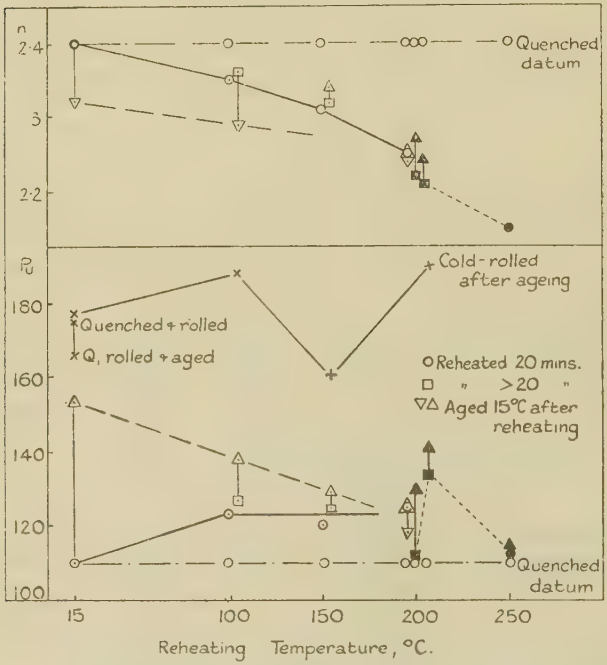

Quenched duralumin, reheated and then aged.

results obtained are given in Table IV. and plotted in fig. 2.

Examination of fig. 2 suggests that for the short periods of reheating here employed the treatments fall into two divisions :

Group (*c*). Treatment for 20 min. (or more at low temperatures) in the range 15°–200° C. (approx.).

Group (*d*). Treatment at temperatures of 200° C. (approx.) for two hours or more, or at higher temperatures.

In other words there is evidence of a boundary or threshold between 150° C. and 200° C. when reheating treatments of about one hour or so are applied.

Group (*c*) *treatments* are characterized by a hardening of the quenched alloy during the heating, and by a further hardening during room-temperature ageing after the treatment. The n value *falls* during *both* these stages of hardening. When the region 150°–200° C. has been reached, the ageing fraction of the hardening has decreased to nothing, and it is at about this stage that the n value ceases to fall during ageing. Beyond this point we enter Group (*d*), where n rises during the room-temperature hardening. It is apparent from fig. 2 that reheating or "accelerating" freshly quenched duralumin in the Group (*c*) range does not permit it to become as hard as by simple room-temperature ageing (15° C.) alone. These facts suggest that this particular Group (*c*) heating is, therefore, progressively inhibiting a fraction of hardening which is of a type associated with a fall of n value. The obvious analogy is the cold-working of a metal at increasing working temperatures, for in such a case strain-hardening is induced to a decreasing and vanishing extent as the working temperature approaches the recrystallization temperature. *We are, therefore, led to infer that Group* (*c*) *treatments include a hardening having effects similar to the strain-hardening of a metal.* It is quite likely that practically all the hardening in Group (*c*) is of this type, the fraction occurring before ageing being simply the same as the other, but generated during the actual period of heating.

The cold-rolling experiments in this section are difficult to interpret. The cold-rolling and indentation testing of a specimen, when completed within 16 minutes of quenching, gave as high a hardness as that of a fully aged and subsequently rolled specimen. Upon ageing the former, however, both n and P_u decreased, indicating that this treatment was ultimately inferior to ageing first and rolling afterwards (Table III.). In each case the rolling operation itself reduced n by 0·23–0·25, and the ageing process lowered it by 0·08–0·10. Rolling the quenched specimen gave an immediate increase of

hardness of 59 per cent., whereas rolling the aged metal only gave a 16 per cent. rise, but the final hardness after rolling was the same in both cases. One might infer, therefore, that in the second case (aged specimen) the metal had already become partly "strain-hardened," which again leads to the inference that ageing is analogous to strain-hardening. Whether this be justified or not, the final fall of n and Pu during ageing in the quenched-rolled-aged material is difficult to account for. A somewhat similar behaviour of the Meyer constants occurs in the tempering of the martensite of hardened steel, and it may be that the heavy distortion is in some way causing a precipitation tempering. When X-ray spectrograms were subsequently taken of this particular specimen, and although the metal had not been reheated at all, its lattice size was 4·038($\pm$·001) Å.U., as compared with the usual 4·036 Å.U. for unheated aged alloy. It must be remarked, however, that the initial quenching temperature happened to be 490° C. as compared with the quenchings at 510° C., which gave the normal value of 4·036 Å.U.

Very heavy rolling (92 per cent. reduction) of simply aged duralumin also gave a surprising result, for n had *risen* to 2·18 and P_u to 191 kg./mm. An analogous behaviour has been observed in austenitic 18/8 Ni-Cr alloy. There is the danger, of course, that since these duralumin specimens cracked and opened during cold-rolling, they may not have distorted uniformly, and the results may be inaccurate.

Group (*d*) *treatments* were first in evidence when a piece of freshly quenched duralumin was at once heated for two hours at 200° C. and immediately tested. There was but very little hardening of the metal, and the limits of accelerated ageing had, therefore, been passed. n was lowered by the treatment, but room-temperature ageing subsequent to this reheating produced both a slight *rise* in n and a rise in hardness. Group (*c*) treatments had given a fall in n, and this change over suggests the advent of a new state of affairs. A similar treatment at 200° C., but for three hours' duration, gave a minimum n value of 2·21, accompanied by a rise of hardness to 134 kg./mm.^{2} These figures are almost the same as those obtained previously for a 4-hour Group (*b*) treatment of aged alloy at 150° C. or 200° C.

(Table III.). The hardness after cold-rolling is 190 kg./mm.^{2} with $n=2{\cdot}09$, which is very similar to that after the Group (*b*) process at 150° C. for 40 hours ($P_u=192$, $n=2{\cdot}08$). We have previously decided that Group (*b*) reheatings are true "precipitation" treatments, and consequently are now led to the suggestion that the present Group (*d*) treatments are of the same type. If this is correct, then since 3 hours' reheating described above gives about the same hardness properties as 4 hours' treatment of the aged series at 200° C. (see fig. 1), then more severe heating should induce troostitic qualities, followed eventually by "coarsening." The test at 250° C. for 20 minutes confirms this view, the results obtained being similar to those on aged duralumin after reheating at 200° C. for 40 hours. It will be observed that this last Group (*d*) treatment is not followed by any appreciable ageing changes.

Mention may here be made of an anomalous result obtained when an old piece of this duralumin was quenched at 510° C. and immediately reheated at 250° C. for 20 minutes. The particular specimen employed had been previously used for heat-treatment experiments, and it may be that its constituents were in an abnormal condition as compared with the original plate. Anyhow, tests immediately after this reheating gave $n=2{\cdot}25$ and $P_u=127$, but the metal then proceeded to age-harden and acquire the properties of a normal age-hardened specimen, having, in fact, the values $n=2{\cdot}31$ and $P_u=151$. X-ray examination of this specimen immediately after the reheating gave the abnormal lattice-size of 4·034 Å.U., which changed to the usual 4·036 Å.U. on ageing (*cf.* Table V.).

Tests on Duralumin with the X-ray Spectrograph.

We have tested our conclusions by examining changes of lattice parameter in the actual duralumin specimens which had been used for the hardness work. Unfiltered copper X-radiation was employed, with a precision "back-reflexion" method, using a camera of 6·60 cm. diameter. Exposures of about 90 minutes were required, and without making any allowance for film shrinkage we believe that the third decimal figure in the calculated parameters is accurate. The α_1 reflexion from the (511) and (422) planes was used for purposes of measurement.

TABLE V.—Correlation of Heat Treatment and Lattice Parameter.

Film no. (Pl. XXVIII.)	Heat treatment.				Lattice-size, Å.U.	Remarks.
		Temp.	Time.	Group-type.		
	W.Q. 415° C. and aged ...	15° C.	5 days	—	4·040	
1.	„ 510° C. „ „ ...	15° C.	1 hr.	—	4·036	Sharp lines.
2.	„ „ „ „ ...	„	5 days	*a*	4·036	
	Do., aged and reheated ..	100° C.	100 hr.	?	4·036	
	„ „ „ „ ..	„	145 hr.	?	4·036	
3.	„ „ „ „ ..	150° C.	20 min.	*a*	4·036	
	„ „ „ „ ..	„	4 hr.	*b*	4·037	
4.	„ „ „ „ ..	„	40 hr.	*b*	4·041	Blurred lines.
	„ „ „ „ ..	250° C.	20 min.	*b*	4·037	
	„ „ „ „ ..	300° C.	20 min.	*b*	4·038	
	W.Q. 510° C., reheated ...	100° C.	20 min.	*c*	4·036	
	Then aged	15° C.	Several days	*c*	4·036	
5.	Do., do.....	200° C.	20 min.	*c*	4·036	Sharp lines.
6.	Then aged	15° C.	Several days	*c*	4·036	Sharp lines.
	Do., do.....	200° C.	2 hr.	*d*	4·037	
	Do., do.....	„	3 hr.	*d*	4·039	Blurred lines.
	Do., do.....	250° C.	20 min.	*d*	4·040	
7.	W.Q. 490° C., aged and cold-rolled 92 % r.-t.....	15° C.	5 days	—	4·038	Very blurred lines; doublets not resolved; (511) lines extremely diffuse. General radiation increased.
	W.Q. 490° C., cold-rolled 83 % reduc. at once and then aged	15° C.	4 mth.	?	4·038 ±·001	
8.	W.Q. 490° C., aged, reheated, and cold-rolled..	360° C.	20 min.	*b*	4·042	

In all cases we found that the alloy freshly quenched from 510° C. and the same after room-temperature age-hardening both gave a lattice-size of 4·036 Å.U.

This confirms recent observations that no easily measurable change of the spacing occurs during simple age-hardening. To that extent it is now generally held that such age-hardening of aluminium alloys is not a "precipitation" effect, for if copper, for instance, were rejected from the solid solution, the lattice-size should increase. This conclusion is most convincing in the case of pure Al-Cu alloys, but commercial duralumin contains so many added elements of differing atomic volumes (see Table I.) that their mutual precipitation might have balancing effects upon the atomic spacing. For present purposes it will be sufficient to state that where there *is* an increase of lattice-size there is strong evidence for the precipitation of a metal of small atomic volume such as copper and/or iron. A cold-working operation does not cause a well-defined change of the lattice-size, but produces a blurring and broadening of the lines of the spectrum. Some of the X-ray spectrograms are shown in fig. 3 (Pl. XXVIII.), those which have been taken from the heavily cold-rolled specimens showing this broadening quite definitely. The age-hardened alloy gives lines which are nearly as sharp as those from the quenched metal before ageing, but the early stages of precipitation are accompanied by diffuse lines.

It is obvious from Table V. that heat-treatment of the types Group (*b*) and Group (*d*) bring about real precipitation, as was inferred from the hardness tests. Group (*a*) and Group (*c*) treatments are shown to be alike in producing no measurable change in lattice-size. This again confirms the deductions made from hardness tests, but throws no light upon the nature of the processes at work. It seems safe to say, however, that the four types of reheating which have been examined reduce to three, which we propose to designate, for purposes of discussion, as "precipitation" (*b* and *d*), "release" (*a*), and "acceleration" (*c*). There is, further, the process of age-hardening at room-temperature, which will be referred to as "incubation."

Discussion.

The "precipitation" process in duralumin appears to be similar to that for quenched Standard silver and

calls for no special comment here. The other three reheating effects may be set out as follows :—

" Incubation "	Age-hardening of quenched duralumin.	Rise of hardness; relatively small fall of n.
" Acceleration " (c).	Heating of quenched duralumin up to 150°–200° C. Resembles " incubation."	Rise of hardness; fall of n—but effect decreases as temperature reaches 150°–200° C.
" Release " (a)	Heating of fully age-hardened duralumin *e. g.*, to 200° C. for 20 min.	Fall of hardness; slight rise of n.

Taken together, we suggest that these processes indicate that the factors operating during the room-temperature age-hardening of duralumin are similar to those which cause strain-hardening during plastic deformation. If the general statement is to be accepted that the age-hardening is accompanied by a rise in electrical resistivity, then this too is consistent with our suggestion. Plastic deformation of an aggregate generally produces a slight fall in density. Some results for duralumin indicate a slight net rise in density, though opposite findings have been reported, and the evidence here is not entirely conclusive. Sometimes the property-curves have an inflexion after 3–4 hours' ageing, and, therefore, rather suggest that two processes are at work.

It seems that the following possibilities must be taken into account during simple age-hardening :—

(1) *Release of Quenching Stresses.*—This effect is likely to take place during " acceleration " and, perhaps, during ordinary ageing. It will probably cause a slight rise in the n value, and we do not think that it contributes to the hardening.

(2) *Segregation of Solute Atoms.*—By this we mean a departure from the so-called random arrangement of the dissolved atoms on the aluminium space-lattice, after quenching, to a more ordered or stratified arrangement. When such a process proceeds to completion, " super-lattices " are produced in the X-ray spectrum, the electrical resistivity is reduced, and the density tends to rise, but the hardness undergoes no important change (*e. g.*, Fe–Al). The " intermediate state " before complete order is reached, however, may give rise to a considerable

increase of Brinell number (Au–Cu), and super-lattices may be absent. We have looked for super-lattices in age-hardened duralumin, but have not succeeded in detecting them. This segregation process can be imagined as beginning during the " incubation " or " acceleration " treatments, but the latter (or " release " heating too) should tend to allow it to approach completion. We cannot say definitely whether this segregation effect actually occurs, but its commencement is a very important possibility.

(3) *Molecule Formation.*—The idea that atoms of aluminium combine in one way or another with some of the solute atoms is involved in theories put forward by Fraenkel and his collaborators and by Gayler and Preston. The former suggests a chemical combination of the constituent atoms. The latter workers consider that molecules may be formed which cause lattice-distortion and increased resistance to slip. If strain-hardening is to be attributed to lattice-distortion, as many believe, then this theory in broad outline would be consistent with our deductions from the hardness results.

We would venture to call attention to Dean and Gregg's general theory of metallic hardening, which is applicable to strain-hardening, and which in some ways is a bridge between (2) and (3) above and our suggestion. Discussing the effect of any factor which tends to upset the normal lattice-spacing of a metal, Dean and Gregg say :—" If the atoms are separated by some distance greater than that of the normal space-lattice, but less than the distance in a gas, there will be a tendency for the separated atoms to take on electrons, with the result that some pairs of atoms will share electrons. This is, in effect, a forced molecule formation, and the theory . . . is that when atoms are separated to a distance greater than their normal lattice-distances they form these pseudo-molecules. . . . The increased hardness is due to the progressive formation of pseudo-molecules of greater energy and strength." These remarks apply to a pure metal, but the same argument would, presumably, suggest the formation of pseudo-molecules of " $CuAl_2$ " and/or Mg_2Si in a duralumin solid solution.

Finally, we would point out that on alloying aluminium

with silver the normal solid solution obtained with low concentrations eventually becomes mixed with Ag_3Al crystals as the aluminium content is increased. The careful work of Phelps and Davey [6] leads them to suggest that this initial solid solution involves a type of chemical combination which, nevertheless, will not produce new lines in the X-ray spectrum, and is similar to molecule formation. Perhaps some such structure builds up during the ageing of light alloys. A comparison of the compressibilities of duralumin in the freshly-quenched and the age-hardened conditions would probably help in the elucidation of the problem, but so far the data do not seem to be available.

Conclusions.

(1) Ball-hardness tests on the basis of "Meyer analysis" indicate that the normal age-hardening of quenched duralumin, or its accelerated ageing at temperatures below 150°–200° C., are not "precipitation" treatments. The age-hardening process has effects somewhat similar to those obtained when a metal is slightly cold-worked.

(2) "Precipitation" can be induced in either freshly-quenched or fully-aged duralumin by sufficiently severe heat-treatment. It has not been found in general to give hardness (P_u) results superior to those obtained from the normal ageing treatment at room-temperature.

Acknowledgments.

This work was carried out with facilities kindly placed at our disposal by Professor F. C. Thompson, and with apparatus provided by financial grants from Messrs. Imperial Chemical Industries, Ltd. We are also indebted to Dr. L. Aitchison for kindly supplying the duralumin which was used, and one of us (G. S. F.) makes acknowledgments to the Royal Commission of the Exhibition of 1851 for an Overseas Research Scholarship.

References.

(1) O'Neill, H., and Cuthbertson, J. W.—J. Inst. Metals, xlvi. p. 273 (1931).
(2) Meissner, K. L.—J. Inst. Metals, xliv. p. 207 (1930).

(3) O'Neill, H.—Carnegie Schol. Mem., Iron Steel Inst., xv. p. 233 (1926).
(4) O'Neill, H., Farnham, G., and Jackson, J.—J. Inst. Metals, lii. (1933).
(5) Fraenkel, W.—*Z. anorg. Chem.* cliv. p. 386 (1926).
(6) Phelps, R. T., and Davey, W. P.—Trans. Amer. Inst. Min. Met. Eng. xcix. p. 234 (1932).

Metallurgical Department,
University of Manchester.
May 1933.

LXXVIII. *The Energy Levels of the Hydrogen Molecular Ion.* *By* C. Gilbert, *A.R.C.S.*, *B.Sc.* *.

Summary.

The differences between the most recent calculations of the energy levels of the hydrogen molecular ion are discussed, with special reference to the degeneracy of symmetric and antisymmetric states. A perturbation theory is given and results calculated which are in close agreement with those obtained by the variation method. A method is also stated whereby the higher energy levels can be easily obtained, and curves are drawn for the energy levels up to the second excited states of the hydrogen molecular ion. The lower energy levels compare favourably with those obtained by the more exact variation method. No published results of experiment appear to give sufficiently large moments of inertia to be in agreement with the theoretical values for the *excited* H_2^+ molecule.

1. *Introduction.*

SEVERAL of the methods of the wave mechanics have been applied successfully to the determination of the discrete energy levels of the hydrogen molecular ion (H_2^+). The earliest work approached the problem from two points of view. The electronic energy for infinite separation of the nuclei is the same as that of the hydrogen atom, and for the united nuclei it is the same as that of the helium ion (He^+). The theoretical work of F. Hund † showed how these two sets of energy levels

* Communicated by W. H. McCrea, M.A., Ph.D.

† References are given by Morse and Stueckelberg (see footnote ‡, p. 930).

could be correlated with each other by making certain assumptions about the number of possible intersections of the energy levels for intermediate distances apart of the nuclei. R. S. Mulliken *, starting from another hypothesis, has obtained similar results. Both methods have been successful and are of especial interest when applied to more complicated diatomic molecules. These results, moreover, were found very valuable when the problem of the hydrogen molecular ion was attacked by means of the perturbation method of the wave mechanics. This method only extends the results already mentioned, for infinite separation of the nuclei and the united nuclei, to the corresponding cases of large internuclear separation and short internuclear separation, so that interpolation is necessary for the intermediate distances. The results of Hund and Mulliken thus show how the two sets of electronic energy curves, as functions of the internuclear distance, are to be joined together.

The energy values for the ground state of the ion were first calculated successfully by Burrau † by a numerical method applied directly to the wave equation separated in elliptic coordinates. A successful perturbation theory for the hydrogen molecular ion was given by Morse and Stueckelberg ‡, who calculated the energy levels for the ground state and the first excited states. At about the same time a variation method was used by V. Guillemin and C. Zener § to calculate the energy values for the ground state of the ion.

The most recent work on the subject has been done by E. Teller || using the variation method, and E. A. Hylleraas ¶ using a "separation method," which is essentially an algebraic solution of the wave equation separated in elliptic coordinates. Teller's calculations give the energy levels for the ground state and first excited states, and are the most complete results so far published. From these results it would appear that the variation method has entirely superseded the perturbation method for the

* References are given by Morse and Stueckelberg (see footnote ‡).

† Burrau, *Kgl. Danske Vid. Selskal. Math-Fys. Med.* vii. No. 14 (1927).

‡ P. M. Morse and E. C. G. Stueckelberg, Phys. Rev. xxxiii. pp. 932–947 (1929).

§ V. Guillemin, Jr., and C. Zener, Proc. Nat. Åcad. xv. pp. 314–318 (1928).

|| E. Teller, *Zeits. f. Phys.* lxi. pp. 458–480 (1930).

¶ E. A. Hylleraas, *Zeits. f. Phys.* lxxi. pp. 739–763 (1931).

accuracy with which the energy levels can be calculated. The energy values can, moreover, be calculated for all ranges of values of the internuclear distance except those which are less than about one hydrogen atomic radius. The latter is the range for which the perturbation method for short internuclear distances gives good results. Hylleraas has made a very detailed study of the ground state of the hydrogen molecular ion, and has also obtained results for the ground state and excited states of the hydrogen molecule.

The original object of this paper was to find as accurately as possible, without extensive calculations, the higher energy levels of the hydrogen molecular ion. On reviewing the work already published in this connexion, considerable diversity was found in the results of the investigators for the first excited states. From the point of view of the method given in this paper, the electronic energy curves obtained by Morse and Stueckelberg seemed most useful, but these had been corrected at a later date by J. E. Lennard-Jones *. It has been shown in § 2 that, though this correction is justified, the results are not so inaccurate as would appear from Lennard-Jones' paper.

The eigenfunctions of the molecular ion at large internuclear distances, referred to as the molecular eigenfunctions, are formed either by addition or subtraction of the separate eigenfunctions for a given state of a hydrogen atom referred to each of the two nuclei as origin. The former are classified as symmetric and the latter as antisymmetric eigenfunctions, and the corresponding states are described in a similar manner. It is well known that the symmetric and antisymmetric states whose molecular eigenfunctions are formed from the same hydrogen eigenfunctions become degenerate at infinity, and it was further shown, by Morse and Stueckelberg, that the two energy levels lie close together until internuclear distances of about ten hydrogen atomic radii are reached. Lennard-Jones' electronic energy curves for the first excited states, on the other hand, show considerable splitting of the symmetric with respect to the corresponding antisymmetric states for large internuclear distances, and actually his calculations show that all the antisymmetric states have

* J. E. Lennard-Jones, Trans. Farad. Soc. xxiv. pp. 668-686 (1929).

higher energy levels than any of the symmetric states for distances up to at least fifteen hydrogen atomic radii.

The calculations by Teller, using the variation method, again show a fairly rapid approach to degeneracy of the respective symmetric and antisymmetric states. An attempt has therefore been made to verify Teller's curves by a perturbation method.

Lennard-Jones has taken no account of degeneracy among the molecular eigenfunctions in his theory, and evidently this does not give a good enough approximation. As a first approximation we shall consider degeneracy among the eigenfunctions of the first excited states only; but evidently the theory can be extended in principle to include all possible forms of degeneracy, in which case an infinite determinant must be evaluated to determine the perturbation energies.

2. *The Perturbation Theory for the Energy Levels of the First Excited States of the Hydrogen Molecular Ion.*

We consider an electron of charge $-e$, under the influence of two nuclei of charges ze ($z=1$ in the particular case of the hydrogen molecular ion), at a distance ρ apart. The internuclear distance ρ is measured in units of a, the radius of the first Bohr orbit for the hydrogen atom; the distances of the electron from the nuclei I and II are r_1 and r_2 respectively.

The Schrödinger equation for the system, if the effect of the motion of the nuclei is neglected, is

$$\mathrm{L}(\chi)\equiv\Delta\chi+\frac{8\pi^2m}{h^2}\left(\mathrm{E}-\mathrm{W}(\rho)+\frac{ze^2}{r_1}+\frac{ze^2}{r_2}\right)\chi=0, \quad . \quad (1)$$

where m is the mass of the electron, h Planck's Constant, and $\mathrm{W}(\rho)(=z^2e^2/\rho a)$, the Coulomb interaction energy of the nuclei. The whole energy E is called the potential energy of the ion, and by subtracting the Coulomb interaction energy we get the electronic energy $\mathrm{E}-\mathrm{W}(\rho)$. We wish to find those values of E, belonging to the first excited states of the system, for which there exists a solution χ of this equation.

We define $\psi(n, l, m)$, $\phi(n, l, m)$ as eigenfunctions for atoms with an electron of charge $-e$ and nuclei I and II respectively, where n is the principal quantum number, l the "azimuthal" quantum number, and m the "equa-

torial" or "magnetic" quantum number. Since in this theory we shall only require the eigenfunctions for the first excited states of the atoms ($n=2$), we shall abbreviate the notation as follows:—

$$\psi_1=\psi(2,0,0),\ \psi_2=\psi(2,1,0),\ \psi_3=\psi(2,1,1),\ \psi_4=\psi(2,1,-1),$$

$$\phi_1=\phi(2,0,0),\ \phi_2=\phi(2,1,0),\ \phi_3=\psi(2,1,1),\ \phi_4=\phi(2,1,-1),$$

and the collection of eigenfunctions for the first excited states will be represented by ψ_i, ϕ_i ($i=1\ldots4$). These eigenfunctions satisfy the eight equations

$$\Delta\psi_i+\frac{8\pi^2m}{h^2}\left(\mathrm{E}_2+\frac{ze^2}{r_1}\right)\psi_i=0, \quad . \quad . \quad . \quad . \quad (2)$$

$$\Delta\phi_i+\frac{8\pi^2m}{h^2}\left(\mathrm{E}_2+\frac{ze^2}{r_2}\right)\phi_i=0, \quad (i=1\ldots4), \quad (3)$$

where, if $z=1$, E_2 is the energy of the first excited state of a hydrogen atom.

To a first approximation we expand χ, the solution of equation (1), in terms of the eigenfunctions ψ_i, ϕ_i ($i=1\ldots4$), with an additional perturbation eigenfunction v. Quite generally we can write

$$\chi=\sum_{i=1\ldots4}\{a_i(\psi_i+\phi_i)+b_i(\psi_i-\phi_i)\}+v, \quad . \quad . \quad . \quad (4)$$

where a_i, b_i are functions only of the internuclear distance ρ. The expansion is written in this form because the one set of eigenfunctions $\psi_i+\phi_i$ ($i=1\ldots4$) is orthogonal to the other set $\psi_j-\phi_j$ ($j=1\ldots4$), and these eigenfunctions with the appropriate normalizing factors are respectively the symmetric and antisymmetric eigenfunctions already referred to.

We also write

$$\mathrm{E}=\mathrm{E}_2+\epsilon,$$

where ϵ is a small perturbation energy.

Substituting these values of χ and E in equation (1), we get

$$\mathrm{L}(v)+\sum_{i=1\ldots4}\Big[a_i\Big\{\Delta(\psi_i+\phi_i) + \frac{8\pi^2m}{h^2}\left(\mathrm{E}_2+\epsilon-\mathrm{W}(\rho)+\frac{ze^2}{r_1}+\frac{ze^2}{r_2}\right)(\psi_i+\phi_i)\Big\}$$

$$+b_i\left\{\Delta(\psi_i-\phi_i)+\frac{8\pi^2m}{h^2}\left(\mathrm{E}_2+\epsilon-\mathrm{W}(\rho)+\frac{ze^2}{r_1}+\frac{ze^2}{r_2}\right)(\psi_i-\phi_i)\right\}\Big]=0. \quad . \quad . \quad . \quad (5)$$

Putting $\eta=\epsilon-\mathrm{W}(\rho)$ and using equations (2) and (3), we get from equation (5)

$$\mathrm{L}(v)+\frac{8\pi^2m}{h^2}\sum_{i=1\ldots4}\left[a_i\left\{\eta(\psi_i+\phi_i)+\frac{ze^2\psi_i}{r_2}+\frac{ze^2\phi_i}{r_1}\right\}+b_i\left\{\eta(\psi_i-\phi_i)+\frac{ze^2\psi_i}{r_2}-\frac{ze^2\phi_i}{r_1}\right\}\right]=0. \quad (6)$$

The usual procedure is to make the non-homogeneous part of this equation orthogonal to the solution χ of equation (1). At large internuclear distances ψ_i and ϕ_i are both approximate solutions of equation (1) having the same energy value, hence any linear combination of ψ_i and ϕ_i will also be an approximate solution of this equation having the same energy value. In particular we can say that, at large internuclear distances $\psi_i+\phi_i$ and $\psi_i-\phi_i$ are solutions of equation (1), with a degenerate energy value, and v tends to zero. Hence we can make the non-homogeneous part of equation (4) orthogonal to the symmetric and antisymmetric parts of χ separately.

We then get

$$\sum_{i=1\ldots4} a_i(\eta\mathrm{N}_{ij}+u_{ij})=0, \quad . \quad . \quad . \quad . \quad . \quad (7\,a)$$

$$\sum_{i=1\ldots4} b_i(\eta\mathrm{N}'_{ij}+u'_{ij})=0, \qquad (j=1\ldots4), \quad (7\,b)$$

where

$$\mathrm{N}_{ij}=\int(\psi_i+\phi_i)\,\overline{\psi_j+\phi_j}\,d\tau,$$

$$\mathrm{N}'_{ij}=\int(\psi_i-\phi_i)\,\overline{\psi_j-\phi_j}\,d\tau,$$

$$u_{ij}=ze^2\int\left(\frac{\psi_i}{r_2}+\frac{\phi_i}{r_1}\right)\overline{\psi_j+\phi_j}\,d\tau,$$

$$u'_{ij}=ze^2\int\left(\frac{\psi_i}{r_2}-\frac{\phi_i}{r_1}\right)\overline{\psi_j-\phi_j}\,d\tau,$$

the integrations being taken over all space.

The determinantal equations obtained by eliminating a_i, b_i $(i=1 \ldots 4)$ from equations $(7\,a)$ and $(7\,b)$ will determine the energy values at a given internuclear distance of all the symmetric and antisymmetric first excited states.

In the case of the symmetric states the equation to determine η becomes

$$\begin{vmatrix} \eta N_{11}+u_{11} & \eta N_{12}+u_{12} & 0 & 0 \\ \eta N_{21}+u_{21} & \eta N_{22}+u_{22} & 0 & 0 \\ 0 & 0 & \eta N_{33}+u_{33} & 0 \\ 0 & 0 & 0 & \eta N_{44}+u_{44} \end{vmatrix} = 0, \quad (8)$$

and the equations $(7\,b)$ give an equation of the same form to determine the energy values for the antisymmetric states, with their corresponding integrals.

The quadratic part of equation (8) gives

$$\eta^2\left(1-\frac{N_{12}^2}{N_{11}N_{22}}\right)+\eta\left(\frac{u_{11}}{N_{11}}+\frac{u_{22}}{N_{22}}-\frac{2u_{12}N_{12}}{N_{11}N_{22}}\right) + \frac{u_{11}u_{22}}{N_{11}N_{22}}-\frac{u_{12}^2}{N_{11}N_{22}}=0. \quad (9)$$

The results given by Lennard-Jones are obtained by omitting the terms containing N_{12}, u_{12} in this equation, and the terms containing N'_{12}, u'_{12} in the corresponding equation for the antisymmetric states. The introduction of these extra terms alters the relative positions of the curves considerably. In fact, the results obtained by this method are in good agreement with those obtained by Teller by the variation method. In fig. 1 the full lines show the results of the calculations using this method, and for purposes of comparison the curves of Teller are shown in dashed lines. Where the dashed lines are not shown the two results are in close agreement. The approximation is not good enough to carry the curves as far as the minima, and does not give good results for internuclear distances less than six hydrogen atomic radii.

It has already been shown by Lennard-Jones * that in general a perturbation theory, to any required degree

* J. E. Lennard-Jones, Proc. Roy. Soc. A, cxxix. p. 604 (1930).

of accuracy, can be obtained by expressing the solution of the wave equation

$$L(\psi)+(E-v)p\,\psi=0$$

(where L denotes a self-adjoint linear partial differential operator and v is the perturbation potential energy), as a linear expansion of the solutions of the equation

$$L(\psi)+Ep\psi=0.$$

Fig. 1.

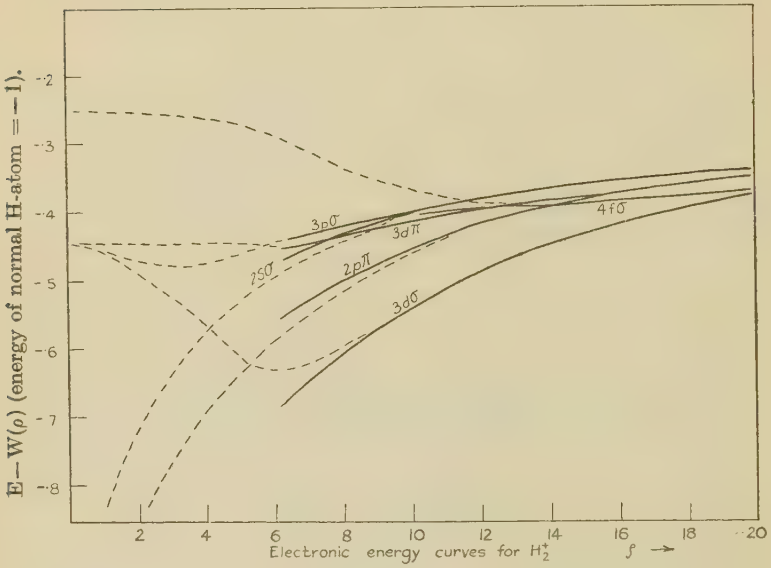

In our particular case we have the ψ- and ϕ-sets of eigenfunctions to consider, and in general a member of the one set is not orthogonal to a member of the other. When we expand in terms of *all* the ψ- and ϕ-eigenfunctions we therefore get a determinantal equation which contains the unknown energy in some non-diagonal terms as well as in the diagonal terms.

3. *The Higher Energy Levels of the Hydrogen Molecular Ion.*

Owing to the great amount of labour involved in the calculations, no theoretical energy curves have been

obtained for any molecule or molecular ion for states higher than the first excited states. The simplest case to consider is the hydrogen molecular ion. Moreover, the results are of interest in the theory of the pressure shift and broadening of spectral lines, since they give the perturbation by a free ion of an atom emitting the Balmer lines.

The method was designed to determine the higher energy levels, to a fair degree of accuracy, at large internuclear distances. It originated in a surprisingly simple way of determining the energy curves for the ground state of the hydrogen molecular ion. For large values of ρ the effects of electron exchange between the two nuclei can be neglected, and the energy of the ion can be found by considering the effect of a distant charge e on an isolated hydrogen atom. This is done by calculating the perturbation energy of the ground state of the atom, from the Stark effect *, caused by a uniform field $e/(\rho a)^2$ throughout space in the direction of the line joining the distant charge to the hydrogen atom.

The Stark effects of the first and second orders, calculated according to the formulæ given below, are inappreciable for the ground state for values of ρ greater than five hydrogen atomic radii. Hence for these values of ρ the energy due to the Stark effect is approximately represented by the line AB, fig. 2 *a*. For large internuclear distances this line will give the potential energy of the ion : but it will not be nearly correct for distances much less than about ten hydrogen atomic radii. To obtain the curve for the latter values of ρ we resort to the electronic energy curves : for we then have additional information about the energies at short internuclear distances. The approximate electronic energy curve CD, for the ion at large internuclear distances, is found by subtracting the Coulomb interaction energy.

When ρ tends to zero the electronic energy of the hydrogen molecular ion will be the same as that of the helium ion in an unexcited or excited state. Nodal reasoning † shows that the unexcited symmetric state of H_2^+ has the same energy as the unexcited He^+ when ρ is zero. This energy value is -4 (in units such that

* *Cf.* Note on formulæ used at the end of this paper.

† Morse and Stueckelberg, *loc. cit.* The notation (for the states) given by these authors is used throughout this paper.

the energy of the normal H-atom $= -1$). Hence an approximate electronic energy curve for H_2^+ is formed by joining O to CD by a smooth curve. If the interaction energy is now added we obtain the usual potential energy curve, fig. 2 *b*, for the unexcited symmetric state of the hydrogen molecular ion. The value of ρ for

Fig. 2 *a*.

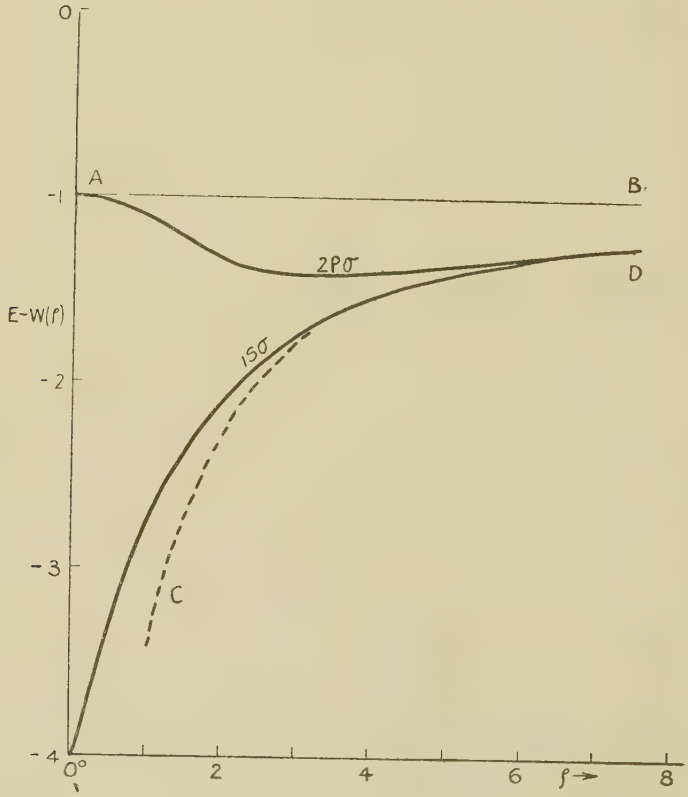

a minimum value of the energy is $\rho_0 = 2{\cdot}1$ hydrogen atomic radii, whereas Teller and Hylleraas found the value 2·0, which is the same as the experimental value *. The value of ρ_0 is found to alter very little with varying smooth curves drawn from O to CD. The nature of this curve can be made still more precise by calculating the

* W. Jevons, 'Report on Band-Spectra of Diatomic Molecules,' p. 268 (1932).

energy values for short internuclear distances by the method of Morse and Stueckelberg. The energy curve corresponding to the antisymmetric state of the unexcited ion is found by joining the point A to CD by a smooth curve. The Morse and Stueckelberg calculations give a good indication here of how the curve is to be drawn.

Fig. 2 *b*.

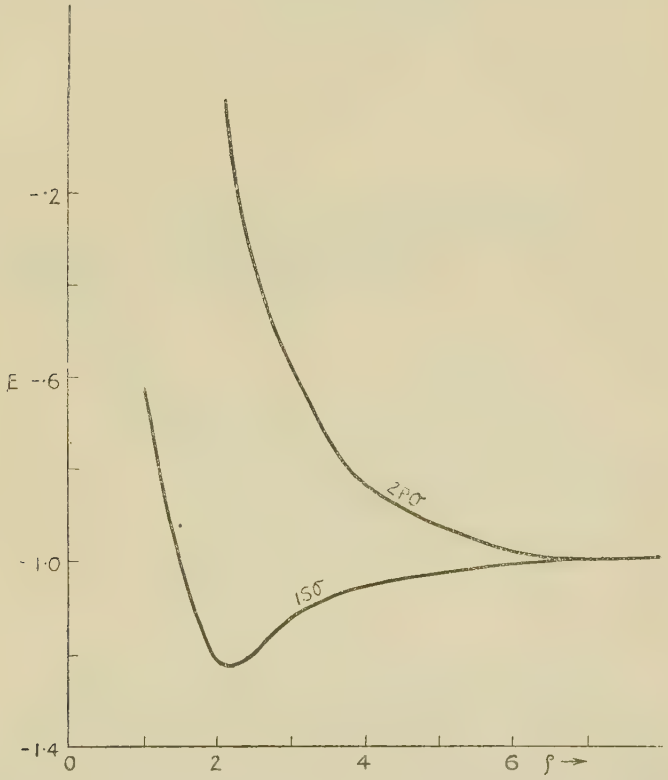

The potential energy is obtained by adding the interaction energy, and shows the usual Van der Waals repulsion. The curves, which were drawn quite independently of any other results, never differ by as much as one volt from those given by Teller.

The method, which has been described in detail above for the calculation of the levels in the ground state of the ion, was extended to the determination of the levels

of the first and second excited states. In these cases it was found necessary to use the method of Morse and Stueckelberg for short internuclear distances, although in the case of the second excited states the perturbation energies become so small that only the sign of the perturbation is necessary to show whether the curve passes through a minimum value or not.

The curves for the first and second excited states are

Fig. 3 *a*.

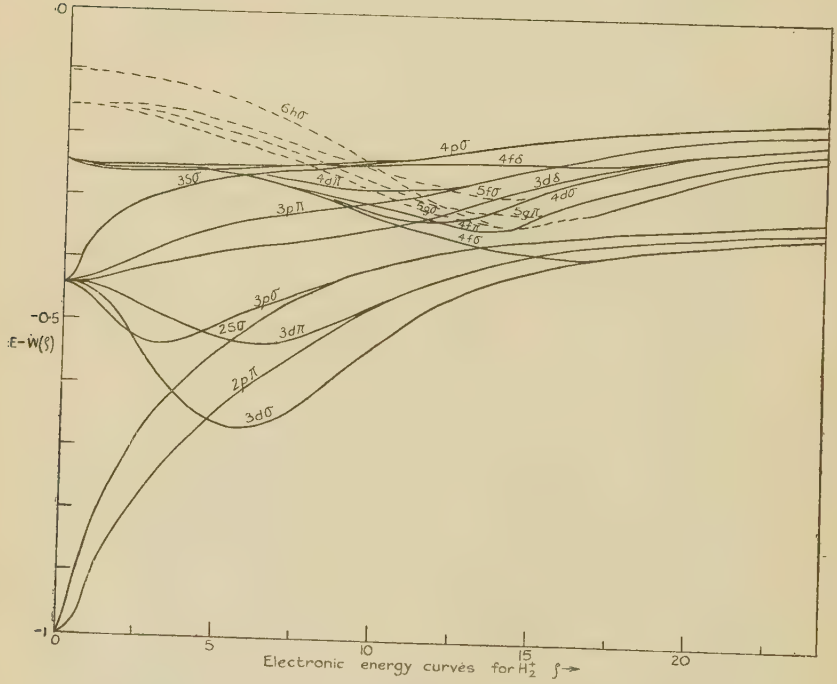

shown in figs. 3 *a* and 3 *b*, and in Table I. certain numerical results are given for most of those curves which show a minimum value of the potential energy. These results, which are taken at the least accurately known parts of the curves, agree with those of Teller. The state $3d\sigma$, which shows the greatest discrepancy in the value of ρ_0, has a very pronounced minimum in the electronic energy curve and was the most difficult case of interpolation. The energy levels which at short internuclear distances approximate to the levels of the helium ion, with the

same degree of excitation as that of the hydrogen molecular ion at large internuclear distances, are the most accurate, for in these cases the electronic energy curves do not show any minima. Other curves which are called promoted, doubly promoted, etc., according as the state of the helium ion is excited once, twice, etc., more than the corresponding state of the hydrogen molecular ion at large internuclear distances, are not so reliable. In fact, doubly and higher promoted curves

Fig. 3*b*.

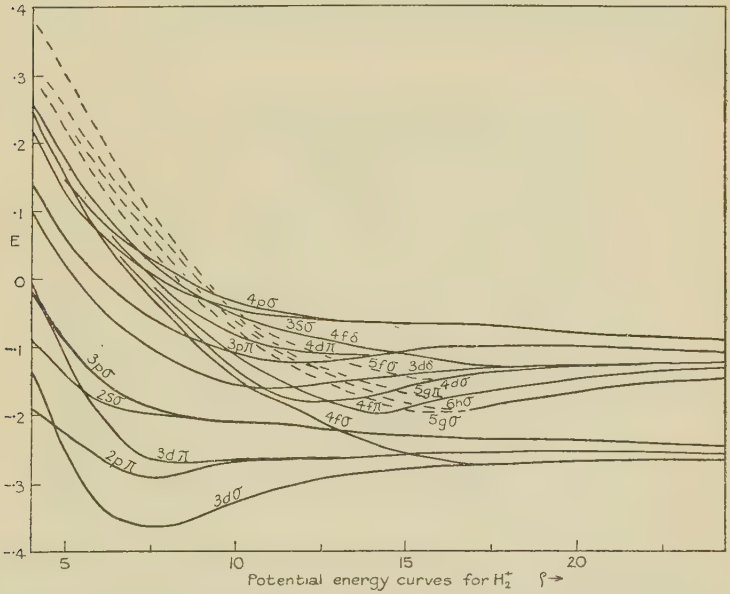

are shown in dashed lines because they are so indeterminate. This difficulty is well illustrated in the case of the doubly promoted $4f\sigma$ state, for according to Teller the electronic energy curve for this state does not approach near to the curve for the $3d\sigma$ state until internuclear distances larger than about ten hydrogen atomic radii are reached.

The results show that the number of states in which formation of a molecule is possible increases with the degree of excitation, but the molecules in the higher excited states will be very unstable. We should therefore

TABLE I.

State.	ρ_0.	γ.	$I_0 \times 10^{40}$.	V.
$1s\sigma$	2·1 (2·0)	1·22 (1·204)	·94	2·97
$3d\sigma$	7·5 (8·9)	·37 (·350)	13·2	1·61
$2p\pi$	7·4 (7·2)	·29 (·265)	12·9	·54
$3d\pi$	8·4	·27	16·6	·27
$3d\delta$	10·4	·15	25·4	·54
$4d\sigma$	12·3	·17	35·6	·81
$4f\pi$	13·8	·20	44·8	1·21

(The results given in parentheses are deduced from Teller's results.)

where,

ρ_0=the internuclear distance, in hydrogen atomic radii, for minimum potential energy of the state under consideration ;

γ=the value of the minimum potential energy in units of $-R$, where $-R\left(=\frac{-2\pi^2me^4}{h^2}\right)$ is the energy of the ground state of a hydrogen atom ;

$I_0=\mu\rho_0{}^2a^2/2$ is the moment of inertia of the molecular ion, in its position of minimum potential energy, about a principal axis through the centre of mass perpendicular to the nuclear axis (where μ is the mass of a proton and a is the radius of the first Bohr orbit for a hydrogen atom) ;

$V=(E-\gamma)R/e$ is the energy of dissociation in volts.

expect the lines in the secondary spectrum of hydrogen to be very weak, and probably only the lowest vibrational bands are possible. The simplest way of verifying the theoretical curves would be from the moments of inertia of the molecule about a principal axis perpendicular to the nuclear axis. From Table I. it can be seen that the moments of inertia for different excited levels will lie within well-defined regions, and so should provide an excellent means of comparison with spectroscopic results.

Certain lines in the secondary spectrum of hydrogen have been assigned to transitions between excited levels

of H_2^+ by C. J. Brasefield *. He has only been able to group the lines into one series of branches so that he assumes they are Q branches. A simple calculation, however, shows that if this were true the value of ρ_0 for the final state of the ion would be less than 2·6 hydrogen atomic radii. As the lines are situated in a region of the spectrum which makes it impossible for them to be caused by transitions to the ground state of H_2^+, this identification must be wrong. In a later paper † Brasefield has determined four P, Q, and R bands, but the calculated values of the moments of inertia are again too small for them to be caused by transitions from excited states of H_2^+. These results are taken over a range in which

Table II.

ρ.	10.	12·5.	15.	20.	25.	50.
$4p\sigma$	·036	·052	·062	·076	·086	·104
$3s\sigma$	·045	·061	·065			
$4d\pi$	·086	·113	·107	·099	·100	·108
$3p\pi$	·107	·117	·107			
$4f\delta$	·051	·085	·110	·120	·115	·111
$3d\delta$	·153	·152	·137			
$4d\sigma$	·129	·169	·150	·122	·116	·111
$4f\pi$	·120	·184	·185	·144	·130	·115
$5g\sigma$	..	..	..	·166	·144	·119

the frequencies are too large, according to my calculations, to include transitions from the lowest vibration levels of the second excited electronic states to the first excited electronic states. There are few other experimental results available, and so it would appear that the analysis of the hydrogen spectrum is not yet sufficiently advanced to give any satisfactory check to the theoretical curves.

The results in Table II. give the potential energies in units of $-R$ for the second excited states, and were taken from fig. 3 *b* for values of ρ up to fifteen hydrogen atomic radii. Consequently, for these results there is

* C. J. Brasefield, Proc. Nat. Acad. of. Sc. xiv. pp. 686–689 (1928).
† C. J. Brasefield, Phys. Rev. xxxiii. pp. 925–931 (1929).

not much accuracy in the third decimal figure. For larger values of ρ the potential energies were calculated by the Stark effect method, and are probably correct to this order of magnitude.

Note on Formulæ used.

The potential energies for large internuclear distances, used in the method given above, and calculated from the Stark effect of the field due to a proton (taken as being $e/(\rho a)^2$ on a hydrogen atom, are obtained from the following formulæ :—

Energy from the first order Stark effect

$$E' = -R\{1/n^2 + 3(n_1 - n_2)n/\rho^2).$$

Energy from the second order Stark effect

$$E'' = -R \cdot \tfrac{1}{8}(n/\rho)^4\{17n^2 - 3(n_1 - n_2)^2 - 9m^2 + 19\},$$

where R, h, n, and m have previously been defined and n_1, n_2 are parabolic quantum numbers, defined by Sommerfeld *, which can take the values 0, 1, 2 . . . etc.

The electronic energies given by the Stark effect are

$$E_e = E' + E'' - W(\rho) = E - W(\rho),$$

where

$$W(\rho) = 2R/\rho$$

is the Coulomb interaction energy of the nuclei.

It has already been mentioned that nodal reasoning similar to that given by Morse and Stueckelberg was used to correlate the levels at large internuclear distances with those at short internuclear distances. The quantum numbers n_1 and n_2 are equal to the quantum numbers n_ξ and n_η used by Morse and Stueckelberg, although the separation into parabolic coordinates is not the same. The electronic energy curves (fig. 3 *a*) agree with the schematic arrangement given by F. Hund †.

The author wishes to express his thanks to Dr. W. H. McCrea for the kind interest he has taken in the preparation of this paper.

* A. Sommerfeld, 'Wave Mechanics,' p. 155 (1930).
† F. Hund, *Zeit. f. Physik.* xl. p. 756 (1927).

LXXIX. *A New Method of Colorimetry.* *By* Dr. R. A. Houstoun, *Lecturer on Physical Optics in the University of Glasgow* *.

ALTHOUGH it has been well known for more than seventy years that all colours can be produced by superposing three coloured lights on a screen, and that consequently any colour can be accurately specified by three numbers, no method of specifying colour in this way is in general use. One reason for this is that there is on the market no simple instrument for the measurement of colour which is based on the theory of colour. I have consequently endeavoured for some years to devise such an instrument. My first attempt is described on p. 431 of the 'Proceedings of the International Congress of Photography' in 1928. My second instrument, which was much more successful, is described on p. 199 of the 'Transactions of the Optical Society,' vol. xxxiii. (1931–32).

This instrument has been considerably improved in the past year. The wedge for mixing the colours has been replaced by a rectangular block, the length, height, and breadth of which are respectively 10 cm., 1 cm., and 5 mm. Three different blocks of the same length and height, but of breadths 2·5 mm., 5 mm., and 10 mm. were tried, and the intermediate breadth was found the most satisfactory. As a consequence of the change the mixing of the colours is now perfect, and the quantity of each primary colour directly proportional to the area of the end it covers. At least no deviation has as yet been detected. The rack and pinion motion for the filters has been replaced by a double micrometer, and instead of sealing the filters in glass the gelatine film has been cemented directly to a brass frame by means of Rawlplug Durofix. In this way it is quite easy both to get a better contact of the two components of each filter and also to bring the planes of the filters closer together.

But while this instrument satisfies all my requirements of accuracy and simplicity its calibration is not so simple. The straightforward method is to use the three "unitary stimuli" of the National Physical Laboratory, namely, 700 mμ, 546·1 mμ, and 435·8 mμ, together with a gas-filled lamp operated at a specified colour-temperature. In

* Communicated by the Author.

addition to the standard gas-filled lamp this requires a mercury arc and at least three filters. The operation presents no difficulty to the man who is regularly doing colour work, but the worker in a school laboratory or in a small college who wishes only to make an occasional absolute colour measurement might find the requirements as to auxiliary apparatus rather exacting. I have consequently thought it worth while to investigate a new method of colorimetry altogether. The matter has become urgent since the Commission Internationale de l'Éclairage held at Cambridge in 1931. The recommendations of that body as to the specification of colour will be ignored

Fig. 1.

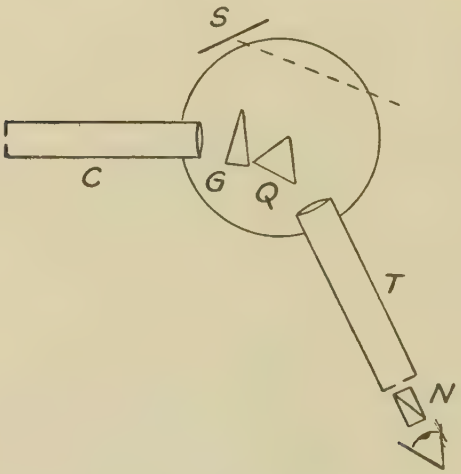

Colour-mixing spectrometer.

by the general physicist, unless an inexpensive and simple method is provided by which he can make absolute measurements of colour himself.

My new method employs a spectrometer, and is represented in plan in fig. 1. The collimator C has a symmetrically opening slit. G is a glass prism and Q a quartz prism cut with its axis parallel to the refracting edge. Two spectra are consequently formed, polarized respectively in the horizontal and vertical planes. Both prisms are set at minimum deviation for Na light, the least deviated image being used in the case of the quartz prism. The telescope T is provided with a Maxwell

slit instead of an eyepiece, and behind this slit rotates a nicol with perpendicular ends. The eye looking into the instrument sees the second face of the quartz prism. This is illuminated by two different colours corresponding to the different spectra superposed on the Maxwell slit, and the relative proportions of these colours can be altered by rotating the nicol. Table I. gives the wave-lengths which are superposed :—

TABLE I.

450 mμ	549 mμ	495 mμ	631 mμ
455	559	500	639
460	568	505	648
465	577	510	658
470	586	515	668
475	595	520	677
480	604	525	686
485	613	530	695
490	622	535	703

It should be stated that the coincidences in this table are only slightly affected by a small displacement of the prisms. The degree of superposition depends principally on the angles of the prisms and the indices of refraction of the glass. The angles of the quartz and glass prisms are respectively 60° 3·1′ and 29° 52·2′, and the refractive index of the glass is 1·5258, 1·5290, 1·5339, and 1·5387 respectively for the four helium lines 6678, 5876, 5016, and 4471 Å.

The second and third columns of Table II. give the internationally accepted colour coordinates for the above thirty-six wave-lengths *. Each colour has a third co-ordinate y, but as $x+y+z$ is always equal to 1, the latter is superfluous.

The thirty-six points are entered in the colour diagram in fig. 2, and corresponding wave-lengths joined by straight lines. When the nicol is rotated, the colour of the field travels from end to end of a straight line. The dotted line joins the extreme ends of the spectrum locus.

* T. Smith and J. Guild, " The C.I.E. Colorimetric Standards and their Use," Trans. Opt. Soc. xxxiii. p. 73 (1931-32).

TABLE II.

λ.	x.	z.	E_λ.	Value.
450	·157	·826	·235	·245
455	·151	·826	·238	·269
460	·144	·826	·242	·267
465	·135	·825	·245	·270
470	·124	·818	·248	·241
475	·110	·804	·251	·213
480	·091	·776	·254	·180
485	·069	·731	·257	·161
490	·045	·660	·259	·138
495	·023	·564	·262	·128
500	·008	·453	·265	·122
505	·004	·341	·268	·121
510	·014	·236	·270	·146
515	·039	·149	·273	·166
520	·074	·092	·276	·193
525	·114	·060	·278	·218
530	·155	·039	·280	·240
535	·193	·025	·283	·280
549	·294	·007	·289	·481
559	·366	·003	·293	·567
568	·430	·001	·297	·652
577	·492	·001	·301	·743
586	·551	·001	·304	·813
595	·603	·001	·308	·835
604	·644	·000	·311	·822
613	·675	·000	·315	·772
622	·695	·000	·317	·656
631	·709	·000	·320	·520
639	·718	·000	·322	·403
648	·725	·000	·324	·282
658	·729	·000	·327	·160
668	·732	·000	·330	·096
677	·733	·000	·332	·061
686	·734	·000	·334	·027
695	·735	·000	·336	·017
703	·735	·000	·338	·011

It will be observed from the diagram, that with the exception of the saturated pinks and purples all actual colours can be matched directly.

It is impossible to use a quartz prism alone, because the relative displacement of the spectra is then too great. The purpose of the glass prism is to diminish this separation.

Fig. 2.

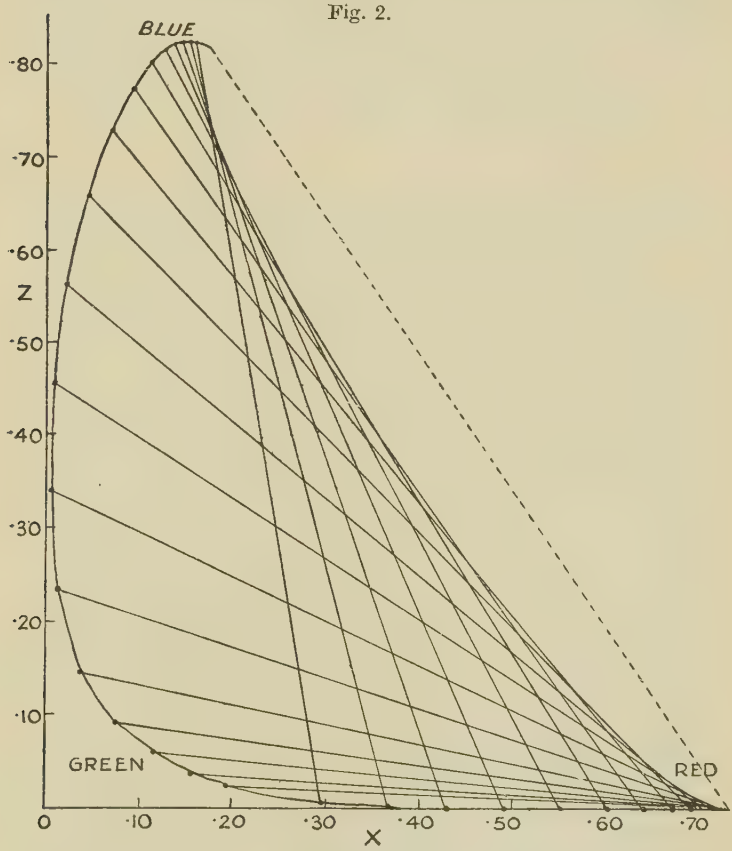

Colour diagram.

The prism chosen was the most suitable at my disposal in the laboratory. If this method of colorimetry finds favour, it will be worth while cementing the two prisms together and making a mathematical examination of the best glass or combination of glasses to employ, but the present arrangement is quite sufficient to explore the possibilities of the method.

The eyepiece slit was $\frac{1}{5}$ mm. broad. As the focal length of the telescope object glass was 24 cm., this subtended 2·9′. The collimator slit subtended usually the same angle, and the spectrum from 450 mμ to 703 mμ measured 94′ or 98′, according to which was taken.

In order to find the coordinates of a colour once it is matched, the spectrum locus must be set down on squared paper and the transversal obtained from the position of the telescope. The position on the transversal must then be obtained from the nicol reading. But before describing how this is done it is necessary to go into the question of the source.

Two sources were tried, a small Pointolite and a 220 volt Pearl Osram run at 250 volts. A magnesium oxide surface was placed at S (fig. 1) and illuminated at 45° by a 150 C.P. lamp which travelled along a rail. In this way it was possible to measure the brightness at various points of the spectrum, and it was found that when the Pearl Osram was used and the slits had the value specified above, an illumination of 1500 metre candles on the magnesium oxide surface matched the spectrum at 638 and 495 mμ, while an illumination of 230 metre candles matched the spectrum at 670 and 468 mμ. The area of the pupil was probably about one square millimetre. Thus with the Pearl Osram the brightness of the field was just sufficient to prevent the Purkinje phenomenon from being an appreciable source of error; for this pupil different authorities state the limit at values ranging from 70 to 1000 metre candles. With the Pointolite it was possible to get the spectrum 20 times as bright with the same slit widths. But the illumination of the face of the quartz was in this case often patchy, so the use of this source was abandoned.

When the Pearl Osram was run at 250 volts, its colour temperature, *i. e.*, the temperature of the black body which has the same colour, was found to be 2841° K. The measurement was made by a spectrophotometric comparison with the Hefner lamp for the wave-lengths 6678 and 5016 Å. It was assumed that the Hefner lamp radiated like a black body of temperature 1875° K. The energy distribution of the spectrum was then calculated by Wien's law,

$$E_\lambda = C_1 \lambda^{-5} e^{-c_2/\lambda T},$$

for $c_2=14350$, and is given in the fourth column of the table in arbitrary units. The result was multiplied by the visibility, the value for the standard observer being employed, and by the slit width correction $d\lambda/ds$. The latter was obtained graphically from the calibration curve. The next point to attend to was loss of light in the instrument. It was assumed that absorption in the lenses, glass and quartz prisms, and nicol would affect all colours to the same extent. These had no visible colour when examined with a contrast filter, so the assumption cannot be far out; in any case I have not the equipment for making a measurement of this absorption.

The reflexion losses are, however, an important factor, as they vary with the state of polarization of the light. Now the electric intensity in the least deviated spectrum is parallel to the refracting edges of the prisms; the electric intensity in the other spectrum is at right angles to this direction. Consequently the least deviated spectrum suffers a greater reflexion loss. The ratio of intensity transmitted for the two spectra is 1 to 0·744, when worked out on the basis of the mean values $\mu=1{\cdot}529$ for glass and $\mu=1{\cdot}537$ for quartz. As it is the blue end of the least deviated spectrum that is used, the results for the first eighteen wave-lengths in Table II. were multiplied by 0·744. The figures then give the variation with wave-length of the brightness of the two overlapping spectra.

It is, however, not brightness that counts in fixing the position of the compound colour on the diagram, because each wave-length has a different unit of brightness. The values of this unit are given in the column y of Table IV., in the paper by T. Smith and J. Guild already referred to, at intervals of 1 mμ throughout the spectrum; my results were divided by this unit, and the final result is given in the last column of Table II. This table gives the value of the different wave-lengths for colour-mixing purposes.

As a check on the calculations the colour of the Hefner lamp was measured. A piece of ground glass was placed at S (fig. 1), and the lamp was placed immediately behind it. Balance was obtained on the transversal that ends at $x=\cdot55$. The wave-lengths mixed were consequently 586 and 470 mμ, the "values" of which are 813 and 241. The setting of the nicol was 24·6° from the position that

totally extinguished the blue. The quantity of yellow was consequently

$$813 \cos^2 24{\cdot}6^\circ$$

and of blue

$$241 \sin^2 24{\cdot}6^\circ.$$

The ratio of blue to yellow is therefore

$$\frac{241}{813} \tan^2 24{\cdot}6^\circ = {\cdot}06213.$$

The point is consequently $\frac{621}{10621}$ of the length of the transversal from the yellow end. The coordinates of this point were found graphically to be $x=0{\cdot}529$, $z=0{\cdot}045$.

In order to check the result I wrote to Mr. Guild for information about the value of these constants. In reply he stated that the Hefner lamp had not been measured at the National Physical Laboratory, but that the black body at 1875° K with which it is said to correspond, had the coordinates $x=0{\cdot}5400$, $z=0{\cdot}0493$. The agreement seems satisfactory enough, when we consider that my determination is the first by a new method.

The amount of calculation involved in determining the "values" of the wave-lengths is great, but has only to be done once for all, and the method works directly in terms of x and z, *i. e.*, we have not to use provisional primaries as in other colorimeters and evaluate afterwards in terms of x and z. Also the apparatus, spectrometer and nicol eyepiece, is such as to be found in any laboratory, and the operations, setting to minimum deviation and adjusting a nicol are of a kind with which every physicist is familiar. Once the apparatus is installed there is little scope for error, though the colour temperature of the source would have to be checked from time to time.

The nicols which are supplied for fitting over the object glass of a telescope have, as a rule, too small an aperture to give accurate results. But if the nicol were big enough it would work quite as well here.

The telescope and nicol readings might themselves be taken as colour coordinates, as they define a colour completely. But they have the disadvantage that they specify the colour at the intersection of two transversals in two different ways.

Note added on correcting the proof, September 21st.—It will be observed that where two transversals intersect the coordinates of the colour are given without using brightness considerations. We are then quite independent of the colour temperature of the source that illuminates the slit. As this method promises great advantages, it is being tested at present with a new arrangement in which an Iceland spar prism is combined with a glass prism. Results will be published in due course.

LXXX. *The Structure of Thin Celluloid Films.*—II. *By* E. Taylor Jones, *D.Sc., Professor of Natural Philosophy in the University of Glasgow* *.

[Plate XXIX.]

IN a recent communication † the writer described a diffraction pattern obtained by transmission of cathode rays through a thin film of celluloid, which could be analyzed into four component patterns or groups of spots, all explicable as being due to reflexions by planes of the same space lattice turned into four positions in the film. Two of the positions differ from each other by a rotation about an axis normal to the film, the other two from these by a rotation about a certain line in the plane of the film parallel to one of the principal axes of the lattice, and probably parallel to the length of the molecular chains of the material.

From the fact that several of the transmitted pencils showed evidence of having been diffracted twice it was concluded that the positions of the lattice which differ by a rotation about a principal axis were in superposed layers of the film, the portion of the film through which transmission took place therefore consisting of two adjacent areas, each occupied by double-layer film, with a break in the chains, or a bend through a certain angle, at the boundary separating the areas.

Another feature of the pattern described in the former paper was that the six spots of the "first ring," easily distinguishable from the others by their much greater

* Communicated by the Author.

† Phil. Mag. xvi. p. 793 (1933).

intensity, lay not on a circle (as is frequently the case), but on an ellipse, two being at the ends of the major axis and the other four at the ends of a pair of equal diameters *. Measured along the length of the major axis the positions of the four latter spots are midway between the centre and the first two, and their distances from the major axis indicate that the spacings of the reflecting lattice planes perpendicular and parallel to the major axis are to a close approximation in the simple ratio 3/2.

In the present communication two other patterns, obtained with celluloid films, will be described which show some of these features but which differ from the pattern just referred to in the number of groups of which the patterns are composed. One of them, in fact, consists of three, the other of two, component groups. Both patterns show evidence of the existence of twice-diffracted pencils.

Beginning with the more complicated pattern (which includes the other as two of its components) the photograph is shown in figs. 1 and 2 (Pl. XXIX.). As before, two copies of the same photograph are reproduced, one (fig. 1, Pl. XXIX.) to show the details of the central portion, the other (fig. 2, Pl. XXIX.) to bring out the outlying parts of the pattern. The methods of taking the photograph and measuring the diametral distance of each spot (*i. e.*, the distance of the "head" of each spot from that of the spot diametrically opposite to it) were precisely the same as those described in the previous paper. The exposure was 3000 flashes of maximum potential 52·5 *k*V.

The six intense diffracted spots in fig. 1 (Pl. XXIX.), representing the first ring, lie on an ellipse the major axis of which is horizontal and 9·5 mm. long in the original photograph. Two of these spots lie at the ends of the major axis, and the other four have diametral distances of 8·7 mm. It will be noticed that by far the greater number of the other spots in figs. 1 and 2 (Pl. XXIX.) lie at equal intervals on horizontal lines which are themselves spaced at equal distances above and below the centre of the pattern.

* For some purposes it is convenient to regard the six spots as lying on two concentric circles, four on the inner circle and two on the other.

The pattern is also shown in the diagram of fig. 3, the spots in which represent the "heads" of the radial streamers of the photographs. The relative intensity of the spots is roughly indicated in fig. 3 by their size, and for convenience in reference the spots in one quadrant of the figure are numbered or lettered.

The spots are divided into three groups—those numbered 1, 2, 3, . . . $\bar{1}$, $\bar{2}$, . . . forming what we shall call the *first*

Fig. 3.

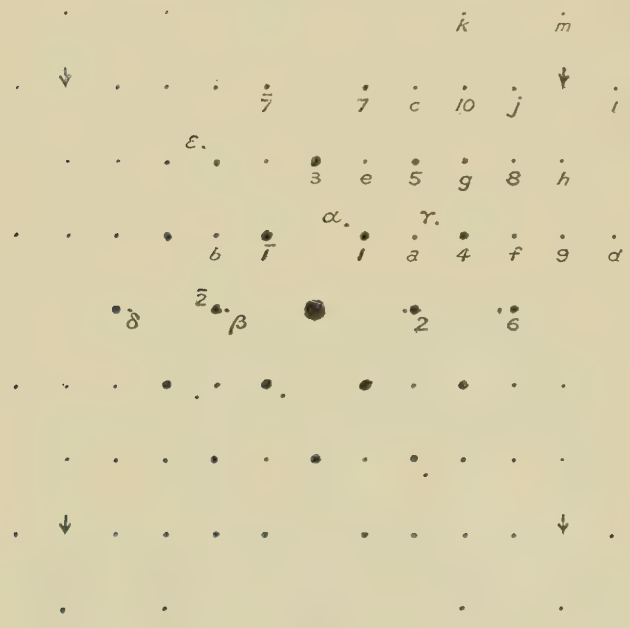

or *principal* pattern; those marked *a*, *b*, *c* . . . will be called the *second pattern* (this group includes certain spots formed by two reflexions); and the *third pattern* is marked α, β, γ . . .

The First Pattern.

Again assuming that the lattice planes which produce the diffracted pencils are normal to the film, the necessary glancing angles being provided by the slight curvature of the film, we find that all the spots of the first pattern can be accounted for by a lattice the projection

of which on a plane parallel to the surfaces of the film is shown in fig. 4. The projection shows an array of points arranged in triangular order, the principal axial ratio (*i. e.*, the ratio of AH to AE) being 3/2. The greatest

Fig. 4.

First Pattern.

No. of spot.	D/D_1.	Lattice planes.	Spacing ratio.	Spacing ratio $\times D/D_1$.
1	1	AM	1	1
2	1·095	AE	0·901	0·987
3	1·645	AH	0·601	0·989
4	1·86	AK	0·537	0·999
5	2·0	AM_2	1	2
6	2·21	AE_2	0·901	1·99
7	2·55	AL	0·391	0·997
8	2·78	AP	0·360	1
9	2·90	AR	0·345	1
10	2·97	AM_3	1	2·97

spacing of normal planes is that of the planes parallel to AM or AN, which produce the spots 1, $\bar{1}$, and their opposites, these being the nearest to the centre of the pattern (fig. 3). The diametral distance of these nearest spots being denoted by D_1, the diametral ratios D/D_1

for all the other spots in the upper right-hand quadrant of the first pattern (fig. 3) are collected in the Table, with the corresponding lattice planes (fig. 4) and the ratio of the spacing of the planes to the greatest spacing. The diameters D were measured on the original negative, and the spacings were calculated from the lattice of fig. 4. The last column of the table shows the product of the diametral ratio D/D_1 and the spacing ratio. When allowance is made for the order of the reflexion (indicated by the suffix in AM_2 etc) the numbers in the last column are seen to be practically constant and equal to unity, showing that the distances of the diffracted spots from the centre of the pattern are correctly accounted for by the lattice of fig. 4. It is easily seen that the directions of the spots with respect to the centre of the pattern are parallel to the normals of the corresponding lattice planes, and it follows from the horizontal and vertical symmetry of figs. 3 and 4 that the spots in the other quadrants of the first pattern are equally well explained by the same lattice.

It should be added that the proportions and the absolute dimensions of the lattice represented in fig. 4 are identical with those of the lattice responsible for the formation of a "principal pattern" described in the previous paper, to which reference has already been made.

The Second Pattern.

It will be seen in the photographs of figs. 1 and 2 (Pl. XXIX.), or in the diagram (fig. 3), that the second pattern consists of a group of much weaker spots, *a*, *b*, *c*, . . . all of which lie in the same horizontal lines as the spots of the first pattern and in positions midway between them. The nearest to the centre are those marked *a*, *b* and their opposites, these having in the original photograph a diametral distance of 12·2 mm.

We notice that in fig. 3 the spots *a*, *b* are twice as far from the vertical axis of the figure (*i. e.*, the line joining the spot no. 3 to the centre) as are the first-pattern spots 1 and $\bar{1}$, and this suggests that the lattice which produces the spots of the second pattern has the same vertical dimension but only one-half the horizontal dimension of that of fig. 4, and can be set into the correct position by a rotation of the lattice of fig. 4 through 60° about

a line parallel to AE. This was the explanation suggested in the former paper for the formation of the "secondary patterns," and, as there explained, it is based upon the assumption that fig. 4 may be regarded as representing an actual net-plane (not merely a projection of the lattice), and that the parallel planes above and below it are spaced at intervals of $AH/\sqrt{3}$.

The projection of the rotated lattice on a plane parallel to the surfaces of the film is shown in fig. 5. The normal planes having the greatest spacing, and being therefore responsible for the spots *a*, *b* and their opposites, are those parallel to AF and AG. Normal planes parallel to AE and to ST (fig. 5) give rise to spots which coincide with spots of the first pattern (viz., nos. 6 and 3), and

Fig. 5.

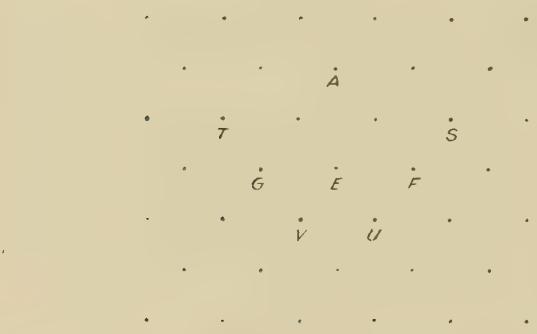

therefore cannot be expected to be visible in the photograph.

The only other visible spots of the second pattern which are formed by a single reflexion are those marked *c* and *d* and their opposites, with corresponding spots in the other two quadrants of fig. 3. The diametral ratios for these spots are 1·93 and 2·40 respectively, the corresponding spacing ratios (planes AS, AT, and AU, AV 0·508 and 0·404, the latter numbers being with fair approximation the reciprocals of the former.

All the other spots, *e*, . . . *m*, of the second pattern appear to be formed by twice-diffracted pencils, showing that the first and second patterns are formed in different layers of the film through which the rays pass in succession. Thus the spot *e* is derived from the pencil

to $\bar{1}$ as a is from the primary pencil; the spot f in the same way from the pencil to no. 2; g from no. 1; h from 4; j from 2 as c is from the primary pencil; k from 7; l from 3 or 6; and m from $\bar{7}$.

It will be noticed that the four positions marked ↓ in fig. 4 are vacant, though the neighbouring spots j and l are present. The vacant positions should be occupied by first-pattern spots, the absence of which is probably due to the curvature of the film being insufficient to allow normal planes to reflect rays at such a large angle. The spots k, l, m, still further from the centre, are, however, present because they are produced after two reflexions (by different normal planes of the film), the resultant deflexion due to which is greater than that which can be produced in a single reflexion by any of the normal planes.

Another conceivable mode of derivation of the second pattern may be mentioned here, though it does not appear to the writer to offer the correct explanation of this group. In fig. 3 the spot a of the second pattern is seen to be exactly midway between the centre and the first-pattern spot no. 8, and might therefore be thought to be a "half-order" spot of the first pattern. In a similar way all the spots of the second pattern might appear to be half-order spots of the first. An attempt to account for the second pattern on these lines by a lattice having net-planes alternately strong and weak in scattering centres was, however, not successful.

The Third Pattern.

The third pattern is a group of rather faint spots each of which is very near a spot of the first or of the second pattern. The nearest to the centre are α, β (fig. 3) and their opposites, these being slightly further from the centre than the innermost spots 1 and $\bar{1}$ of the first pattern, their diametral distance being 8·8 mm. The line joining γ to its opposite is parallel to and twice as long as $\alpha\beta$, and the line joining ϵ to the centre is perpendicular to these lines. The spot ϵ is not visible in the photographs of figs. 1 and 2 (Pl. XXIX.), but it is clearly seen in some of the other plates taken with the same film. It is probably the second order of a spot hidden in the "tail" of the strong first-pattern spot $\bar{1}$.

The ratio of the diametral distances of ϵ and γ is 4/3, and, the former being regarded as a second-order spot, it is clear that the third pattern is produced by a lattice of principal axial ratio 3/2 and of practically the same dimensions as that responsible for the first pattern. The spot δ is clearly the second order of β. It will be observed that there are no spots corresponding to γ in the second and fourth quadrants of fig. 3 and none corresponding to ϵ in the first and third quadrants.

There is no evidence of the existence in the third pattern of spots resulting from two reflexions, and we conclude that this pattern is formed in a portion of the film which is adjacent to (not above or below) that in which the first pattern originates. The angle between the principal axes of the first and third lattices (*i. e.*, the angle between the line joining the spots γ and the vertical axis of fig. 3) is 56° 19′. Probably only a small portion of the primary pencil is transmitted through the region of the film in which the third pattern is formed.

In addition to these three patterns there are, in figs. 1 and 2 (Pl. XXIX.), faint traces of other spots not sufficiently numerous to enable their complete patterns to be identified, and the continuous concentric circular rings frequently found in photographs taken with celluloid films are also present.

The other photograph, showing a pattern of the same type as that of figs. 1 and 2 (Pl. XXIX.), but simpler, is reproduced in fig. 6 (Pl. XXIX.) *. It was taken with another celluloid film and an exposure of 1800 flashes at a sparking potential of 40 kv.

The pattern in fig. 6 (Pl. XXIX.) is clearly identical with the first and second patterns of figs. 1 and 2 (Pl. XXIX.), and it shows the same evidence of having been formed in two superposed layers of the film, the lateral dimension of the lattice in one layer being one-half the corresponding dimension in the other. There is evidently a tendency in celluloid films to this kind of double-layer formation,

* The photograph of fig. 6 (Pl. XXIX.) was printed from the negative through a diaphragm which allowed the central portion to be submitted to greater exposure than the more distant parts. It therefore does not show in correct proportion the relative densities at different distances from the centre.

and, as already remarked, the suggestion was made in the previous paper that the apparent lateral contraction of the lattice is due to a rotation of the material through 60° about a certain direction parallel to the plane of the film. This seems to be the most probable explanation of the contraction, but it is not the only explanation that could be offered. It may be, for instance, that the two layers are of different substances, the width of the molecular chains in one being one-half the width in the other. There is, however, no other evidence, so far as the writer is aware, of such large variation in the chain-width in cellulose and its nitrates.

Natural Philosophy Department,
The University, Glasgow.
July 1933.

LXXXI. *Nature of Polish Layers.*

By J. A. Darbyshire *and* K. R. Dixit *.

[Plate XXX.]

Introduction.

In a recent paper French † examined by means of electron diffraction the surface layers of copper, silver, gold, and chromium after various degrees of polishing. He commenced by polishing on No. 0 emery, using benzene as lubricant, and followed on with 00, 000, 0000 emery, taking photographs at each stage ; finally using chromium oxide or rouge on chamois. He observed that the rougher surfaces gave polycrystalline rings characteristic of the metal concerned, but these became more and more diffuse as the surfaces became smoother, and the highly polished surfaces gave only two very diffuse rings.

The metals he examined were all cubic, and in these cases the ring-system for the polycrystalline material could be regarded as being built up of two main groups. Thus the rings from the planes 111 and 200 go together to form the first, and 220, 311, 222 to form the second. A third group, comprising 331, 420, 422, 333, might also

* Communicated by Prof. G. P. Thomson, M.A., F.R.S.
† R. C. French, Proc. Roy. Soc. A, cxl. p. 637 (1933).

be considered, but in general this would be much weaker than the first two. If the individual rings comprising these groups were diffuse we would expect to get merely two diffuse rings on the plate.

French points out that his results may be considered as supporting the theory of Sir George T. Beilby *, who suggested that the surface layer of a highly polished metal is amorphous and resembles closely a supercooled liquid. French draws attention to the fact that it is not possible to decide whether this liquid layer is to be regarded as a monatomic liquid or as a molecular liquid, the molecules being possibly colloidal particles of actual crystalline material—that is, it is impossible to say definitely whether the diffuse rings are due to interatomic interferences in accordance with the Ehrenfest formula as described later, or to lattice interference from very small crystallites (colloidal particles). The metals he examined are all situated near the minima of the atomic volume curve, and the evaluation of the interatomic distances gives almost exactly the same result whichever way the effect is regarded, corresponding closely in each case to the value observed by X-ray crystallography. In either case the results may be taken as confirmation of Beilby's theory, since for this the very small crystallites arranged at random may be regarded as a liquid layer almost as much as if the particles were individual atoms arranged at random.

The metals examined by French have very nearly the same density in the molten as in the solid state, and so we should expect the interatomic distances to be the same for a layer of truly amorphous nature (monatomic liquid) as for the colloidal or crystalline layer. Thus the metals he examined do not give very definite information as to the real nature of the polished surface.

In the case of certain metals such as bismuth there is a marked contraction of volume when passing from solid to liquid, and the present work was undertaken in the first place to see if a corresponding change could be observed in the interatomic distances as revealed by the diffuse rings which are obtained when an electron beam is reflected from the polished surface of such a specimen. Instead of the small contraction expected, which would

* Sir G. T. Beilby, ' Aggregation and Flow of Solids.'

have been hardly beyond the limits of experimental error, a very considerable contraction was found. This seems to indicate that here the liquid layer is of very high density, and it was then decided to examine as many metals as possible to see if similar discrepancies appeared in other cases. The following elements were polished and examined :—Bi, Sb, Zn, Te, Cd, Au, Ag, Pb, Mo, Cu, Cr, Se, Si. The last two have very high electrical resistance, but the others are all fairly good conductors. In addition we studied the semiconductors, galena (PbS), and iron pyrites (FeS_2).

Method of Working.

The apparatus used to take the electron diffraction photographs was similar to the one designed originally by Professor G. P. Thomson * for reflexion experiments. Most of the metals examined were polycrystalline aggregates, although in the case of antimony, bismuth, zinc, and tellurium single crystal specimens were also examined after polishing. The metals were ground down successively, commencing on 0 emery and working up to 0000, using benzene as lubricant. Then the specimens were polished on chamois, using a finely decanted suspension of chromium oxide in distilled water. Photographs were not taken at each stage, but generally only after a highly polished surface had been obtained. In one or two cases intermediate photographs were taken to investigate special points.

The surfaces were carefully washed with benzene, ether, and other solvents in order to remove all traces of grease. It was suspected at first that perhaps the rings had nothing to do with the polished layers, but were due to grease or a film of gas, or, perhaps, preferential orientation.

Numerous experiments were carried out to prove that the observed effects could not be due to such causes. Thus the surfaces were photographed after washing with ether in successive stages, but no perceptible diminution in the intensity of the rings could be detected. Various polishing materials were used, but all gave very similar effects. The results were also reproduced consistently by different observers using different apparatus. A

* G. P. Thomson and C. G. Fraser, Proc. Roy. Soc. A, cxxviii. p. 641 (1930).

number of photographs were taken by reflexion from very smooth cleavage planes of single crystals of Zn, Te, Sb, and Bi, but diffuse rings were in general not observed. In one or two exceptional cases there were traces of similar rings, and it is possible that under certain conditions an amorphous layer is left on the surface after cleavage has taken place. These rings were always much weaker than the rings obtained by polishing. These results may be taken to exclude the possibility of gas films giving the effects described, because such films would have been equally evident in the case of these cleaved surfaces.

In Table I. the observed $\frac{d}{n}$ values for the two rings are given. These are derived directly from the Bragg

TABLE I.

$\frac{d}{n}$ values for the two rings.

	Bi.	Sb.	Zn.	Te.	Cd.	Au.	Ag.	Pb.	Mo.	Cu.	Cr.	Se.	S
First ring ...	2·24	2·25	2·40	2·30	2·37	2·34	2·27	2·40	2·38	2·28	2·24	2·90	2·
Second ring .	1·25	1·24	1·28	1·25	1·28	1·29	1·23	1·31	1·27	1·26	1·23	1·54	1·
Ratio	1·81	1·82	1·88	1·84	1·85	1·82	1·85	1·84	1·88	1·83	1·82	1·89	1·

equation $n\lambda = 2d \sin\theta$. The ratio of these two quantities are also given in the third line. The $\frac{d}{n}$ spacings given here are essentially experimental and have no direct interpretation as in the case of the plane spacing for a crystalline solid. They are related to the interatomic distance in the amorphous polish layer by a factor which will be dealt with more fully later on.

The ratio to be expected theoretically from the Ehrenfest formula $I = 2N\psi^2\left(1 + \frac{\sin x}{x}\right)$ is 1·84. This is evidence in favour of the assumption that the diffraction is due to a model of the kind considered by Ehrenfest. A typical photograph from polished cadmium is reproduced in fig. 1 (Pl. XXX.) showing the two diffuse rings.

In the case of the trigonal metals Sb, Bi the rings

could be explained to some extent by assuming preferential orientation with the trigonal axis parallel to the direction of the electron beam. However, the effects did not change in any way when the specimen was rotated about an axis normal to its surface ; hence it seems very improbable that this could be the explanation of the observed rings. Similarly in the case of the cubic metals no consistent explanation by preferential orientation could be given.

The spacings deduced from the rings for any one polished material were in good agreement in the different photographs. The values given in the table are the mean obtained from six photographs of each material. The experimental error is rather large on account of the very diffuse nature of the rings, but the $\frac{d}{n}$ values are accurate within 8 per cent. in all cases.

The results obtained are rather unexpected, and so every precaution was taken to eliminate external influences such as grease or gas, and we believe that the diffraction is definitely due to the atoms of the various elements forming the polished layer. In all cases two diffuse rings were visible, although in the case of bismuth alone other feeble rings were sometimes seen. Bismuth is very soft and behaved differently in a number of ways from the other metals. Also it was found that the polish layer in bismuth could easily be rubbed off by slight pressure on a piece of paper. We found that when the specimen polished was a single crystal, the surface appeared to have a still higher polish after treatment in this manner, but the photographs gave a well defined cross-grating * pattern and there was no trace of the usual polish rings. If the metal were polycrystalline feeble polycrystalline rings were observed after rubbing gently on paper. The other metals did not behave like this, and the polish layer seemed to be quite well attached to the surface. Brisk rubbing on rough paper sometimes produced scratches, and traces of polycrystalline rings were then observed.

Discussion.

As already remarked, the presence of the two rings observed by French did not enable him to decide whether

* Kirchner and Raether, *Phys. Zeit.* xxxiii. p. 510 (1932).

the surface layer was a truly amorphous (monatomic liquid) layer or merely a very finely divided layer (colloidal). The amorphous point of view receives strong support from the fact that we also observed only two diffuse rings from bismuth, antimony, and tellurium. If we consider the ordinary polycrystalline rings of these substances to become blurred, as they would for small particle size, they will not group together to form merely two diffuse rings as in the case of the face-centred cubic substances. Thus the evidence seems to point to a complete breaking up of the lattice structure, and suggests that the atoms are then packed together at their distance of closest approach as in a monatomic liquid. The striking thing about our results is that this distance of closest approach is apparently much less in some cases than the corresponding distance in the actual crystal lattice.

If we assume the Ehrenfest formula to hold good for the diffraction by such a layer, we have for the intensity of the diffracted beam in any direction inclined at an angle ϕ to the incident beam

$$\mathrm{I}=2\psi^2\mathrm{N}\left(1+\frac{\sin x}{x}\right), \quad . \quad . \quad . \quad . \quad . \quad . \quad (1)$$

where N is the total number of atoms concerned, ψ is a monotonic function of ϕ representing the amplitude of the wavelet scattered by an atom in any direction (ψ is the atom form factor, or "f" curve, for electrons), and

$$x=\frac{4\pi l}{\lambda}\sin\frac{\phi}{2}. \quad . \quad . \quad . \quad . \quad . \quad . \quad (2)$$

In this formula l is the interatomic distance and λ is the electron wave-length. The formula (1) is strictly applicable only to a diatomic gas, but a much more elaborate treatment of diffraction by a liquid indicates that this formula is a good approximation in these cases. The intensity would have maximum values at $x=7{\cdot}72$ and $x=14{\cdot}06$ if ψ were constant, but if we allow for the decrease of the scattering power of the atom with increasing angle we have maxima at $x=7{\cdot}00$ and $13{\cdot}00$. These depend, strictly speaking, on the actual form of the "ψ" curve for the elements considered, but the results do not differ much for the substances we are

concerned with here, and the two maximum values of x quoted represent a mean value applicable to all materials examined here.

Since $\frac{d}{n} = \frac{\lambda}{2 \sin \phi/2}$, we have from equation (1) the following relations between the observed $\frac{d}{n}$ values and the interatomic distance l.

(1) Without f curve.		(2) With f curve.	
First max.	Second max.	First max.	Second max.
$\frac{d}{n} = \cdot 81\, l.$	$\frac{d}{n} = \cdot 45\, l.$	$\frac{d}{n} = \cdot 89\, l.$	$\frac{d}{n} = \cdot 48\, l.$

It will be seen from these figures that the effect of the "f" curve is to draw the maxima inwards in each case.

However, the diatomic gas formula (1) is not strictly applicable to our problem, and the peaks are rather sharper than would be allowed by this equation. The effect of the "f" curve in causing a shift of the maxima is correspondingly less, and a detailed calculation based on the average breadth of the diffraction rings actually observed indicates the most suitable values to be

$$\frac{d}{n} = \cdot 85 l \quad \text{or} \quad l = 1 \cdot 18 \frac{d}{n} \text{ for first maximum,}$$

$$\frac{d}{n} = \cdot 47 l \quad \text{or} \quad l = 2 \cdot 13 \frac{d}{n} \text{ for second maximum.}$$

We use these relations to deduce the interatomic distance from the observed positions of the diffuse rings.

If we regard the atoms in the polish layer as being packed closely together as in a liquid we have a simple relation given by Keesom * expressing the interatomic distance b in terms of the atomic weight and the density

$$b = 1 \cdot 33 \sqrt[3]{\frac{\mathrm{A}}{\mathrm{D}}},$$

where A is the atomic weight and D the density of the liquid. The expression $\frac{\mathrm{A}}{\mathrm{D}}$ is, of course, the atomic volume as usually defined. The density of a molten metal is in general very little different from that of the solid, and

* W. H. Keesom and J. de Smedt, Proc. Amsterdam, xxv. p. 118 (1922).

so we can insert the ordinary density of the solid in this equation in order to calculate b. This gives us the interatomic distance to be expected in a liquid layer where the atoms preserve the same interatomic distance that they have in the solid. This is very closely true for a metal in the molten state. The slight difference in density in the case of bismuth, for which the change is greatest, leads to a change of interatomic distance of less than 1 per cent. The calculated values of b for all the metals examined here are given in column one of Table II., and the observed values of l are given in the second column.

TABLE II.

	$b=1{\cdot}33\sqrt[3]{\frac{A}{D}}$.	$l=1{\cdot}18\frac{d}{n}$.	X-ray interatomic distance.
Bi	3·66	2·64	(i) 3·11 (ii) 3·47
Sb	3·45	2·66	(i) 2·87 (ii) 3·37
Zn	2·77	2·83	(i) 2·65 (ii) 2·90
Te	3·62	2·72	(i) 2·86 (ii) 3·74
Cd	3·09	2·79	(i) 2·96 (ii) 3·28
Au	2·86	2·75	2·86
Ag	2·87	2·68	2·88
Pb	3·48	2·83	3·50
Mo.....	2·80	2·82	2·72
Cu	2·55	2·70	2·54
Cr	2·55	2·64	2·46
Se	3·36	3·42	(i) 2·32 (ii) 3·46
Si.....	3·05	3·03	(i) 2·35 (ii) 3·83

We should expect these two quantities to have the same value if the polish layer is really a supercooled liquid built up of atoms of normal dimensions such as those in the ordinary solid crystal or ordinary molten metal. The interatomic distances deduced by X-ray investigation are given in column three, and it is interesting to note that they are very closely related to those given by the Keesom formula for b in the first column of the table.

It will be seen that the values of l in the second column are all appreciably constant except in the case of Se and Si. This is very surprising in view of the rapid periodic variations of b, which of course follow exactly

the periodic fluctuations of the atomic volume curve. The metals Zn, Cu, Ag, Cr, Au, Mo all lie near the lowest points of the curve. Cd and Si are higher up and Se, Pb, Te, Sb, Bi a little higher still. We then tried metals of greater atomic volumes, such as Ca, Ba, Sr, but could not obtain stable polished surfaces. These metals oxidize very readily, and no conclusions could be arrived at.

The results seem to imply that all atoms of atomic volume higher than the minimum on the curve collapse when polished. They appear to build up a liquid layer of abnormally small-sized atoms corresponding to the minimum regions of the atomic volume curve, thus forming a liquid of particularly high density. This is perhaps the reason why a polished surface oxidizes less readily than one that has not been polished.

It was then decided to test some non-conducting elements, in the hope that perhaps this contraction of atomic radius was a feature peculiar to atoms of good conductors. Unfortunately very few of the non-conducting elements will take a polish, and we were only successful in the case of selenium and silicon. The former can be very easily polished, but the latter required several hours before a polished surface could be obtained. These two specimens gave photographs of very great interest. It will be seen in Table II. that here the values of l and b are closely in agreement, and, moreover, the values of l for these two substances are considerably different from each other and also from the appreciably constant values for the conducting elements. Thus in the case of Se and Si the decrease of atomic radius does not take place, and the normal interatomic distance is preserved even in the polished layer. This difference in the behaviour of Se and Si from the conductors must in some way be associated with the binding forces controlling the outer electronic orbits, indicating some feature which distinguishes conductors from non-conductors.

As already remarked we cannot regard the rings given by Bi and Sb as corresponding to the polycrystalline rings made diffuse on account of small particle size. The same thing applies to the body-centred cubic substances such as Mo, Cr, because here the rings would be evenly spaced and could not be divided into two distinct groups. For the face-centred cubic metals, Cu, Pb, Au,

and Ag, such a grouping is possible, as already pointed out.

In Table III. the $\frac{d}{n}$ values to be expected if this were the explanation for the appearance of the two diffuse rings are given in column one. The experimentally observed $\frac{d}{n}$ values are given in column two, and the values of $\frac{d}{n}$ that we should have expected to find experimentally if the surface layer were a super-cooled liquid of normal atomic dimensions are given in column three.

Table III.

	Ring 1.			Ring 2.		
	111 200	$\frac{d}{n}$ obs.	$\frac{d}{n}$ Normal liquid.	220 311	$\frac{d}{n}$ obs.	$\frac{d}{n}$ Normal liquid.
Cu ...	2·02	2·28	2·15	1·20	1·26	1·14
Pb ...	2·77	2·40	2·95	1·62	1·31	1·57
Au ...	2·27	2·34	2·43	1·33	1·29	1·28
Ag ...	2·28	2·27	2·44	1·33	1·25	1·29

It will be seen that in all four cases the $\frac{d}{n}$ values to be expected on the colloidal particle theory are indistinguishable from those to be expected for a liquid layer of normal atomic volume—that is, the figures in the first column are in agreement with those in the third to an extent well within the errors of observation for the measurement of such diffuse rings. The observed $\frac{d}{n}$ values for the polished layers are in agreement with these also, except in the case of lead. Here the observed $\frac{d}{n}$ value is not much different from those for Au, Cu, Ag, whereas, according to the colloidal particle theory or the theory of an ordinary uncompressed liquid layer, it ought to be considerably different.

This seems to indicate definitely that the diffuse rings are not due to very small crystalline particles, and they

are therefore most probably due to a monatomic or nearly monatomic liquid layer of small atoms considerably smaller than the normal lead atom. In order to investigate this further photographs were then taken from lead at the intermediate stages of polishing, and we found diffuse rings of different spacing but corresponding to the theoretical values to be expected for rings from particles of colloidal size and in agreement with those in column one. Thus lead is a very suitable material to use in order to find whether the rings are due to finely divided polycrystalline material or to a nearly monatomic layer resembling a liquid. Apparently, however, the liquid layer is here, as in many other cases, much denser than ordinary molten metal, indicating some curious contraction of those atoms whose atomic volume is higher than the minimum values of the periodic curve.

In the case of single metal crystals the results were just the same as for polycrystalline material, although in one or two cases spots were visible in addition to the diffuse rings when the polishing had not been carried on as long as usual.

Many estimates have been made of atomic diameters, but the expression "size of atom" is quite vague, and different methods of approaching the problem give different results because various criteria are used to define the boundary. The principal methods of estimating the size are :—

(1) Bragg's estimate from crystal structure.

(2) The viscosity method developed by Rankine *.

(3) Saha's † estimate from measurement of ionization potential.

(4) Method based on ionic refraction by Wasastjerna ‡.

(5) Richards's § estimate from the compressibility of the elements.

The atomic volume varies in a periodic manner with atomic number, and it is also remarkable that the compressibilities of solid elements were found by Bridgman

* A. O. Rankine, Proc. Roy. Soc. A, xcviii. p. 360 (1921).
† M. N. Saha, 'Nature,' cvii. p. 682 (1921).
‡ J. A. Wasastjerna, *Soc. Scien. Fennica*, vi. (21), p. 1 (1932–33).
§ T. W. Richards, J. Amer. Chem. Soc. xliii. p. 1584 (1921).

and Richards * to vary periodically in a similar way. (There are minor irregularities, especially for insulators.) These similar periodic variations appear to indicate that the volumes of the atoms in a compressed state can, under certain conditions, be brought more nearly into agreement with each other than are those in the normal atomic volume curve. These results are to some extent in agreement with those given here, and possibly the polishing process involves a compression similar in principle to that carried out by Bridgman. In his experiments, however, the size of the atom was reduced only whilst the material was under compression, whereas in these experiments it appears as a permanent contraction after polishing. It is possible of course that the surface atoms are constantly under very great pressures, and thus reproduce more nearly the condition of Bridgman's experiments on compression.

It is difficult to give a theory of the reason for this contraction of atomic radius, but one or two possibilities may be discussed. In the first place it may be that the outer electrons have been excited to occupy less eccentric orbits, and if we consider the precession of these orbits around the nucleus it may be shown that they will give an atom of rather smaller diameter than would be the case for the more eccentric orbit. Such excited states are as a rule, however, very unstable, and would return to normal in a fraction of a second if the atom were subject to sufficient impact. In view of the incidence of a high-voltage electron beam which would assist a return to normal state it seems very improbable that this could be the explanation of the reduced size of the atoms. It seems more probable that in the case of the conductors the atoms are stripped of their outer electrons, but that these electrons are still moving as free conductivity electrons in the amorphous layer, apparently no longer contributing to the size of the atom as they do in the usual lattice structure. Our results would then appear to indicate that this stripping process does not occur in the case of the non-conductors. This would be in accord with what we should expect from the present views regarding the difference in binding of the outer electrons in conductors as compared with non-conductors.

* P. W. Bridgman, ' Physics of High Pressure ' (London, 1931).

Galena and Iron Pyrites.

In the case of all substances discussed so far the binding has been homopolar. Two substances were also examined in which the binding is heteropolar, namely, galena (PbS) and iron pyrites (FeS_2). In the case of galena the molecular volume is greater than the sum of the atomic volumes of the individual atoms, whereas for iron pyrites the molecular volume is equal to the sum of the atomic volumes. A photograph obtained by reflexion from the cleavage face of galena showed the usual single crystal pattern of spots, Kikuchi lines, and lines * due to a surface cross grating. The specimen was then rubbed on 0000 emery for 100 strokes in one direction, and gave surface lines along with two faint rings. After another 100 strokes it showed a number of fairly sharp rings typical of powdered galena (Pl. XXX. fig. 2). It was then rubbed for another 200 strokes at right angles, and the rings became more diffuse. After polishing on chamois with chromium oxide the rings became very blurred (Pl. XXX. fig. 3), although it was observed that they became sharp again if the polishing was prolonged, and then diffuse again, and so on. It was not possible to detect any difference by eye during these changes, nor could any difference be observed under the microscope. The surface maintained a good polish appearance throughout these experiments Galena is very soft, and it is possible that the crystallites can be reduced to a certain small size by polishing, but are then very readily removed, leaving a rougher surface for further polishing. This effect was consistently observed with three different specimens polished parallel to the cleavage plane (100) and also in the case of specimens polished on the (110) plane. This process of forming small crystallites which are subsequently rubbed away appears to be a characteristic property of galena.

A photograph was then taken from the cleavage face of a crystal of FeS_2 (Pl. XXX. fig. 4), showing a pattern resembling that from galena. The crystal was then polished parallel to the cleavage plane (100), and another specimen polished on the (110) plane.

For both, surface lines and spots persist throughout; Kikuchi lines were not seen (Pl. XXX. fig. 5), but diffuse polycrystalline rings apparently due to very small particles

* Kirchner and Raether, *loc. cit.*

were observed. The single crystal pattern always persists even after prolonged polishing (Pl. XXX. fig. 6), and this appears to indicate that the structure is preserved except for small particles that are removed to form the finely divided layer. This is probably due to the fact that the binding is stronger in the case of iron pyrites than in the case of galena, as may be inferred from the relation between the molecular volumes and the atomic volume of the component atoms. In both these substances, galena and iron pyrites, the diffuse rings are always due to small particle size, and there is no indication of a layer of supercooled liquid in the form of separate atoms arranged at random. Thus there seems to be no evidence in support of Beilby's theory for substances where the binding is heteropolar.

In conclusion, we must thank Professor G. P. Thomson for useful advice and general supervision throughout the course of the work. One of us (J. A. D.) is indebted to the Department of Scientific and Industrial Research for an award during the tenure of which this work has been carried out.

Summary.

The polished surfaces of the elements Bi, Sb, Zn, Te. Cd, Au, Ag, Pb, Mo, Cu, Cr, Se, Si have been examined by means of electron diffraction. In all these cases the polish layer appears to be amorphous, resembling a supercooled liquid. This was suggested originally by Beilby, and later confirmed by French, who examined Au, Ag, Cr, Cu, using electron diffraction methods. From the positions of the diffraction rings the interatomic distances are deduced, and it is found that in many cases the atoms do not retain their normal size as on the atomic volume curve. In the case of the conductors, which include all but the last two, the atoms appear to be stripped and have atomic volumes corresponding in all cases more nearly to the minimum values of the normal atomic volume curve. In the case of the non-conductors Se and Si, however, the normal interatomic distance is preserved. Two semiconductors, PbS and FeS_2, were also examined, and here the rings are merely due to very small size of the crystal particles after polishing. There was no evidence in these cases of the amorphous rings observed for the elements.

The Imperial College of Science and Technology, London.

LXXXII. *On the Uniqueness of Solution of Problems of Elasticity connected with the Bending of Thin Plates under Normal Pressures,* *By* BIBHUTIBHUSAN SEN *.

1. *Introduction.*

IN this paper a simple method has been used to show that the solution of the problem of a thin plate bent by transverse loads is unique in character when the edge is clamped or supported, and that when the edge is free the solution is indeterminate in the sense that two values of displacements satisfying the equation of equilibrium and the boundary conditions may differ by an expression which is a linear function of the coordinates.

In all these cases the transverse displacement ω of the plate at any point (x, y) satisfies the equation

$$\nabla_1^4\omega = f(x, y), \dagger \quad . \quad . \quad . \quad . \quad . \quad (1{\cdot}1)$$

where ∇_1^4 stands for

$$\frac{\partial^4}{\partial x^4} + 2\frac{\partial^4}{\partial x^2 \partial y^2} + \frac{\partial^4}{\partial y^4}.$$

We shall suppose that ω is single valued and continuous, and has continuous derivatives of the first four orders with respect to x and y at every point in a simply connected region bounded by the edge of the plate.

At every point of a clamped edge the boundary conditions are

$$\omega = \frac{\partial\omega}{\partial\nu} = 0, \quad . \quad . \quad . \quad . \quad . \quad . \quad (1.2)$$

$d\nu$ being an element of outward-drawn normal at a point on the boundary.

For the supported edge we have the conditions

$$\omega = 0, \quad \text{and} \quad \frac{\partial^2\omega}{\partial\nu^2} + \sigma\left(\frac{\partial^2\omega}{\partial s^2} + \frac{1}{\rho^1}\frac{\partial\omega}{\partial\nu}\right) = 0,$$

where σ is Poisson's ratio, ds an element of the bounding curve at a point, and ρ^1 the radius of curvature of the curve at the point.

* Communicated by the Author.

† This equation and the following boundary conditions have been taken from 'The Mathematical Theory of Elasticity,' by A. E. H. Love, 4th edition, p. 488.

Since

$$\nabla_1^2\omega=\frac{\partial^2\omega}{\partial x^2}+\frac{\partial^2\omega}{\partial y^2}=\frac{\partial^2\omega}{\partial\nu^2}+\frac{1}{\rho^1}\frac{\partial\omega}{\partial\nu}+\frac{\partial^2\omega}{\partial s^2},$$

we can put the above conditions as

$$\omega=0,$$

and

$$\sigma\nabla_1^2\omega+(1-\sigma)\frac{\partial^2\omega}{\partial\nu^2}=0. \quad . \quad . \quad . \quad . \quad (1.3)$$

At every point of a free edge we have

$$\sigma\nabla_1^2\omega+(1-\sigma)\frac{\partial^2\omega}{\partial\nu^2}=0,$$

and

$$\frac{\partial}{\partial\nu}\nabla_1^2\omega+(1-\sigma)\frac{\partial}{\partial s}\left[\frac{\partial}{\partial\nu}\left(\frac{\partial\omega}{\partial s}\right)\right]=0. \quad . \quad . \quad (1.4)$$

2. *Clamped Edge.*

Applying Green's theorem to the plane region Ω bounded by the curve s, we get

$$\iint_{\Omega}(U\nabla_1^2V-V\nabla_1^2U)d\Omega=\int\left(U\frac{\partial V}{\partial\nu}-V\frac{\partial U}{\partial\nu}\right)ds. \quad (2.1)$$

Putting $V=\nabla_1^2U$ in the above identity, we find

$$\iint_{\Omega}[U\nabla_1^4U-(\nabla_1^2U)^2]d\Omega=\int_s\left[U\frac{}{\partial\nu}(\nabla_1^2U)-\nabla_1^2V\frac{\partial U}{\partial\nu}\right]ds.$$

$$. \quad . \quad . \quad (2.2)$$

If possible let ω_1 and ω_2 be two solutions of the equation (1.1) which satisfy the boundary conditions (2.1).

Then

$$U=\omega_1-\omega_2$$

will satisfy the equation

$$\nabla_1^4U=0$$

throughout the region, and

$$U=\frac{\partial U}{\partial\nu}=0$$

on the boundary.

Hence, from (2.2), we get

$$\nabla_1^2U=0$$

throughout the region.

From Green's theorem we find

$$\int_s U_1 \frac{\partial U_2}{\partial \nu} ds - \iint_\Omega U_1 \nabla_1^2 U_2 d\Omega = \iint_\Omega \left[\frac{\partial U_1}{\partial x} \frac{\partial U_2}{\partial x} + \frac{\partial U_1}{\partial y} \frac{\partial U_2}{\partial y} \right] d\Omega, \quad . \quad . \quad . \quad (2.3)$$

whence, on putting $U_1 = U_2 = U$, we obtain

$$\int_s U \frac{\partial U}{\partial \nu} ds - \iint_\Omega U \nabla_1^2 U d\Omega = \iint_\Omega \left[\left(\frac{\partial U}{\partial x} \right)^2 + \left(\frac{\partial U}{\partial y} \right)^2 \right] d\Omega.$$

If $U = \frac{\partial U}{\partial \nu} = 0$ on the boundary, and $\nabla_1^2 U = 0$ throughout the region Ω, we have everywhere

$$\frac{\partial U}{\partial x} = \frac{\partial U}{\partial y} = 0 \quad \text{or} \quad U = \text{constant},$$

and since it is zero on the boundary, $U = 0$ everywhere or $\omega_1 = \omega_2$ at every point.

3. *Supported and Free Edge.*

Whatever may be the boundary conditions, we can deduce from the results (1.2), (1.3), and (1.4) the identity

$$\int_s \left\{ \frac{\partial}{\partial \nu} \nabla_1^2 \omega + (1-\sigma) \frac{\partial}{\partial s} \left[\frac{\partial}{\partial \nu} \left(\frac{\partial \omega}{\partial s} \right) \right] \right\} \omega \, ds - \int_s \left\{ \sigma \nabla_1^2 \omega + (1-\sigma) \frac{\partial^2 \omega}{\partial \nu^2} \right\} \frac{\partial \omega}{\partial \nu} ds = 0.$$

This identity can be rewritten as

$$\begin{aligned} &(1-\sigma) \int_s \omega \frac{\partial}{\partial \nu} \nabla_1^2 \omega \, ds \\ &+ \sigma \int_s \left[\omega \frac{\partial}{\partial \nu} \nabla_1^2 \omega - \nabla_1^2 \omega \frac{\partial \omega}{\partial \nu} \right] ds \\ &+ (1-\sigma) \int_s \omega \frac{\partial}{\partial s} \left[\frac{\partial}{\partial \nu} \left(\frac{\partial \omega}{\partial s} \right) \right] ds \\ &- (1-\sigma) \int_s \frac{\partial^2 \omega}{\partial \nu^2} \frac{\partial \omega}{\partial \nu} ds = 0. \quad . \quad . \quad . \quad . \quad . \quad (3.1) \end{aligned}$$

Putting ω for U_1 and $\nabla_1^2\omega$ for U_2 in (2.3) we get

$$(1-\sigma)\int_s \omega \frac{\partial}{\partial \nu}\nabla_1^2\omega\, ds=(1-\sigma)\iint_\Omega \omega\nabla_1^4\omega d\Omega$$

$$+(1-\sigma)\iint_\Omega\left[\frac{\partial\omega}{\partial x}\frac{\partial}{\partial x}\nabla_1^2\omega+\frac{\partial\omega}{\partial y}\frac{\partial}{\partial y}\nabla_1^2\omega\right]d\Omega \quad . \quad (3.2)$$

From (2.2) we find that

$$\sigma\int_s\left[\omega\frac{\partial}{\partial\nu}\nabla_1^2\omega-\nabla_1^2\omega\frac{\partial\omega}{\partial\nu}\right]ds=\sigma\iint_\Omega[\omega\nabla_1^4\omega$$

$$-(\nabla_1^2\omega)^2]d\Omega. \quad . \quad . \quad (3.3)$$

The expression

$$(1-\sigma)\int_s \omega\frac{\partial}{\partial s}\left[\frac{\partial}{\partial\nu}\left(\frac{\partial\omega}{\partial s}\right)\right]ds$$

on partial integration yields

$$(1-\sigma)\left[\omega\frac{\partial}{\partial\nu}\left(\frac{\partial\omega}{\partial s}\right)\right]_1^2-(1-\sigma)\int_s\frac{\partial\omega}{\partial s}\frac{\partial}{\partial\nu}\left(\frac{\partial\omega}{\partial s}\right)ds.$$

The first expression vanishes when $\omega=0$ on the boundary, as in the case of clamped and supported edges. If ω be not zero on the edge, but is a single-valued function having continuous derivatives, the expression will vanish when the bounding curve is a closed one. The remaining integral taken with the last integral on the left-hand side of (3.1) gives

$$-\frac{(1-\sigma}{2}\int_s\frac{\partial}{\partial\nu}\left[\left(\frac{\partial\omega}{\partial s}\right)^2+\left(\frac{\partial\omega}{\partial\nu}\right)^2\right]ds,$$

which is equal to

$$-\frac{1-\sigma}{2}\int_s\frac{\partial}{\partial\nu}\left[\left(\frac{\partial\omega}{\partial x}\right)^2+\left(\frac{\partial\omega}{\partial y}\right)^2\right]ds, \quad . \quad . \quad (3.4)$$

since

$$\frac{\partial}{\partial\nu}=l\frac{\partial}{\partial x}+m\frac{\partial}{\partial y},$$

and

$$\frac{\partial}{\partial s}=l\frac{\partial}{\partial y}-m\frac{\partial}{\partial x},$$

l and m being the direction cosines of the outward drawn normal.

We know from Green's theorem that

$$\int_s \frac{\partial V}{\partial \nu} ds = \iint_\Omega \nabla_1^2 V d\Omega.$$

With the help of this result (3.4) reduces to

$$-\frac{(1-\sigma)}{2}\iint_\Omega \nabla_1^2\left[\left(\frac{\partial\omega}{\partial x}\right)^2+\left(\frac{\partial\omega}{\partial y}\right)^2\right]d\Omega$$

$$=-(1-\sigma)\iint_\Omega\left[\left(\frac{\partial^2\omega}{\partial x^2}\right)^2+\left(\frac{\partial^2\omega}{\partial y^2}\right)^2+2\left(\frac{\partial^2\omega}{\partial x\partial y}\right)^2\right.$$

$$\left.+\frac{\partial\omega}{\partial x}\frac{\partial}{\partial x}\nabla_1^2\omega+\frac{\partial\omega}{\partial y}\frac{\partial}{\partial y}\nabla_1^2\omega\right]d\Omega \quad . \quad . \quad . \quad . \quad (3.5)$$

Using the results (3.2), (3.3), and (3.5) in (3.1), we get

$$\iint_\Omega \omega\nabla_1^4\omega\, d\Omega=\iint_\Omega\left[\sigma(\nabla_1^2\omega)^2+(1-\sigma)\left\{\left(\frac{\partial^2\omega}{\partial x^2}\right)^2\right.\right.$$

$$\left.\left.+\left(\frac{\partial^2\omega}{\partial y^2}\right)^2+2\left(\frac{\partial^2\omega}{\partial x\partial y}\right)^2\right\}\right]d\Omega. \quad . \quad . \quad (3.6)$$

Now, if possible, let there be two solutions ω_1 and ω_2 which satisfy the equation (1.1).

Then $$W=\omega_1-\omega_2$$

will make $\nabla_1^4 W=0$ everywhere.

Whatever may be the boundary conditions, W will satisfy the identity (3.6). The left-hand side of this identity is zero, since

$$\nabla_1^4 W=0.$$

Hence we obtain

$$\nabla_1^2 W=\frac{\partial^2 W}{\partial x^2}=\frac{\partial^2 W}{\partial y^2}=\frac{\partial^2 W}{\partial x\partial y}=0 \text{ everywhere.} \quad (3.7)$$

In the case of a supported edge $W=0$ on the boundary, and from the result, $\nabla_1^2 W=0$, we can deduce, as in the case of a clamped plate, that $W=0$ everywhere, or $\omega_1=\omega_2$ at every point of the plate.

From (3·7) we find that when the edge is free, W may be a linear function of x and y.

It can be easily seen that the results obtained in this paper can be extended to problems of transverse vibration of thin plates.

LXXXIII. *The Inner Potential of Semi-Conductors.*

By K. R. Dixit *.

[Plates XXXI. & XXXII.]

Inner Potential.

When an electron enters an electric field its velocity changes, changing thereby the wave-length of the electron waves $\left(\lambda=\frac{h}{mv}\right)$. Therefore, the wave-length of the waves in the field will be different from the wave-length in the free-space. The field acts on these waves in just the same way as a refracting medium acts on, let us say, light waves; it simply alters the wave-length. We can easily calculate how much it alters the wave-length, and so obtain the refractive index. Let E be the energy of each electron, and V(xyz) the potential energy that it would have at any point (xyz) in the electric field. Then the velocity of the electron at that point is given by

$$\tfrac{1}{2}mv^2=(\mathrm{E}-\mathrm{V}), \quad i.e., \quad v=\sqrt{\frac{2(\mathrm{E}-\mathrm{V})}{m}}.$$

This gives the wave-length of the waves at the point (xyz) as

$$\lambda_v=\frac{h}{\sqrt{2m(\mathrm{E}-\mathrm{V})}}.$$

The wave-length in free space, *i. e.*, where the field V=0, is

$$\lambda_{v_0}=\frac{h}{\sqrt{2m\mathrm{E}}}.$$

The refractive index at the point (xyz) is equal to the ratio of these two velocities, *i. e.*,

$$\sqrt{\frac{\mathrm{E}}{\mathrm{E}-\mathrm{V}}}=\left(1-\frac{\mathrm{V}}{\mathrm{E}}\right)^{-1/2}=\left(1+\frac{\mathrm{V}}{\mathrm{E}}\right)^{1/2}, \quad \text{approx. as } \mathrm{E}>>\mathrm{V}.$$

The refractive index depends on E and therefore on the wave-length of the waves in the free space, as is the case with light. Now if E and V are both expressed in volts, we get the usual notation

$$\mu=\sqrt{1+\Phi/\mathrm{P}}.$$

* Communicated by Prof. G. P. Thomson, M.A., F.R.S.

Bethe * gives the result that the mean potential of the crystal V_0 may be expressed as

$$V_0 = \frac{2\pi N}{3} \int_0^\infty p(r) r^4 \, dr, \quad . \quad . \quad . \quad . \quad . \quad (1)$$

where N is the number of atoms per unit volume and $p(r)r^2\,dr$ is the number of electrons at a distance r from the nucleus or the charge density in electronic units at a distance r from the nucleus.

This method of calculating inner potentials can be conveniently applied to the case of metals or any substance composed of one kind of atoms only. In the case of natural crystals like Galena (PbS) this method cannot be applied. Firstly because we cannot accurately estimate the effective nuclear charge, and secondly because the conductivity electrons of lead are absent, and sulphur has got two extra electrons. The formula (1) can, however, be modified so as to apply to our case.

For a crystal where there are two kinds of atoms or ions this may be written as

$$V_0 = \Sigma_i V i = \frac{2\pi}{3} \Sigma_i N_i e \int_0^\infty P_i(r) r^4 \, dr, \quad . \quad . \quad (2)$$

where

N_i is the number of ith atoms or ions per unit volume,

$P_i(r)$ its charge density.

The charge density or electronic distribution can be determined from a knowledge of the structure factor. There are three methods of attacking this problem; they are :—

(1) A method of trial.

(2) The use of an empirical formula.

(3) An application of Fourier series.

Of these three, by far the most satisfactory method is that of Fourier analysis. Thus we may write with Compton †

$$P i(r) r^2 \, dr = \frac{8\pi r}{d^2} \sum_1^\infty n F_n \sin 2\pi n \frac{r}{d} \, dr. \quad . \quad . \quad (3)$$

* Bethe, *Ann. der Physik*, lxxxvii. p. 95 (1928).

† Compton, 'X-rays and Electrons,' p. 164.

d denotes the spacings of the net planes for which the intensities of X-ray reflexions are measured. It is not necessary to consider the intensity of reflexion of the electrons, for we are only using our knowledge of the intensities of X-ray reflexions to determine the electronic distribution. F_n is the structure factor.

Substituting this in (2) we get

$$V_i = \frac{2\pi N i e d^2}{3} \sum_1^\infty F_n (-1)^{n+1} \left(\frac{1}{2} - \frac{3}{\pi^2 n^2} \right) . \quad . \quad . \quad (4)$$

Now the only question that arises is as to the values of F_n and d to be used. In making measurements of inner potentials by the method of visual observations the Laue spots from the cleavage face are measured. Moreover the cleavage face and the Bragg d corresponding to it are the characteristics of a crystal. It seems natural to use that value of d which corresponds to the cleavage face.

The values for X-ray atomic scattering factors for the charged particles were calculated by Hartree's method of self-consistent fields, using the method of interpolation as developed by James and Brindley *. In the case of Pb^{+2} the distribution was supposed to be that given by Thomas-Fermi's method for Pb, subtracting the effect due to two electrons. Those values of F_n were used, for which $\sin\theta/\lambda$ satisfies the Bragg relation, so that $\frac{\sin\theta}{\lambda} = \frac{n}{2d}$. If these values are substituted in (4) for V_i, we get the contribution of these particular ions to the mean potential of the crystal. For V_i we get an infinite series of terms, which are alternately positive and negative, and in summing up the series we can neglect the terms when the differences between the numerical values of two successive terms become very small (less than 4 per cent.).

In this method the assumption $V = \Sigma_i V_i$ is justifiable, when the atoms of which the crystal is composed retain their volume, that is their individual electron distribution peculiarities in the crystal. For example, Fe atoms, atomic volume $8(10^{-24}$ c.c. omitted as common), combine with two sulphur atoms, volume 16 each to form FeS_2

* James and Brindley, Phil. Mag. xii. p. 81 (1931).

of molecular volume 39·4. Here the electron distribution may be supposed to be unaltered, except for the conductivity electrons. But in the case of PbS, Pb atomic volume 18 combines with S atomic volume 16, to form PbS of molecular volume 52. In this case the outer electron shells are considerably altered, and it is these outer electrons which contribute the major part of inner potential; therefore in such a case the method cannot be expected to give an accurate estimate of the inner potential.

$$Fe(8),\ S_2(32)=FeS_2(39{\cdot}4)\ ;$$

$$Fe_2(16),\ O_3(33)=Fe_2O_3(50{\cdot}7)\ ;$$

but

$$Pb(18),\ S(16)=PbS(52{\cdot}0)\ ;$$

$$Zn(10),\ S(16)=ZnS(39{\cdot}8).$$

TABLE I.

Substance.	Φ observed in volts.	Φ calculated in volts.
PbS	12·5	23·5
ZnS	−4·8	−2·1
FeS_2 ..	5·1	7·3
Fe_2O_3 ..	12·6	16·0

In the case of galena the calculated value is much higher, while the values for iron pyrites and hematite are slightly higher than the observed—as was also the case for nickel calculated by Bethe—due to the distribution of electrons not being spherical, as is assumed throughout the calculation.

The theory of occurrence of the spot diagram on a photographic plate or a willemite screen has been explained by Professor Thomson *. With a favourable setting of the crystal a few bright spots can flash up simultaneously on the screen. These spots are due to planes with a common zone axis and lie on a circle passing through the undeviated spot. The centre of this circle is the point of intersection of the common zone axis with the plate. Now it may be possible that other spots due to planes belonging to this zone can flash up

* G. P. Thomson, Proc. Roy. Soc. A, cxxxiii. p. 1 (1931).

simultaneously by increasing the angle of incidence. Here again these spots would lie on a circle passing through the undeviated spot. The centre of this second circle gives another point of intersection of the same common zone axis with the plate. By increasing the angle of incidence we have made the common zone axis move in a definite direction and this motion of the zone axis may enable us to assign orders to the spots. It may happen that with two different positions of the zone axis spots occur which can be assigned to the same reflecting plane (not the cleavage plane) in different orders. In this case, since the act of diffraction does not affect the distance of a spot from the plane of incidence, these distances for the two spots are in the ratio of the corresponding orders, which are thus determined irrespective of any assumption as to inner potential.

Zinc-blende.

Zinc-sulphide occurs in nature, crystallized in two different forms. The common zinc-blende or sphalerite crystallizes in the cubic system and the other comparatively rarer wurtzite belongs to the hexagonal system. The sphalerite used came from Wrexham, Denbighshire, Wales, and was as pure as natural crystalline zinc-blende can be.

The substance zinc-blende is highly interesting, as having been the first studied by Laue for the production of Laue diagrams. The crystal structure was determined by Bragg *, and his conclusions were theoretically justified by P. P. Ewald †.

There are as many atoms of Zn and S in a unit crystal cube of zinc-blende as there are of Na and Cl in a unit crystal cube of rock-salt. The structures, however, are not identical. Both Zn and S atoms lie on a face-centred cubic lattice, but the relative positions of the two lattices are not the same as those of the face-centred lattices of Na and Cl in rock-salt. Zn atoms are placed at the corners and the centres of the faces of the large cubes like Na atoms in rock-salt ; but S atoms occupy the centres of four alternate small cubes, eight of which make a large structural unit cube. The words zinc and sulphur are interchangeable in the above description.

* Bragg, Proc. Roy. Soc. A, lxxxviii. p. 435 (1913).
† P. P. Ewald, *Ann. der Physik* (4), xliv. p. 259 (1914).

The apparatus used was a modified form of Professor Thomson's * electron camera. The voltage used varied from 21 kilo-volts to 44 kilo-volts. Ten different specimens of zinc-blende from the same source were used, and for each one of them four slightly different mountings in the crystal holder were adjusted. Some plates were taken showing Kikuchi lines and spots. Visual measurements were also made, in the same way as by Professor Thomson †.

The specific resistance of the zinc-blende used is of the order of 10^8 ohms (compared with 10^{16} ohms of rock-salt). The specimen showed signs of electrostatic charging up at grazing angles of incidence, which is not perceptible at slightly larger angles. In all cases the free surface exposed to the beam was the cleavage surface (110). There was a sort of time-effect in the production of diffraction spots possibly due to a local rise of temperature. The brightness of the spot on the willemite screen appeared to diminish after long exposure, but the intensity was observed to increase on change of azimuth, as this exposed a different portion of the surface to the beam.

At any given voltage and with correct setting successive orders of spots could be followed by changing the incidence only. The central line spots are due to reflexion from the cleavage face. These spots are best investigated by visual measurements on the fluorescent screen. If x is the displacement on the screen, P the voltage, n' the number found by dividing the spacing calculated from the value of $x\sqrt{\mathrm{P}}$ into 7·64, the 110 spacing of zinc-blende, then the inner potential

$$\Phi = \frac{150n^2}{4d^2}\left[1-\frac{n'^2}{n^2}\right], \quad . \quad . \quad . \quad . \quad . \quad (5)$$

where $d=a\sqrt{2}$, a is the cube side, and n the integral order corresponding to n'. Considerations of the structure of zinc-blende indicate that the values of n' must be nearly $4p$, where p is an integer. In Table II. four is taken out as a common factor.

The correctness of the orders assigned was verified by noting the position of the spots, that flash up simultaneously on the screen, for a definite incidence,

* Thomson and Fraser, Proc. Roy. Soc. A, cxxviii. p. 641 (1930).
† G. P. Thomson, Proc. Roy. Soc. A, cxxxiii. p. 1 (1931).

and then changing the incidence and noting the position of the new spots that may flash up. The spots which flash up successively on the screen, when the angle of incidence alone is changed, belong to a definite zone axis. The successive positions of the intersections of this zone axis with the plate are determined from the positions of the spots. This enables one to make an estimate of the orders to be assigned to the spots.

Besides, if the values of p in Table II. are supposed to be 4, 5, and 6, instead of 3, 4, and 5, we get the corresponding values of Φ positive, but 68·9, 90·1, and 111·2 volts respectively; but these values are very unlikely to be correct. The orders assigned 3, 4, and 5 to p appear to be the correct ones.

TABLE II. (for centre-line spots).

Number of readings.	p'.	p.	Φ in volts.
8....	3·0775	3	−4·84
70....	4·0581	4	−4·84
30....	5·0441	5	−4·52
		Weighted means	−4·8

Galena.

The natural crystals of PbS belong to the cubic variety. The lead and sulphur atoms are arranged in a cubic lattice just like Na and Cl in rock-salt. It has a cubic cleavage and the face exposed to the beam of electron is (100) face. The resistivity of galena is 3×10^{-3} ohm cm.

The massive lead atoms in the surface cause a considerable number of electrons to be reflected at the surface, and so these lead atoms in the surface serve as a two-dimensional or cross grating *.

The electrons reflected by the atoms on the line AD, parallel to the plane of incidence, lie on cones with the line AD as the axis and small semi-vertical angles. The intersections of these cones with the photographic plate will be circles approximately with the incident beam-spot as the centre. Because of the very small angles

* Kirchner and Raether, *Phys. Zeits.* xxxiii. p. 510 (1932).

between the incident and reflected ray and the line of reflecting atoms, the reflected rays from the atoms would not be out of phase over a considerable distance. If θ is the angle of incidence, ϕ the angle of reflexion, and d the distance between two consecutive atoms in the direction of the incident beam, the path difference between the rays reflected by these two atoms would be

$$d \cos \phi - d \cos \theta = \frac{d}{2} \times (\phi^2 - \theta^2),$$

θ and ϕ being both small. These rays would get out of phase when the path difference becomes $\lambda/2$. Thus for the rays to get out of phase

$$\frac{d}{2}(\phi^2 - \theta^2) = \lambda/2, \quad i.\,e., \quad (\phi - \theta) \sim \lambda/d(\phi + \theta);$$

Fig. 1.

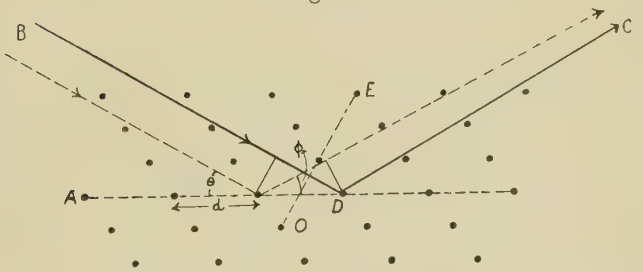

as θ and ϕ are very small the rays would not be out of phase over a considerable distance and the rings would be diffuse. For higher orders ϕ increases, while θ remains the same and the orders become sharper and sharper.

The atoms that lie on a line like OE, perpendicular to the plane of incidence, give rise to reflected rays which lie on cones with semi-vertical angles nearly 90°. The intersections of these cones with the plate are nearly straight lines, perpendicular to the shadow. These lines are fairly sharp, due to the large number of scattering centres being able to scatter coherently.

It is the massive lead atoms which form the cross grating, as the contribution of the sulphur atoms to the reflexions is negligible. Now lead atoms lie on a face-centred lattice, say of side $2a$. If the incident beam is parallel to the cube edge, the distance between the atoms, which would give rise to surface lines, is $2a$;

while if the incident beam is parallel to the face diagonal, the corresponding distance is $a\sqrt{2}$. Naturally the ratio of the distance between the surface lines on the photographic plate in the two cases would be as $1:\sqrt{2}$, provided the energy of the electrons is the same. The crystal of PbS has a fourfold symmetry. If we suppose that for zero azimuth the incident beam is parallel to the cube edge, the distance between the surface lines would be the same for 0°, 90°, 180° of azimuth, while for 45°, 135° it would be $\sqrt{2}$ times that for the zero azimuth. This effect, which was observed by Kirchner and Raether, was confirmed in the present experiment, see fig. 2 (Pl. XXXI.). But although the lines observed are the same as would be produced by a surface grating, Kirchner's deduction that the second and lower layers play no part does not seem to be justified. Kikuchi lines which are due to penetrating electrons were always seen.

In general, when two Kikuchi * lines intersect, the intensity of both the lines is observed to have diminished near the intersection. This is due to the fact that the corresponding point of intersection of the two white lines has to supply simultaneously electrons to give two black lines, and as a result it robs both the lines and the intensity is observed to be reduced. But if a Kikuchi line intersects a surface line—as the two effects are due to entirely different causes and produced by different electrons—we actually get an increase in the intensity. and sometimes enough to produce a spot. Kikuchi lines are due to the diffuse scattering and subsequent selective reflexion of the electrons, while surface lines are due to electrons reflected at or near the surface. In the case of galena where the surface lines are very strong, this increase of intensity effect is observed, and spots besides Laue spots due to reflexion from the crystal can be seen on the screen, and their position has to be noted when making visual measurements. But the position of the Kikuchi lines, and with them the positions of these secondary spots, would alter by changing the azimuth, while the positions of the Laue spots due to the cleavage face, for which the visual measurements are made, would remain unaltered. The positions of these secondary

* Shinohara, Scientific Papers, I.C.P.R. Tokyo, No. 401 (1932).

spots would correspond to those for fractional orders. In making calculations of the inner potential, only those spots were taken as due to reflexion from the cleavage face, which are present for the majority of cases. The energy of the electrons used varied between 20 to 40 K. volts. The formula (5) for the inner potential may be written as

$$\frac{\Phi}{P} = \frac{x_0^2 - x^2}{4L^2}, \quad \ldots \ldots \quad (6)$$

where

P is the energy of electrons used ;

L is the length of the camera ;

x_0 the distance between the initial beam spot and the reflected spot when $\Phi = 0$;

x the actual distance corresponding to x_0.

TABLE III.

Number of readings.	Φ in volts.
16	12·7
6	12·6
20	12·5
6	12·4
5	12·3
15	12·2
5	11·9
6	11·7
Weighted mean	+12·5

The results are given in Table III. The correctness of the orders assigned was verified by the method of noting all the spots that appear on the screen at once, measuring all the spots that flash successively by changing the incidence only, and considering the motion of the zone axis. This method has been already described for zinc-blende.

This result was checked by calculating the inner potential from the Kikuchi * lines due to the cleavage face. The method consists in measuring the distance

* Shinohara, Scientific Papers, I.P.C.R. Tokyo, No. 375 (1932).

between the line of intersection of the cleavage plane with the photographic plate, known in practice as the shadow edge, and the lines parallel to it. Orders are assigned to these lines and $P \sin^2 \theta$ is plotted against n^2.

The modified Bragg relation, taking account of the refractive index, becomes with usual notation

$$\mu^2 - 1 = \frac{n^2\lambda^2}{4d^2} - \sin^2 \theta. \quad . \quad . \quad . \quad . \quad . \quad (7)$$

For electrons $\mu = \sqrt{1 + \Phi/P}$

and $\lambda = \sqrt{150/P}$

in Angstrom units. Substituting in (7) we get

$$P \sin^2 \theta = \frac{150n^2}{4d^2} - \Phi. \quad . \quad . \quad . \quad . \quad . \quad (8)$$

The curve of $P \sin^2 \theta$ against n^2 should be a straight line whose intersection on the $P \sin^2 \theta$ axis gives Φ, while the slope gives d for the cleavage face, in the present case the side of the unit cell.

In practice this method of calculating the inner potential from Kikuchi lines serves only as a check on the experimentally determined value, because the shadow edge in general is not very sharply defined. Thus, in drawing the curve, the correct intercept corresponding to the determined value of Φ is taken as one point on the curve. The value of d as determined from the slope in this case comes out to 6·07 Å. as compared to 5·97 Å, which shows fairly good agreement.

One more point should be specially mentioned. The Kikuchi lines due to the cleavage face are produced by electrons diffusedly scattered, after they have penetrated inside the crystal, perpendicularly to this face. Thus in a case like galena, where the surface effect is very predominant, Kikuchi lines due to the cleavage face would be seen very rarely, as was observed to be the case.

Iron Pyrites.

The crystal of iron pyrites * FeS_2 is cubic. The iron atoms are arranged on a face-centred cubic lattice. If the larger cube is divided into eight smaller cubes and a series of non-intersecting three-fold axes are chosen,

* W. H. and W. L. Bragg, 'X-rays and Crystal Structure,' pp. 119–140.

one passing through each iron atom, each small cube has a single diagonal which is a three-fold axis. Each cube contains one sulphur atom, which lies on the diagonal near the empty cube corner and divides the diagonal in the ratio of 1 : 4. The symmetry of the structure is still that of the cubic class. Roughly speaking the structure may be supposed to be similar to that of rock-salt, iron atoms taking the place of sodium atoms, and sulphur molecules that of the chlorine atom. The natural crystal has a cubic cleavage and the face exposed to the electron beam was (100). The resistivity of the crystal is $2{\cdot}4 \times 10^{-2}$ ohm cm.

The cube of iron pyrites belongs to a class known as tesseral central. The natural cube has striations on its faces and those on each face are parallel to the cube edge and perpendicular to those of the neighbouring faces. This shows that the crystal does not possess a four-fold axis of symmetry perpendicular to the face, but merely a two-fold axis. The cube has a centre of symmetry which distinguishes it from zinc-blende. It has planes of symmetry parallel to (100).

The surface effect was observed with iron pyrites as in the case of galena, but the iron atoms are not so heavy as lead and the surface lines were very much less intense. No secondary spots were seen as with galena. The Kikuchi lines due to the cleavage face are present on almost every plate. Plates were taken showing the surface lines for 0°, 45°, 90°, 135°, 180°, and 225° of azimuth, the incident beam being parallel to the cube edge for the zero azimuth. The distance between the surface lines is the same for 0°, 90°, and 180°. It is also the same—but different from that for zero—for 45° and 225°, but it is different for 135°. This is to be expected, as the considerations of symmetry will show. The crystal has only a two-fold axis of symmetry, while it has planes of symmetry parallel to (100).

Visual measurements of the spots were made on the screen, and inner potential was calculated just as in the case of galena. The results are given in Table IV. The orders assigned are seen to be the right ones by the " motion of zone axis " method.

This value of Φ was checked by the method of Kikuchi lines. The slope of the straight line $P \sin^2 \theta$ against n^2 gives the value of d as 5·53 Å as compared with 5·40 Å.

Hematite.

The structure of hematite * Fe_2O_3 is exactly similar to that of corundum Al_2O_3. It is a trigonal crystal of the calcite type. The oxygen atoms form a close-packed hexagonal arrangement ; the iron atoms lie at some of the gaps in between the oxygen atoms.

The plane exposed to the beam of electrons was (111). The resistivity of hematite is about 0·7 ohm cm.

TABLE IV.

Number of readings.	Φ in volts.
6	5·3
26	5·2
34	5·1
26	5·0
7	4·9
Weighted mean	= +5·1

TABLE V.

Number of readings.	Φ in volts.
5	12·4
10	12·5
29	12·6
16	12·7
15	12·8
Mean	+12·6

The inner potential was calculated from the visual measurements on the screen as before. The orders assigned were seen to be the right ones from the motion of zone axis method. The results are given in Table V.

In this case, as with FeS_2, Kikuchi lines due to the cleavage face are seen on all plates. The value of d determined from the slope comes out exactly at 2·29 Å, thus serving as a good check on the experimentally determined value.

* Pauling and Hendricks, J. Amer. Chem. Soc. xlvii. p. 781 (1925).

Discussion.

The experimentally obtained value of the inner potential of zinc-sulphide is negative, which is rather unusual. In order to make sure that this is not an experimental error, more than twice the number of readings were taken than with any other substance, using ten different specimens. The orders assigned also appear to be the right ones as we have seen. The method of determining the inner potential from Kikuchi lines due to the cleavage face—which in practice only serves as a check on the experimentally determined values of the inner-potential as the shadow edge is not sharp—could not be used, as Kikuchi lines due to the cleavage face were not seen on any plate.

The value of Φ calculated above comes out to be negative. Probably the potential is actually negative. Negative values of Φ have been observed before by Laue * and Rupp for a number of ionic crystals, including zinc-blende, for which a value $-5{\cdot}8$ volts was obtained. The substances used by them were insulators, and they used slow electrons. The effect observed by them is generally supposed to be the charging-up effect, and the agreement does not mean much. When a beam of electrons is incident on an insulator, and if it receives more electrons than the number of electrons which leave it, it will acquire a negative charge. The greater the specific resistance of the substance the greater will be the effect. Rock-salt has a much higher specific resistance than zinc-blende, and yet the apparatus used in the present work gives it a positive inner potential of about 10 volts, as observed by Professor Thomson †. It seems very unlikely that the effect observed with zinc-blende is due to electrostatic charging up.

Kirchner ‡ and Raether calculated Φ from pictures for a number of substances, including NaCl, FeS_2, and PbS, and they state that the values obtained by them are always positive and lie between 5 and 15 volts.

Emslie § obtained a value for the inner potential of galena of 18·2 volts. Professor Thomson ‖ observed

* Laue and Rupp, *Ann. der Physik*, iv. p. 1097 (1930).

† G. P. Thomson, *loc. cit.*

‡ *Loc. cit.*

§ Emslie, 'Nature,' cxxiii. p. 977 (1929).

‖ G. P. Thomson, 'Wave Mechanics of Free Electrons,' New York (1930).

a gradual change of Φ from 9 to 18 volts, accompanied by a discoloration of the surface of galena used. No such discoloration was observed in the present work, even after exposing the specimen to the electron beam for three hours.

In general the values of Φ obtained above appear to agree fairly well with those found by other investigators.

Summary.

(1) By using fast electrons and the method of visual measurements the inner potentials of ZnS, PbS, FeS_2, and Fe_2O_3 have been determined, the substances used being all natural crystals. The values found are $-4{\cdot}8$, $+12{\cdot}5$, $+5{\cdot}1$, and $+12{\cdot}6$ volts for ZnS, PbS, FeS_2, and Fe_2O_3 respectively. These are checked by Kikuchi line measurements. A method called the motion of the zone axis method is developed to check the orders assigned.

(2) Theoretical estimations of Φ have been made by using a modified form of Bethe's formula.

(3) Presence of surface effect has been observed, and the positions of the surface lines correspond to those to be expected from the crystal symmetry.

Finally, I would like to express my sincere thanks to Professor Thomson, in whose laboratory this work was done.

LXXXIV. *Paschen Back Effects in the Spectra of Thallium.* *By* A. M. Crooker, *M.A., Research Student University of Toronto* *.

Abstract.

The Paschen Back effect of several visible thallium lines has been investigated at a field strength of 25·3 kilogauss in the second order of a three metre concave grating. The complex patterns obtained are shown to agree well, within the limits of experimental error, with the theoretical ones deduced from the intermediate field equations of Goudsmit and Bacher.

* Communicated by Professor J. C. McLennan, F.R.S.

Introduction.

CONSIDERABLE interest and importance are attached to the Zeeman effect of lines ordinarily displaying h.f.s. It is well known that the complete Paschen Back effect of such lines, if this can be attained and the resulting pattern resolved, provides the most unequivocal determination of the spin moment of nuclei. This follows from the fact that the nuclear spin makes itself manifest by splitting each "anomalous Zeeman Component" into $2I+1$, equally spaced, equally intense fine components. As this splitting is quite independent of the gross structure term, a spectrum which has not been analyzed might be investigated immediately for a nuclear moment. The number of fine components of any ordinary Zeeman component need only be observed and the "I" value follows directly. The classical experiments of Back on the Bismuth arc line λ 4722 well illustrate the power and definiteness of this method under the best modern spectroscopic technique.

Although the complete Paschen Back effect is capable of such a unique interpretation, it is very rarely obtained experimentally, for if the h.f.s. intervals are small enough to permit the effect being realized the resulting pattern is difficult to resolve. This is the case since the separation of the fine Paschen Back components is determined by the difference of the h.f.s. intervals of the two terms involved. Thus, in practice, most patterns are obtained in an intermediate field, and the resulting asymmetrical pattern fitted to a theoretical one.

On account of the experimental difficulties the Zeeman effects with thallium lines have been investigated only by Durnford[1], by Back and Wulff[2], and by Green and Wulff[3]. In these experiments the difficulties of the method have been superseded, with the result that the theory of the Zeeman effect at intermediate field strengths has been in these three cases verified well within the experimental limits. The purpose of the present communication is to report some work done on visible Tl lines lying in the grating region, $n\lambda=10$, 700–11, 900 Å.U.

Theory.

The theory of the Zeeman effect in intermediate fields developed by Heisenberg and Jordon[4], and by C. G.

Darwin[5] for the case of multiplets, has been modified for the case of hyperfine structure by Goudsmit and Backer[6]. Now from the simple model treated by Darwin we expect the results to be only valid for multiplets displaying LS coupling. Such multiplets with separations of the order necessary for Paschen Back effects (1 cm.$^{-1}$), occur rarely with any intensity in the spectra of light atoms. Hyperfine multiplets, however, are admirably suited for a test of the theory ; they have small separations and the (IJ) coupling is analogous to extreme (LS) coupling. The theoretical expressions for the line positions and intensities are deducible from the key equation for the separate term splitting, namely

$$-X_{m_J-1,\,m_I+1}\cdot\frac{A}{2}(J-m_J+1)(I+m_I+1)$$
$$+X_{m_J,\,m_I}(W-Am_Jm_I-gm_Jw)$$
$$-X_{m_J+1,\,m_I-1}\cdot\frac{A}{2}(J+m_J+1)(I-m_I+1)=0,$$

where A is the h.f.s. interval factor, w the Lorentz unit ($4{\cdot}674\times10^{-5}$ cm.$^{-1}\times$H)[7], W the energy of the magnetic level referred to the centre of gravity of the field free hyperfine levels, and the X's are the coefficients in the expansion of the wave function, and are used in the calculation of the line intensities. For a given value of $m_F=m_J+m_I$ this leads to a set of equations, the number of which $2J+1$ or $2I+1$ is restricted by m_J or m_I respectively. The roots of the determinant of this set of equations gives the values of W associated with the given m_F. These values are then correlated to the different combinations of m_I and m_J by the familiar " non-crossing over " rule implicitly contained in the equations above. When these energy values are put in the equations only the ratios of the X's result, but their absolute values become determined by the addition of the normalizing relations. These normalizing relations and the formulæ for the computation of the line intensities have been given by Goudsmit and Backer and are not reproduced here.

In the case of thallium the above calculations are reduced to a minimum. Even in this case, however, the complete calculations require considerable lengthy arithmetic. The necessary work may be considerably reduced

if one notices that for the case of $I=\frac{1}{2}$ the general key equation may be rewritten in a simplified form: in this case, for any $m_F'=m_J-I$ or $(m_J-1)+I$, the determinant of the chain of equations becomes

$$\begin{vmatrix} -A/2(J-m_J+1) & W+m_J(A/2-gw) \\ W-(m_J-1)(A/2+gw) & -A/2(J+m_J) \end{vmatrix}$$

As a check on the calculations one may use the easily proved theorem that the roots for $-m$ may be derived from those of m_F by simply changing the sign of g. As the previous experimenters have verified the application of the above theory to any field strength if to one, the line patterns discussed in this communication will be understood to hold for a field strength of 25·3 kilogauss.

Experimental.

The apparatus used has already been described by Durnford[1]. Moreover, his detailed description of the experimental technique involved makes a lengthy description of this unnecessary. Only a few minor alterations made will be considered in a sketch of the general method.

The same vacuum arc chamber, electrode assembly, and magnet of du Bois type, wire wound of 3100 turns, were used[1]. At a current of 12 amperes a field of 23·3 kilogauss was attained with a pole gap of 4 mm. As the magnet was cooled only by radiation the current was turned on and the ventilation adjusted until the room reached an equilibrium in thirty minutes. This was also necessary in order to control the temperature of the three-metre grating in a heavily lagged Eagle mount. The field current was adjusted constantly by hand to balance out the effect of small fluctuations of the line voltage. The arc current was adjusted at three to five amperes. The focal properties of the condensing lens were changed to allow a more advantageous use of the light. A Wollaston double image prism was always used so as to separate the components vertically on the slit. Thus both polarisations were obtained in the same exposure. This adjustment was made critically and no relative shifts of the π and σ components were observed. Ilford Special Rapid Panchromatic plates were used throughout. The exposures varied from thirty minutes to eight hours. As recommended by Dr. Durnford[8] it was found advisable to experiment at night.

Results.

The observed patterns may now be compared with those predicted by the theory outlined above. This comparison is made for three lines, one arc line, one first spark line, and one second spark line. The lines are so chosen that all the terms involved are independent of

Fig. 1.

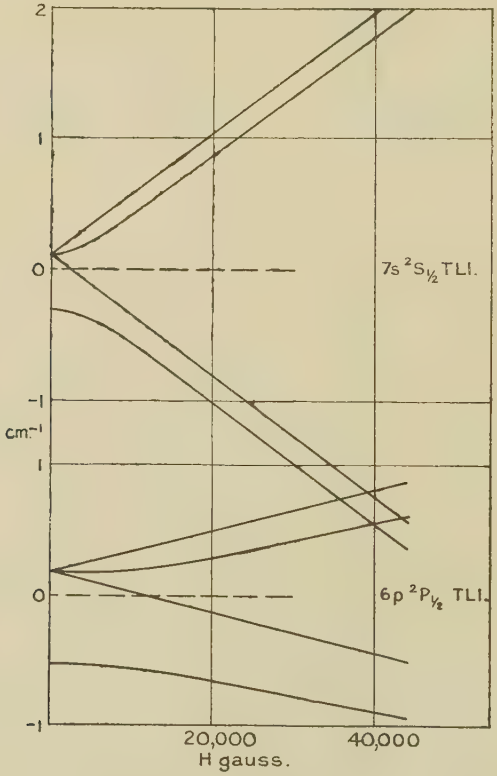

coupling, so there is no indeterminacy in the g factor, with the possible exception of perturbation effects. Since the agreement between theory and experiment is in all cases good, such perturbation effects must be inappreciable.

A graphical method of presentation is used as it is felt that the magnetic term splitting is most readily followed by this method. In this respect it is interesting to note how a large g factor will compensate for a large A

Fig. 2.

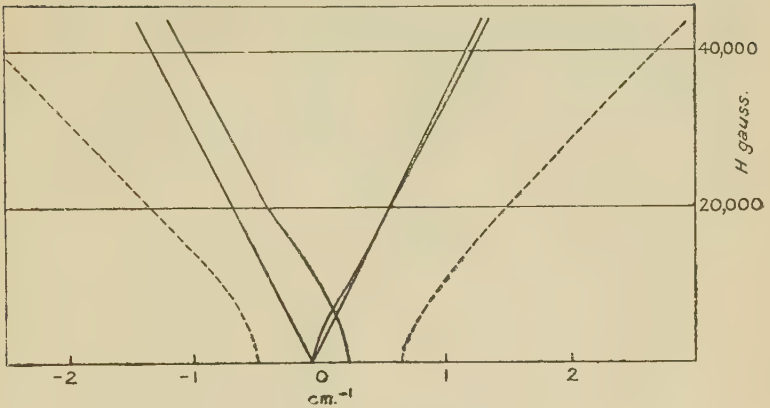

Theoretical π components of Tl I, λ 3776.

Fig. 3.

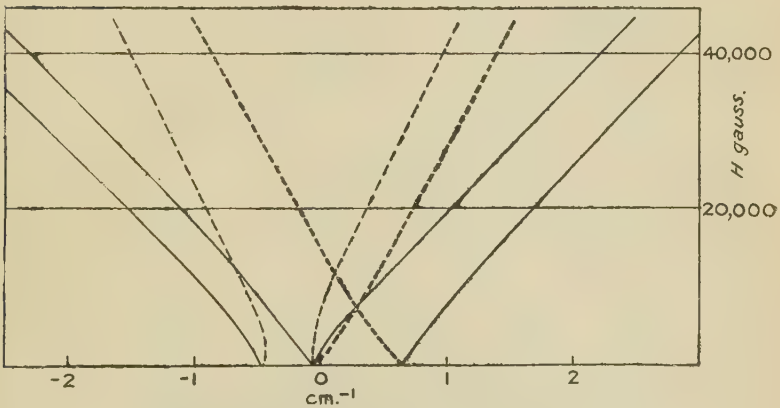

Theoretical σ components of Tl I, λ 37J6.

Fig. 4.

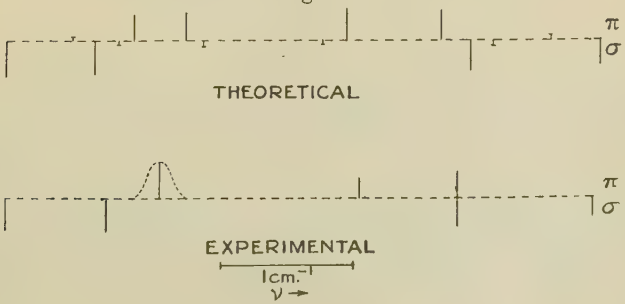

H = 25·3 KG.

Line pattern of Tl I, 3776.

factor and allow a symmetrical complete Paschen Back effect to be realized at relatively small fields. The results are shown graphically in figs. 1–12*.

The line λ 3776, Tl I, $6s^2S\frac{1}{2}-7_p{}^2P_{\frac{1}{2}}$.

This line has been most carefully investigated by Back and Wulff. Their results are in complete agreement

Fig. 5.

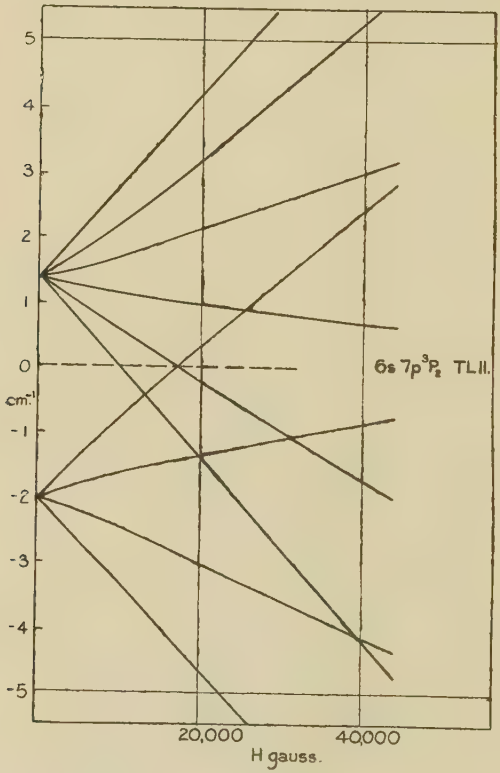

with theory, as are those presented here. The present results, however, are obtained at a new field strength.

As the $^2S\frac{1}{2}$ term has the smaller A factor and the larger

* Fig. 1 shows the magnetic variation of the term values giving rise to λ 3776, Tl I, figs. 5 and 6 that of the term values giving rise to λ 5949, Tl II, and fig. 10 that of the term values giving rise to λ 5362, Tl III. Figs. 2 and 3 show the magnetic resolution of λ 3776, and fig. 4 the intensities of its different components. Figs. 7, 8, and 9 show the corresponding features of λ 5949, and those of λ 5362 are shown in figs. 11, 12, and 13.

g factor, it approaches a symmetrical pattern more rapidly than the $^2P_{\frac{1}{2}}$ term. It is interesting to note that the transition which merges in field free space into the forbidden 0—0 transition, gives rise to a strong observed component in the field. (Measurements made in 3rd order.)

Fig. 6.

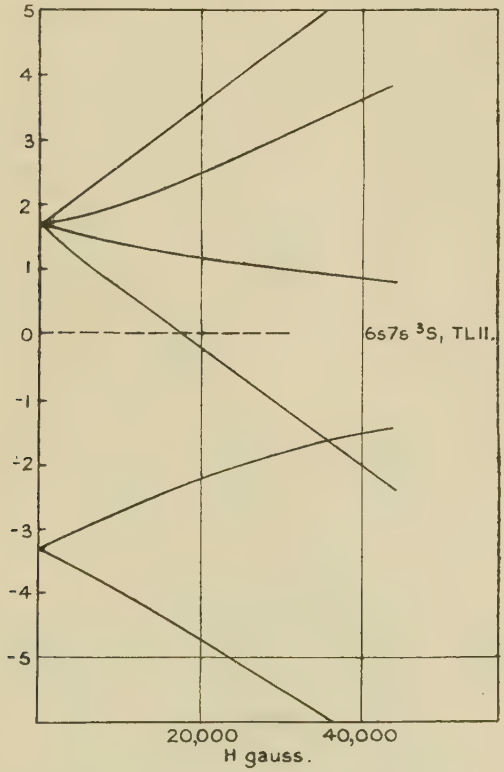

The line λ 5949, Tl II, $6s7s\,^3S_1—6s7p\,^3P_2$.

This line has been previously studied by Durnford, but at different field strengths than used in this investigation.

The fact that the Paschen Back effect is only beginning, caused by the large A factors of the terms involved, is shown by both the highly unsymmetrical observed line pattern, and the extreme intensity of the so-called forbidden transitions $\Delta m_1 = \pm 1$, especially the central

Fig. 7.

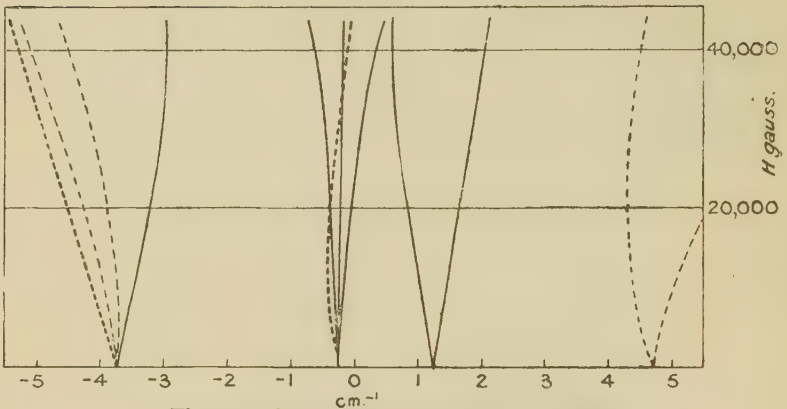

Theoretical π components of Tl II, λ 5949.

Fig. 8.

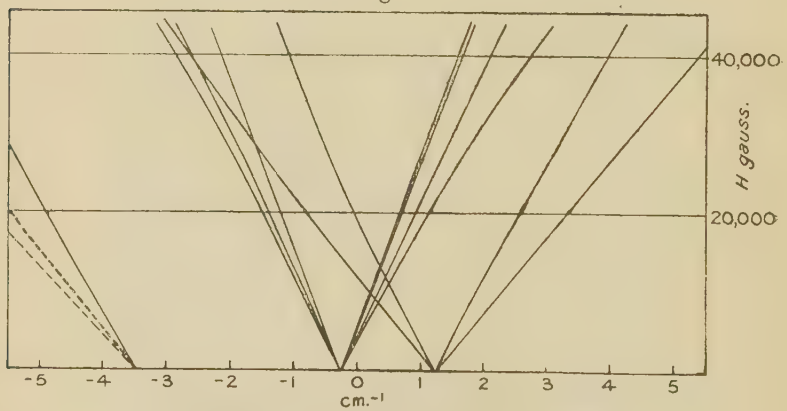

Theoretical σ components of Tl II, λ 5949.

Fig. 9.

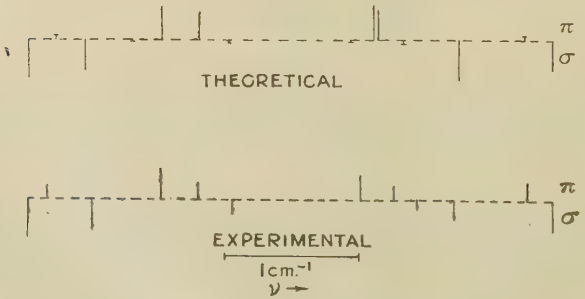

Line pattern of Tl II 5949.

component. (The forbidden transitions are dotted in to distinguish them.) In the case of the σ components only two observed forbidden components are drawn in the theoretical pattern to avoid confusion. Durnford's patterns at various field strengths coincide well with the stronger components in the theoretical patterns.

Fig. 10.

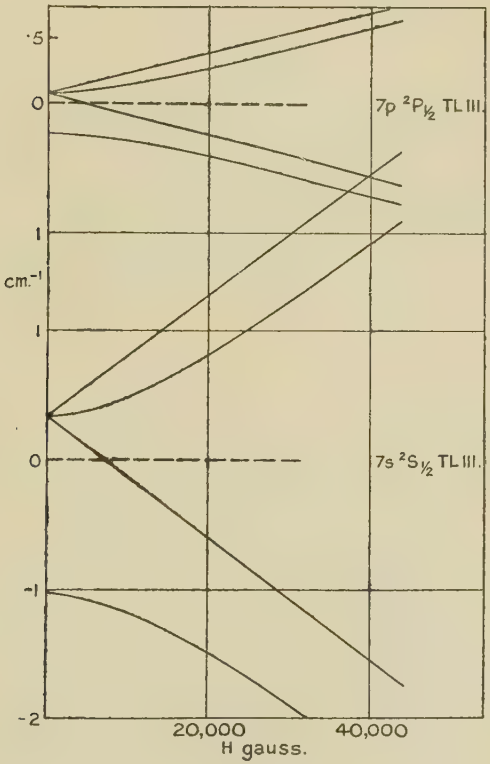

The line 5362, Tl III, $7s^2S_{\frac{1}{2}}—7p^2P_{\frac{1}{2}}$.

This line has not previously been reported upon.

The observed pattern is intermediate between the incipient pattern of λ 5949, and the almost complete pattern of λ 3776. The forbidden components of moderate intensity are not observed with certainty as the pattern is mixed with the ghosts of the strong green arc line λ 5350.

Fig. 11.

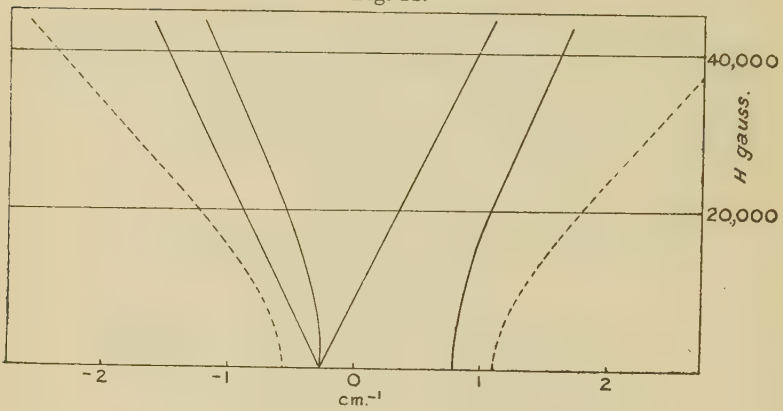

Theoretical π components of Tl III, λ 5362.

Fig. 12.

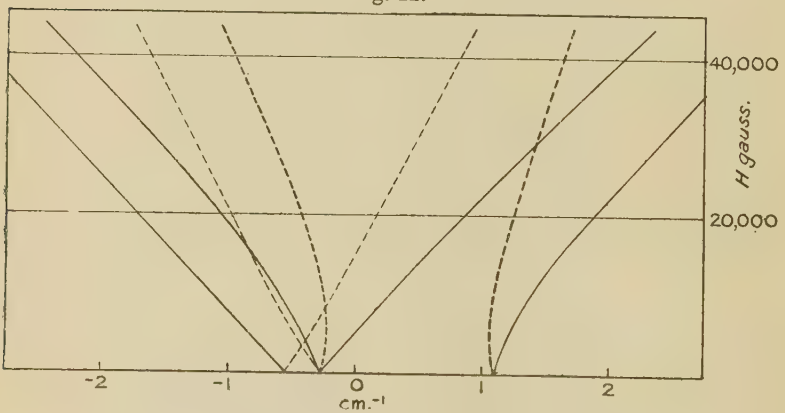

Theoretical σ components of Tl III, λ 5362.

Fig. 13.

THEORETICAL

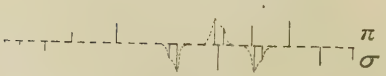

EXPERIMENTAL

1cm.-1
ν →

H = 25·3 KG.

Line pattern of Tl III 5362.

Acknowledgments.

It is a pleasure to recall the helpful enthusiasm of Prof. J. C. McLennan under whose directorship this research was initiated, and more recently the willing co-operation of Prof. E. T. Burton, who has continued to extend the resources of the McLennan Laboratory. The author's warmest thanks are due to Mr. M. F. Crawford for his criticism and numerous friendly discussions.

Bibliography.

(1) A. M. I. A. W. Durnford, Proc. Roy. Soc. A, cxxix. p. 48 (1930).
(2) E. Back u. J. Wulff, *Zeits. f. Phys.* lxvi. p. 31 (1930).
(3) J. B. Green and J. Wulff, Phys. Rev. xxxviii. p. 2177 (1931).
(4) W. Heisenberg u. P. Jordon, *Zeits. f. Phys.* xxxvii. p. 263 (1926).
(5) C. G. Darwin, Proc. Roy. Soc. A, cxv. p. 1 (1927).
(6) S. Goudsmit and R. F. Bacher, Phys. Rev. xxxiv. p. 1499 L (1929); *Zeits. f. Phys.* lxvi. p. 13 (1930) (most complete treatment); also L. Pauling and S. Goudsmit, "Structure of Line Spectra," McGraw Hill, New York (1930).
(7) R. T. Birge, Rev. Mod. Phys. i. p. 1 (1929).
(8) A. M. I. A. W. Durnford, Thesis, Toronto (1930).

LXXXV. *The Supraconductivity of Alloy Systems.* By J. F. Allen, *M.A., Fellow of the National Research Council of Canada, University of Toronto* *.

AT the present time much attention is being focussed upon the problem of supraconductivity. The phenomenon was discovered by Kamerlingh Onnes[1] in 1911, when he found that mercury, on being cooled in liquid helium to a temperature of about 4° K above absolute zero, suddenly lost all resistance to an electric current. Since that time nine other metals have been found to behave similarly, with transition points varying from 1·05° K in the case of Gallium to 8·2° K for Niobium. Whether all metals would exhibit supraconductivity will perhaps never be known, since the lower limit of temperature available for measurement seems to be in the neighbourhood of one degree absolute.

Soon after the phenomenon was discovered in pure metals, it was found to be present also in certain alloys. Continued researches have shown that supraconductivity

* Communicated by Professor J. C. McLennan, F.R.S.

is more generally present in alloys than in pure metals. The known supraconductive alloys are for the most part binary alloys of which one or both of the components are supraconductive. There are several exceptional cases, however, notably the compound CuS and the alloy Au–Bi which becomes supraconducting although none of the elements copper, sulphur, gold, or bismuth are supraconductive.

Previous researches on the supraconductivity of alloys have been designed mainly to determine the extent of the phenomenon, and the alloys tested were usually of the eutectic type. Little attention has been paid to the possible effect upon the phenomenon of varying the proportions of the components. Consequently, whereas the supraconductive alloys now number about forty, complete data on the effect of varying concentrations are lacking in all but a small number of alloy systems.

The recent researches of Meissner and his collaborators, and also reports from the cryogenic laboratory in Toronto, have clearly shown that, as was natural to expect, supraconductivity in alloys depends on their constitution in much the same way as do other physical properties. In a paper published by the writer last year in collaboration with McLennan and Wilhelm[2], results were given of measurements made on various metallic compounds and eutectics in the systems Ag–Sn, Au–Sn and Au–Pb. It was noted at that time that the varying of proportions in these systems had a profound effect on the transition temperatures. The general conclusion was that intermetallic compounds possessed lower supraconductivity points than did eutectics between these compounds, or between compounds and pure metals. Publications by Meissner[3] appearing at about the same time showed that throughout an alloy system of which both components are supraconductors, the supraconducting point varies continuously. Meissner investigated several types of alloys ; namely, systems composed of eutectic mixtures, of mixed crystals with solubility boundaries, and one system in which both components showed unlimited solubility. Each of these types was found to possess distinctive characteristics, which will be discussed together with the results of the present research.

The measurements published from the cryogenic laboratory in Toronto last year on Ag–Sn, Au–Sn, and

Au–Pb were made on alloy systems of which one component only was a supraconductor. The observations, however, were incomplete in that they did not trace the change in supraconducting point throughout the alloy system. This has now been done and the investigation extended to other alloy systems of the same group, Ag–Pb, Cu–Sn, and Cu–Pb. These are all eutectic systems with either mixtures, or mixed crystal series, and most of them contain solubility boundaries. The system Tl–Sn, which had previously been investigated by Meissner, was also examined for purposes of comparison with Meissner's results.

Preparation and Mesaurement of Alloys.

The concentrations of the constituents of the alloys are given throughout the paper in weight per cent. It was necessary to exercise great care in weighing out the metals to be alloyed, since an error of even one per cent. in concentration might, in extreme cases, cause a displacement of the transition temperature of more than half a degree.

The amount of metal in an alloy melt was never greater than half a gram, and was as small as a tenth of a gram in alloys containing gold. Metal filings or scrapings were not used since they are hard to handle in such small quantities. As far as possible, in weighing out metals, a single piece of metal was used, and it was pared down until it was of the correct weight. Only spectroscopically pure metals were employed and these were kept as clean as possible prior to melting.

In order to facilitate the research and also to avoid the complications which might arise from heat-treatment, the melt when once solidified was allowed to cool immediately to room temperature, in all cases except those in which heat-treatment was desirable. When difficulty was encountered in obtaining a specimen suitable for measurement, as in the case of some of the Ag–Sn and Cu–Pb alloys, the alloys were kept in a molten state for a considerable period of time. Annealing, consisting of maintaining the specimens at a high temperature for some time after solidification, was applied only to two alloys of the Tl–Sn system. Full details of these special cases are set forth below.

The method of preparation of alloys depended on their melting-points. In all cases where both constituents of the alloy were of low melting point, or where the concentration of the more refractory constituent was low, they were melted together in pyrex tubes *in vacuo*. In previous researches, after the melt was complete in the pyrex tube, it was strained through glass wool before entering the capillary section of the tube, where casting took place. In the present work, no glass wool was used since it sometimes happened that a piece of metal remained undissolved in its solvent of lower melting-point and became caught in the glass wool. In place of glass wool, a tube with a short but extremely fine capillary section was employed. The melt, forced through it by means of atmospheric pressure, was thereby cleaned effectively, and the tube could easily be inspected for undissolved pieces of metal.

With alloys containing higher concentrations of copper and gold, two methods were used. The first, a method similar to the one described above, required a quartz tube in place of pyrex, and was successfully used in several cases. A second method, however, was equally successful and much simpler. It consisted in placing the metal in a pyrex tube and nearly closing off the tube just above the metal. The tube was then exhausetd and heated until the metal with low melting-point had entirely surrounded the more refractory component. The tube was then filled with air, a quantity insufficient to cause appreciable oxidation, and again heated until the melt was complete. After a thorough shaking-up to ensure the homogeneity of the melt, and continued heating until the softened pyrex completely enclosed the molten pellet of metal, the tube was quickly drawn out, so that the metal solidified in the form of a thin wire suitable for measurement. Finally the glass was cracked away from the ends of the sample, leaving it ready for insertion into the cryostat. The specimens measured varied in size from half a centimetre to 5 cm. in length, and also varied considerably in cross-section. No attempt has been made to obtain values of specific resistance, since these are not pertinent to the present research.

Current and potential leads were attached to each sample, and resistances were measured by recording the potential drop across them. A Cambridge Instrument Co.

Vernier Potentiometer was used for this purpose. The measuring current in all cases was three-tenths of an ampere.

It was possible to make accurate measurements of temperatures below the normal boiling-point of liquid helium, 4·2° K. Temperature was determined by varying the pressure over the surface of the liquid helium by means of a large-capacity vacuum pump. Above 4·2° K, temperatures are more difficult to maintain since they are produced by upsetting the ideal liquefying conditions at the expansion valve of the liquefier. Measurements of temperature in this region are therefore accurate to only one-tenth of a degree. Temperatures above 4·2° K were recorded on a helium gas thermometer and checked with a constantan resistance thermometer.

Description of the Alloy Systems and their Supraconductivity.

Au–Sn.

The phase structure of the alloy system Au–Sn was examined by Vogel[4]. It was found to be comparatively complex and composed of several compounds and eutectics. According to Vogel, the system may be divided into seven regions. The first, a mixed crystal series, with the dominant structure that of gold, becomes saturated at 5 per cent. Sn. The second extends from the solubility boundary at 5 per cent. to the eutectic point at 20 per cent. Sn, and is a mixture of the eutectic and saturated mixed crystals. The eutectic is composed of mixed crystals and the compound AuSn. From 20 to 38 per cent. Sn, the phase consists of AuSn plus the eutectic. The fourth phase is bounded by the two compounds AuSn at 38 per cent. and $AuSn_2$ at 55 per cent. Sn, and consists of a mixture of the two boundary components. The fifth phase, ending at the compound $AuSn_4$ (71 per cent. Sn), is similar to the fourth phase. From 71 to 90 per cent. Sn, the structure is a mixture of $AuSn_4$ and the main eutectic of the system ($AuSn_4$+Sn). The final phase consists of the eutectic and primary Sn crystals.

Examination of the specific resistance, thermo-electric force, and volume of the alloy system has shown that all these phenomena undergo sudden changes at the point where the compound AuSn occurs. It was thought likely

that this point might also be the non-supraconductive boundary in the system.

Fig. 1 gives a composite picture of the variations of both supraconducting point and residual resistance throughout the alloy system Au–Sn. For purposes of comparison, figures of the equilibrium diagrams, reproduced from the National Critical Tables, have been set below each of the supraconductivity graphs of the various alloy systems examined. The supraconductivity diagrams contain three curves each. Two of these curves trace the supraconductivity of the system, and the third curve represents the variation of residual resistance of the alloys throughout the system. Residual resistance is the name given to that value of $R/R_0 = r$ which is exhibited by an alloy or pure metal at a temperature so low that the resistance-temperature curve becomes horizontal or very nearly so. Thus in a supraconductor, the residual resistance is the r-value at a temperature just above the transition interval. The upper supraconductivity curve shows the point where transition begins, that is, where the resistance curve commences to drop toward the supraconducting point. The lower curve traces the change in supraconducting point caused by the change in concentration throughout the alloy system. Thus the temperature interval in which the transition takes place is depicted by the ordinate distance between the upper and lower curves. The temperature scale for these two curves is given at the right of the diagram. Since the cryogenic laboratory in Toronto is not equipped to produce temperatures below 1·88° K, complete paths of the supraconductivity curves for the various alloy systems are not known, and we have therefore extrapolated the curves to meet the zero ordinate.

The supraconductivity of the Au–Sn system agreed, on the whole, with Vogel's phase diagram. Supraconductivity appeared only above 50 per cent. Sn, and rose to a value of 2·48° at $AuSn_2$. Between the two compounds $AuSn_2$ and $AuSn_4$, the supraconducting point rose to a maximum of 3·2° and then dropped to 2·40° at $AuSn_4$. Above $AuSn_4$ the supraconducting point rose abruptly to 3·5°, which is the transition temperature for the eutectic region lying between 71 and 100 per cent. Sn.

The residual resistance curve also coincided with the equilibrium diagram. The most outstanding feature of the

Fig. 1.

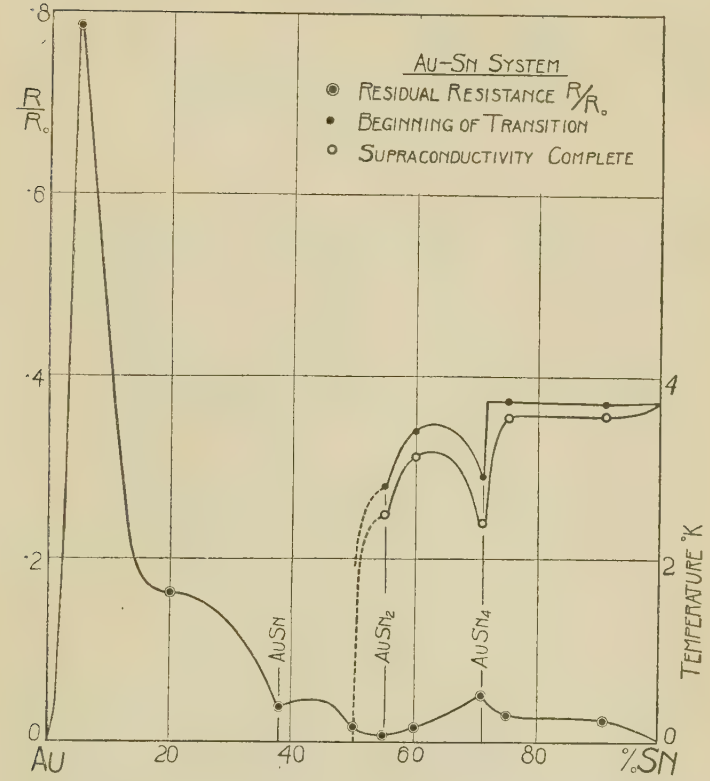
AU-SN SYSTEM
RESIDUAL RESISTANCE R/R₀
BEGINNING OF TRANSITION
SUPRACONDUCTIVITY COMPLETE
R/R₀
·8
·6
·4
·2
0
AU
20
40
60
80
%SN
AUSN
AUSN₂
AUSN₄
4
2
0
TEMPERATURE °K

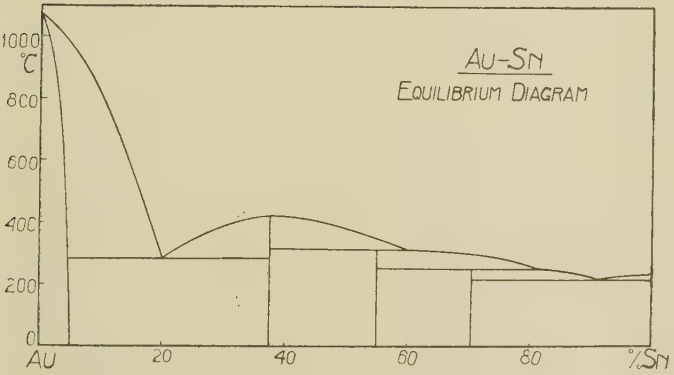
AU-SN
EQUILIBRIUM DIAGRAM
1000
°C
800
600
400
200
0
AU
20
40
60
80
%SN

Fig. 2.

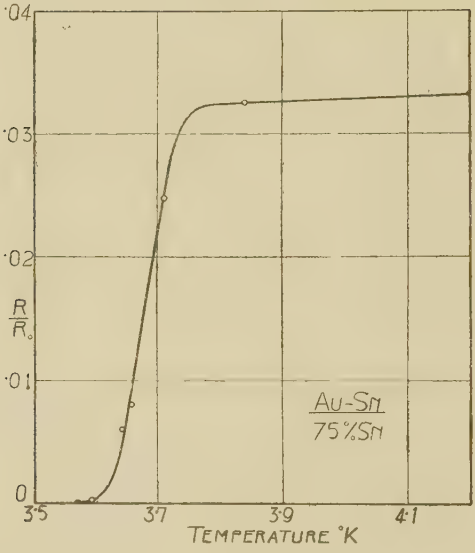

TABLE I.

Au–Sn.

Alloy.	Temperature at beginning of Transition Ta°K.	Supraconducting Temperature T°K.	*r*-value (R/R_0).
Pure Gold	—	—	·00029
5% Sn	—	—	·7850
20% Sn	—	—	·1638
38% Sn	—	—	·0310
50% Sn	—	—	·0147
55% Sn	2·8	2·48	·0084
60% Sn	3·5	3·125	·0156
71% Sn	2·9	2·4	·0551
75% Sn	3·72	3·57	·0325
91% Sn	3·72	3·57	·0230
100% Sn	3·72	3·71	·00079

curve was the sharp maximum which occurred at the saturation point of 5 per cent. Sn dissolved in Au.

The transition curve for the alloy containing 75 per cent. Sn is shown in fig. 2, and the measurements made on this system in the present investigation are given in Table I. The transition curves of the other alloys of the system were published last year.

Au–Pb.

According to Vogel [5], who examined it thermodynamically, the system may be divided into three phases. The first, from 0 to 45 per cent. Pb, is a mixture which contains three structural elements, primary gold crystals, the compound Au_2Pb, and a eutectic. The second phase, extending from 45 to 72 per cent. Pb, is characterized by only two structural elements, Au_2Pb and a eutectic. The third phase, from 72 to 100 per cent. Pb, contains two elements, the eutectic and primary lead crystals. The eutectic is given as a mixture of $AuPb_2$ and Pb.

The analysis of the supraconductivity and residual resistance of the Au–Pb system is shown in fig. 3, and the individual transition curves for alloys are given in fig. 4. The alloys containing 35 per cent., 45 per cent., 67 per cent. and 85 per cent. Pb were examined at an earlier date, and the results and diagrams published in a previous paper [2] by the writer in collaboration with McLennan and Wilhelm. An examination of figs. 3 and 4 shows that, from the standpoint of supraconductivity, the system may be divided into three phases as before, but with other boundaries than those given by Vogel. Here the phase boundaries may be placed at about 8 per cent. Pb, and 35 per cent. Pb (the proportion giving Au_2Pb). Vogel examined no alloy of Au–Pb containing less than 10 per cent. Pb and in consequence found nothing unusual in this region of the equilibrium diagram. At 8 per cent. Pb, however, we found a very pronounced peak of residual resistance, and at the lowest temperature a slight drop in the resistance curve of the alloy itself, which latter fact indicates the proximity of a supraconductive phase in the system. In the region above 8 per cent. Pb, the residual resistance dropped continuously to a minimum at 35 per cent. Pb (Au_2Pb), and at the same time supraconductivity appeared and the transition point rose steadily to the value 3·57° at Au_2Pb.

Fig. 3.

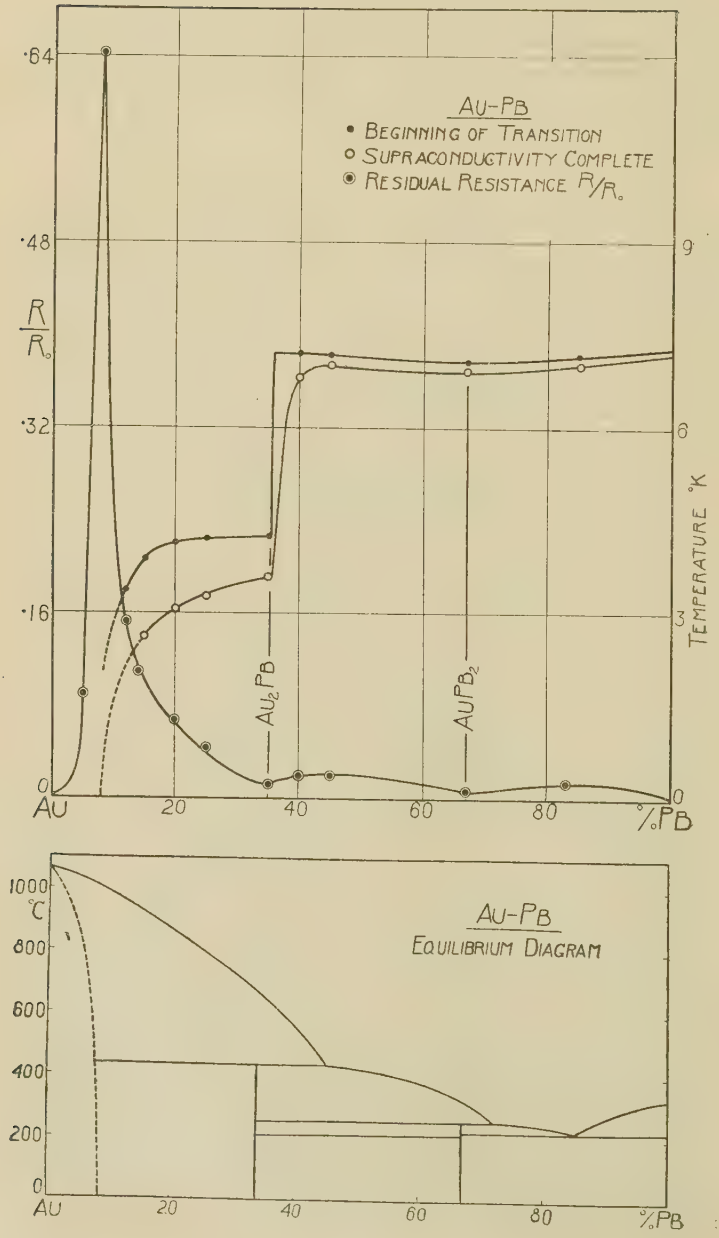
AU-PB
• BEGINNING OF TRANSITION
○ SUPRACONDUCTIVITY COMPLETE
◉ RESIDUAL RESISTANCE R/R₀
·64
·48
·32
·16
0
R/R₀
AU
20
40
60
80
%PB
AU₂PB
AUPB₂
9
8
7
6
TEMPERATURE °K
1000
°C
800
600
400
200
0
AU-PB
EQUILIBRIUM DIAGRAM
AU
20
40
60
80
%PB

Fig. 4.

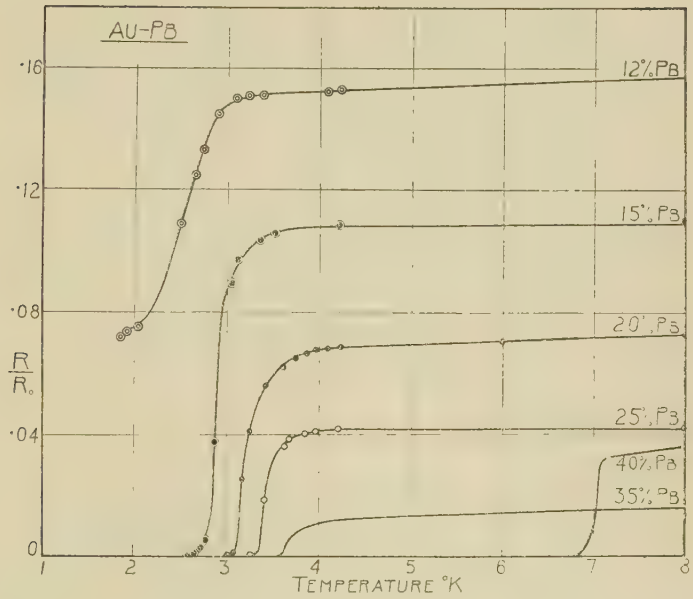

Table II.

Au–Pb.

Alloy.	Ta°K.	T°K.	*r*-value.
Pure Gold	—	—	·00029
5% Pb	—	—	·0881
8% Pb	2·5	—	·6200
12% Pb	3·0	—	·1500
15% Pb	3·7	2·59	·1070
20% Pb	4·0	3·04	·0673
25% Pb	4·2	3·25	·0427
35% Pb	4·2	3·59	·0122
40% Pb	7·2	6·8	·0343
45% Pb	7·2	7·0	·0192
67% Pb	7·1	6·9	·0063
85% Pb	7·2	7·0	·0125
100% Pb	7·3	7·2	·0010

As the concentration of lead increased above Au_2Pb, the supraconducting point rose abruptly to 7·1° at a concentration of 45 per cent. Pb, and remained fairly constant throughout the rest of the system except for a slight minimum at the concentration giving $AuPb_2$. At this concentration occurred also a minimum in the residual resistance curve.

The pronounced peak of residual resistance at 8 per cent. Pb may be indicative of a solubility boundary, since such peaks were observed in several systems such as Au–Sn and Tl–Sn at points where solubility boundaries are known to exist. The solubility boundary indicated has been inserted in the equilibrium diagram as a dotted line.

Measurements made on the alloys of this system are given in Table II.

Ag–Sn.

Petrenko[6] has examined the system thermodynamically and divided it into four phases. The first, 0 to 19 per cent. Sn, is a series of homogeneous mixed crystals. At 19 per cent. Sn appears a new structural element, the compound Ag_3Sn. This phase extends to 27 per cent. Sn, the proportion which forms pure Ag_3Sn. The third phase extends from 27 to 96·5 per cent. Sn, and contains Ag_3Sn plus a eutectic. The eutectic is given as a mixture of Ag_3Sn+Sn. The final phase, above 96·5 per cent. Sn, consists of the eutectic and primary tin crystals.

The alloys containing 27 per cent., approximately 30 per cent., 50 per cent., and 96·5 per cent. Sn, were examined and the results published a year ago. The transition curves for the alloys of the rest of the system are shown in fig. 6. In fig. 5 it is seen that the analysis of the system for supraconductivity and residual resistance is comparatively simple. The compound Ag_3Sn was examined previously by de Haas[7] and found to be non-supraconducting down to 1·0° K. There was, however, a considerable drop in resistance at the lowest temperature, indicating that it was close to a supraconductive alloy region. In alloys immediately above the proportion Ag_3Sn supraconductivity appears, mounts quickly to the value 3·57° K, and, except for a slight minimum at the eutectic point (95·5 per cent. Sn), remains fairly constant throughout the rest of the system.

The residual resistance curve in the silver-rich mixed crystal phase rises to an extraordinarily high value near

Fig. 5.

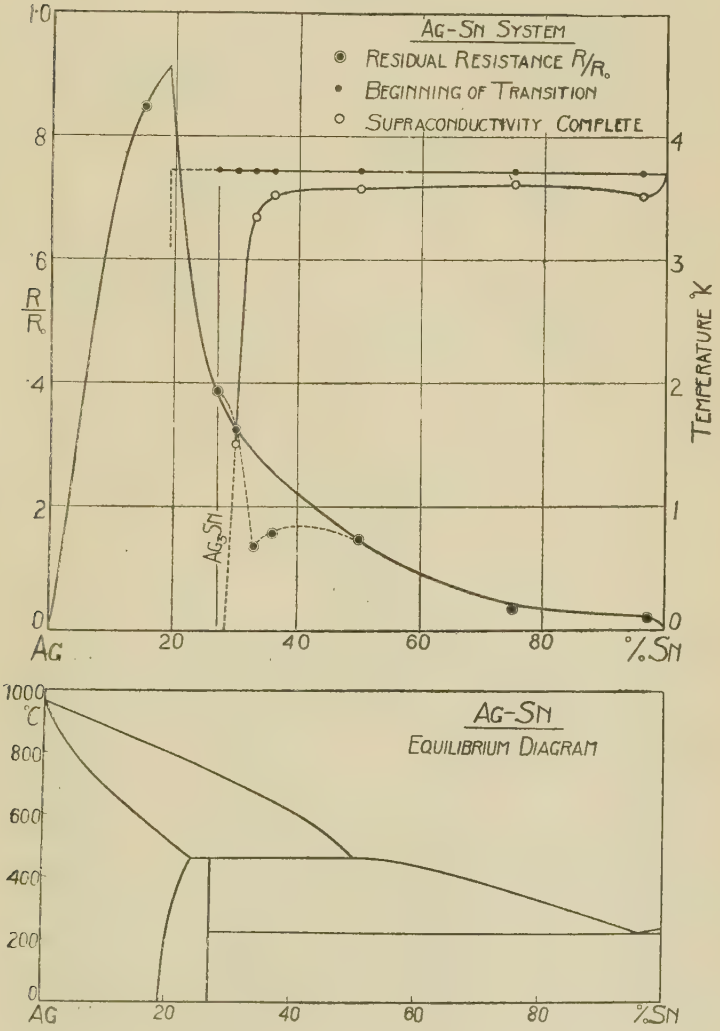

the saturation point (19 per cent. Sn). With higher tin concentration, the r-value drops rapidly toward the eutectic point and then makes a sharper drop to the

value for pure Sn. The r-value obtained by de Haas for Ag_3Sn has been used in fig. 5. Unusually low r-values

Fig. 6.

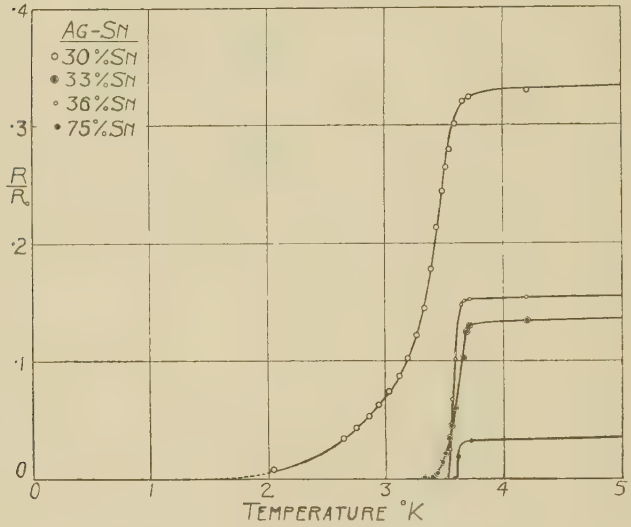

TABLE III.

Ag–Sn.

Alloy.	Ta°K.	T°K.	r-value.
Pure Silver	—	—	·00288
15% Sn	—	—	·8470
27% Sn	3·72	—	·3950
30% Sn	3·72	appr. 1·5	·3240
33% Sn	3·72	3·33	·1301
36% Sn	3·72	3·52	·1520
50% Sn	3·72	3·57	·1504
75% Sn	3·72	3·62	·0311
96% Sn	3·72	3·52	·0209
100% Sn	3·72	3·71	·00079

were obtained for the alloys containing 33 per cent. and 36 per cent. Sn. In the preparation of these two alloys some difficulty was encountered in obtaining, in the

capillary tubes, lengths of metal suitable for measurement. The alloys were remelted and kept in a molten state for some time in an effort to obtain the desired form. The low r-values observed may therefore be an effect due to a closer approach to constitutional equilibrium in the alloys.

Measurements on the Ag–Sn alloys investigated are given in Table III.

Fig. 7.

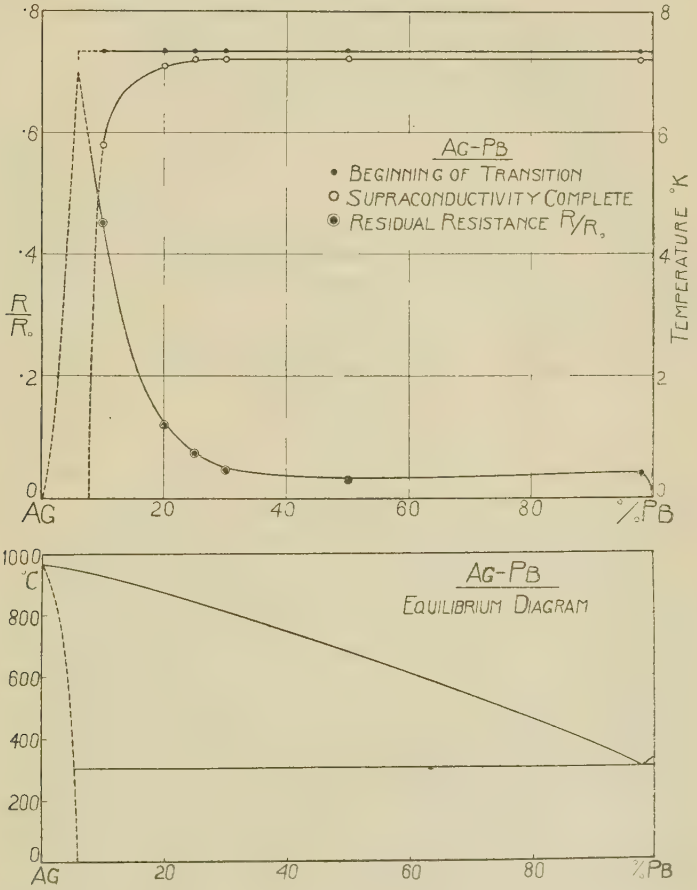

Ag–Pb.

The system Ag–Pb was also examined by Petrenko[6], and found to consist of a single eutectic region. The eutectic, which is a mixture of Ag and Pb, is present

throughout the whole system in conjunction with either primary Ag or Pb crystals.

Fig. 8.

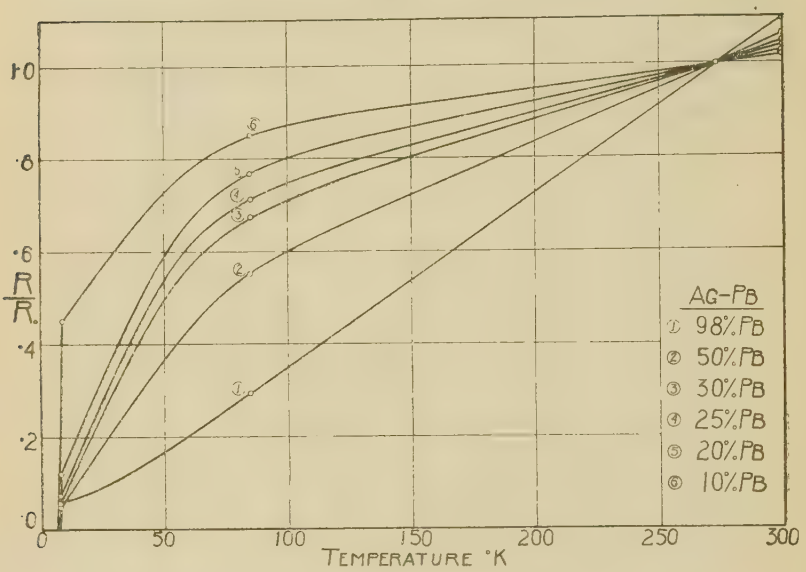

TABLE IV.

Ag–Pb.

Alloy.	Ta°K.	T°K.	*r*-value.
Pure Silver	—	—	·00288
10% Pb	7·3	5·8	·4520
20% Pb	7·3	7·1	·1197
25% Pb	7·3	7·2	·0733
30% Pb	7·3	7·2	·0415
50% Pb	7·3	7·2	·0293
98% Pb	7·3	7·2	·0475
100% Pb	7·3	7·2	·0010

The examination of the system for supraconductivity and residual resistance, fig. 7, seemed to agree, in all but one particular, with Petrenko's phase diagram.

There was observed, in silver-rich alloys, an approach to a peak of residual resistance coincident with a drop of supraconducting point. The peak was not located precisely, but probably occurs in the neighbourhood of 6 per cent. Ag. It was inferred, from similar cases in other alloy systems, that a solubility boundary might occur in this system with silver dissolving as much as 6 per cent. lead. The solubility boundary thus indicated has been entered in the equilibrium diagram by a dotted line. Throughout the Ag–Pb system above 30 per cent. Pb, the supraconducting point remained perfectly constant as far as it was experimentally possible to determine. The residual resistance rose slightly to the eutectic point at 98 per cent. Pb, and then dropped sharply to the r-value for pure lead.

Fig. 8 shows the resistance curves over the entire range of temperatures observed for all the Ag–Pb alloys examined. The results are drawn from Table IV. The curves have been given in complete form in order to show their peculiar nature. The only normal curve is that for the eutectic, 98 per cent. Pb. The rest show varying convexities to the temperatures axis.

Cu–Sn.

Many experimenters have investigated this complicated alloy system, but probably the most complete thermal analysis is that of Haughton[8]. The system contains two compounds, Cu_4Sn and Cu_3Sn, and the rest of the system is broken into numerous solubility and eutectic phases. According to Haughton, Sn is capable of holding only about 1 per cent. Cu in solid solution, which saturated solution forms the eutectic of the system. The analysis for supraconductivity and residual resistance, seen in fig. 9, was simpler than was expected in so complicated a system. The residual resistance rose in the first mixed crystal phase (from 0 to 15 per cent. Sn). The next phase, which terminates in Cu_4Sn (32 per cent. Sn), possessed a uniformly high r-value, which dropped quickly in the following narrow phase to a lower value at Cu_3Sn. De Haas[7] has examined these two compounds and found that neither shows any signs of supraconductivity at a temperature as low as 1·0° K. Since an alloy containing 45 per cent. Sn became supraconducting at

2·7° K, Cu_3Sn at 38 per cent. Sn most likely forms the non-supraconductive boundary to the supraconductive region of the alloy. The phase from 38 to 60 per cent. Sn

Fig. 9.

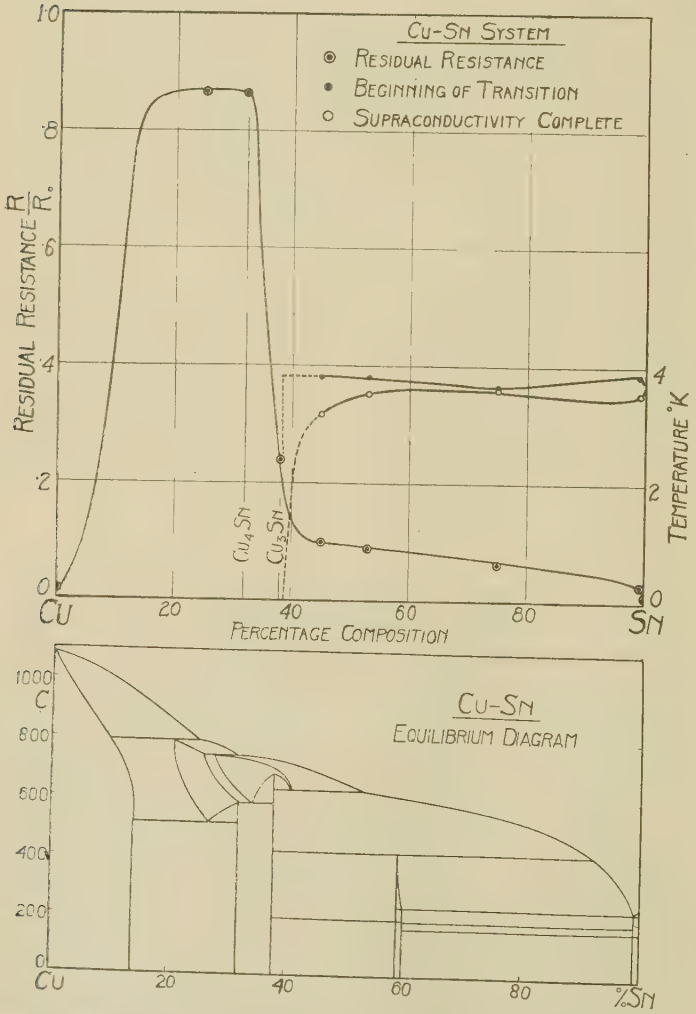

is a mixture of Cu_3Sn plus Sn, and was characterized by a quick rise to a steady value of 3·5° K. The final eutectic region, from 60 per cent. Sn to pure tin, maintained a fairly steady supraconducting point with a

Fig. 10.

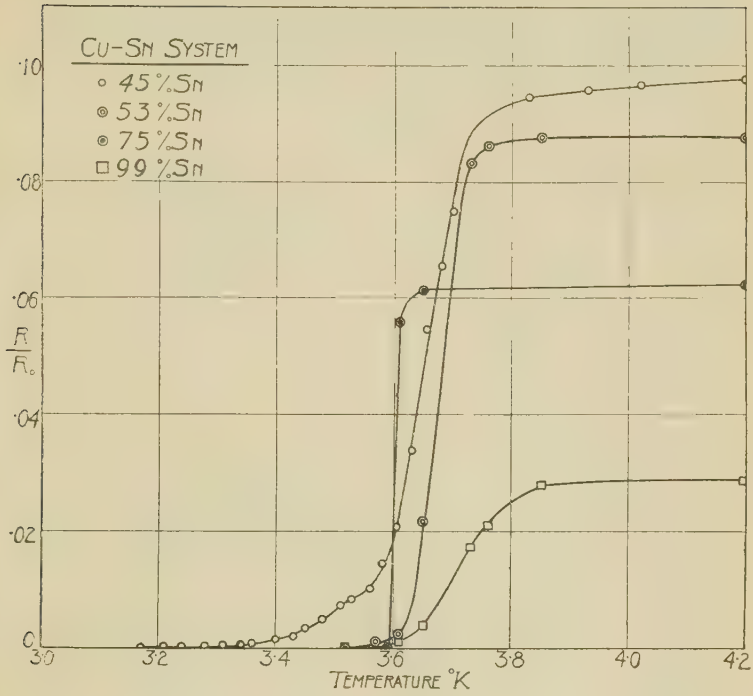

Table V.

Cu–Sn.

Alloy.	Ta°K.	T°K.	τ-value.
Pure Copper	—	—	·00029
25% Sn	—	—	·8640
32% Sn	—	—	·8630
38% Sn	—	—	·2370
45% Sn	4·0	3·17	·0974
53% Sn	3·85	3·52	·0871
75% Sn	3·70	3·59	·0623
99% Sn	3·85	3·52	·0279
100% Sn	3·72	3·71	·00079

slight minimum at the eutectic point. The r-value diminished in a straight line to the eutectic point, and then suffered a sudden drop to the value for pure Sn.

The transition curves drawn from Table V. are shown in fig. 10.

Fig. 11.

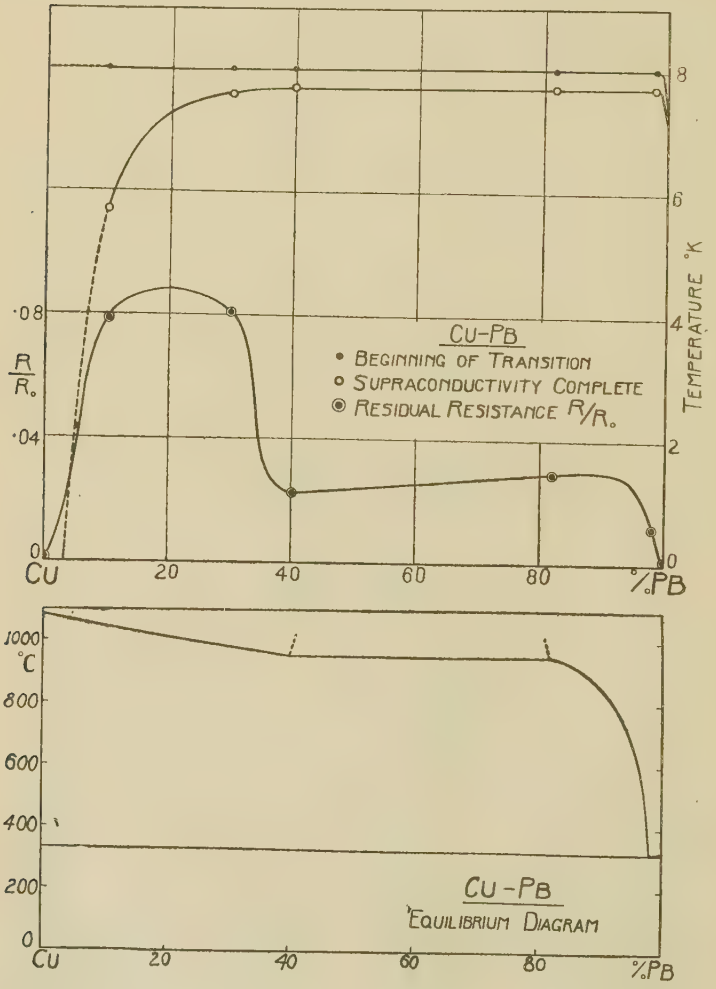

Cu–Pb.

Only a superficial thermal analysis of the Cu–Pb system has been made. Heycock and Neville[9] in 1897

investigated the freezing-point curve of the system and found it to possess a eutectic at 98 per cent. Pb, and the whole system to be a single eutectic region.

Fig. 12.

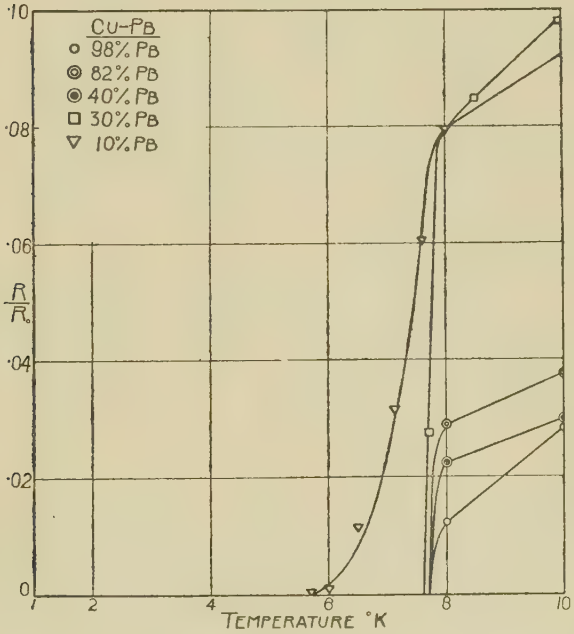

TABLE VI.

Cu–Pb.

Alloy.	Ta°K.	T°K.	*r*-value.
Pure Copper	—	—	·00029
10% Pb	8·0	5·7	·0795
30% Pb	8·0	7·7	·0847
40% Pb	8·0	7·7	·0223
82% Pb	8·0	7·7	·0289
98% Pb	8·0	7·7	·0122
100% Pb	7·3	7·2	·0010

In the analysis of the system with regard to supraconductivity and residual resistance, depicted in fig. 11, the r-value curve showed a broad maximum in alloys of low lead content. Supraconductivity appeared very near the point of pure copper and rose quickly to a constant value of 7·7° K at 40 per cent. Pb. This value was maintained as far as the eutectic point at 99 per cent. Pb, after which it dropped to 7·2° K for pure lead.

In a previous general research on supraconductivity in alloys, a Pb–Cu alloy containing 50 per cent. Pb was examined and reported to be non-supraconductive. The erroneous result may have been due to imperfect mixing, since homogeneity, especially in the copper-rich alloys, was difficult to obtain.

The individual transition curves for the various Cu–Pb alloys examined are shown in fig. 12 from data in Table VI. They resemble closely the transition curves for pure lead and for the lead-rich Au–Pb alloys, in that there is no flattening-out of the resistance curve immediately above the transition region.

Tl–Sn.

This system has been examined thermodynamically by Fuchs[10]. It consists of a eutectic region from 0 to 80 per cent. Tl, which latter figure represents the saturation point of the mixed crystal series that covers the rest of the system to pure thallium.

Preliminary measurements from an X-ray examination of the Tl–Sn system * reveal that whereas pure thallium possesses a close-packed hexagonal structure, the solution of tin in the mixed crystal phase from 80 to 100 per cent. Tl produces a face-centred cubic lattice. This structural change, due to the solution of Sn in Tl, is easily explained since it requires but slight shifting of the Tl atoms to pass from one structure to the other. The lattice constant is changed from $a=3{\cdot}45$ Å for hexagonal close-packed thallium, to an average of 4·80 Å for the face-centred cubic lattice of the solid solution.

In the eutectic alloy region of the system, the two components present are the tetragonal structure of Sn

* 'On the Crystal Structure of the Tl-Sn Alloy System.' Research to be published in the near future by Professor E. F. Burton and Mr. J. P. Blewett of the University of Toronto.

and the face-centred cubic lattice of the solid solution. There is observed, however, a continuously changing lattice constant for each of the structures throughout the whole eutectic region. Incomplete measurements on the solid solution component indicate that the lattice constant has a minimum at the saturation boundary (80 per cent. Tl), and a maximum at the eutectic point (42·5 per cent. Tl). The tetragonal tin lattice constant also shows a maximum at the eutectic point. Such lattice expansions and contractions are unusual in a eutectic region and must involve some form of unlimited solubility of Tl in Sn and *vice versa*.

The supraconductivity of the system was examined by Meissner[3] last year. Meissner had observed oddly shaped transition curves for the alloys in the eutectic region of the system, and curves of a more normal shape for mixed-crystal, thallium-rich alloys. The abnormal curves had the appearance of arising possibly from the presence of a small amount of pure thallium in the otherwise homogeneous alloy sample. The observed results were explained by Meissner as probably due to partial disintegration of an unstable component in the alloys. The supraconductivity curve for the alloy system, as determined from the alloy transition curves, showed violent fluctuations which did not in any way conform to the equilibrium diagram.

In view of the results obtained by Meissner it was decided to examine the system again. The results of the present examination are shown in figs. 13 to 17, which are drawn from Tables VII. and VIII. The data obtained agreed with Meissner's for only the solubility phase between 80 and 100 per cent. Tl. Throughout the eutectic region below 80 per cent. Tl the supraconducting point was found to vary continuously, with a cusp-shaped minimum occurring at the eutectic point 42·5 per cent. Tl, and with a peak at the solubility boundary. The residual resistance followed the same type of path as the supraconductivity curve, with a cusp at the eutectic point and a steady rise to a sharp peak at the boundary between the eutectic and mixed crystal phases.

A feature of this system is the great transition interval of temperature which was found throughout the system. This interval was smallest at the eutectic concentration and immediately increased on both sides of this point.

Fig. 13.

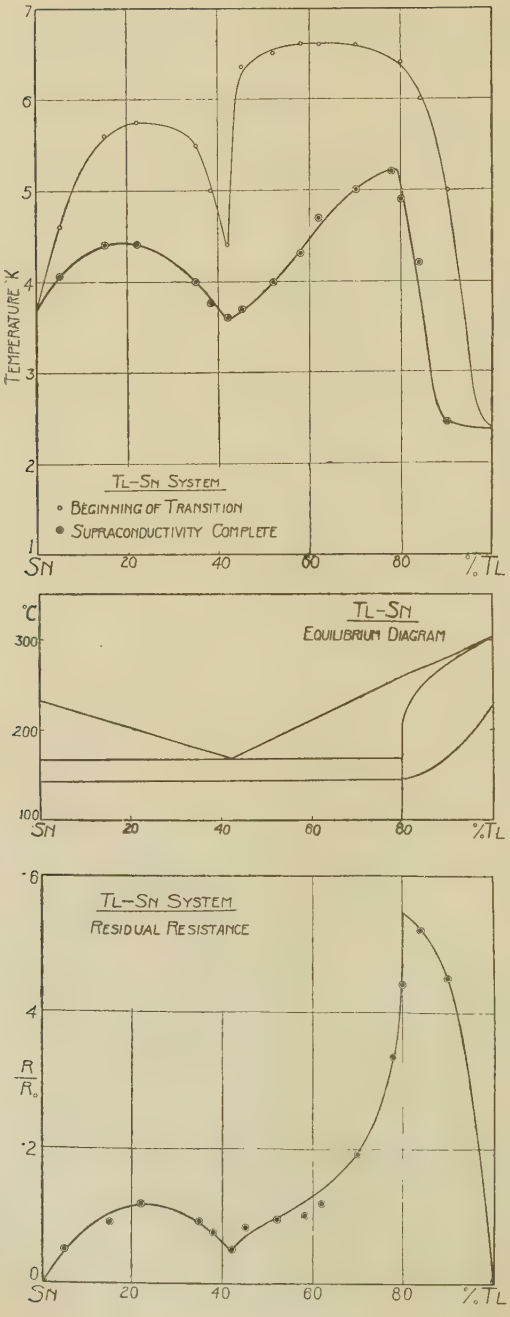
TEMPERATURE °K
7
6
5
4
3
2
1
Tl–Sn System
° Beginning of Transition
• Supraconductivity Complete
Sn
20
40
60
80
% Tl
°C
300
200
100
Tl–Sn
Equilibrium Diagram
Sn
20
40
60
80
% Tl
·6
4
R/R₀
·2
0
Tl–Sn System
Residual Resistance
Sn
20
40
60
80
% Tl

The size of the transition interval is also noticeable in figs. 14, 15, and 16, which show the transition curves for all the Tl–Sn alloys examined. In the results from the alloy group from 45 to 78 per cent. Tl, there is a slight resemblance to the curves obtained by Meissner, in that

Fig. 14.

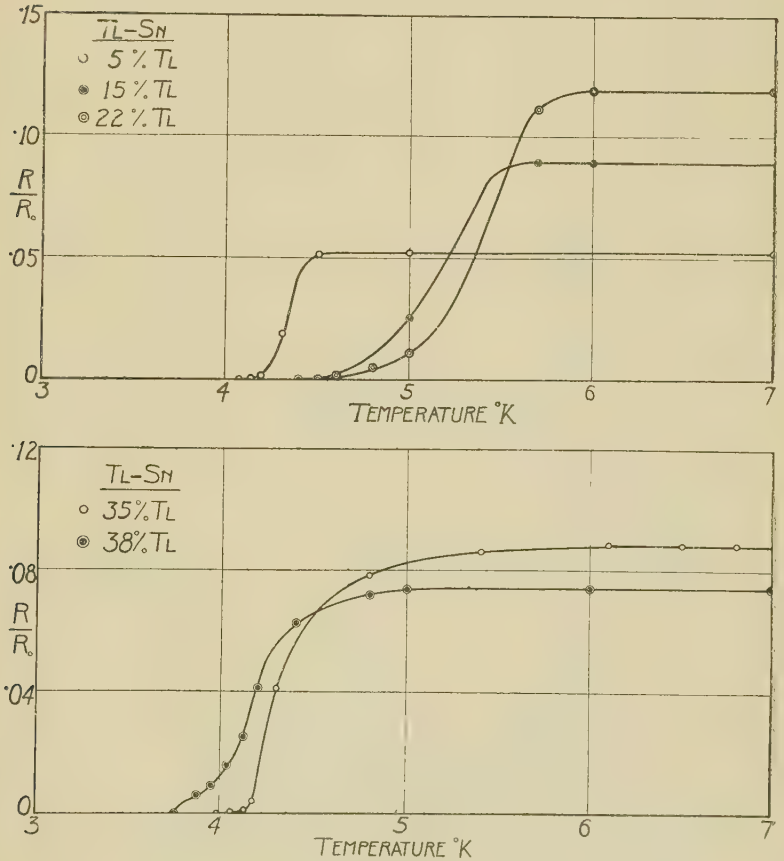

these alloys showed a sharp drop in resistance at the beginning of the transition interval, followed by a more gradual final approach to supraconductivity.

In a further attempt to duplicate Meissner's results an alloy containing 45 per cent. Tl was prepared by the method that Meissner used. This procedure required

both cold-working and annealing. The 45 per cent. Tl alloy was first drawn down to 50 per cent. of its original diameter and a test piece removed. The drawn sample was then rolled to 0·5 per cent. of its original diameter, during various stages of which process samples were

Fig. 14 (*cont.*).

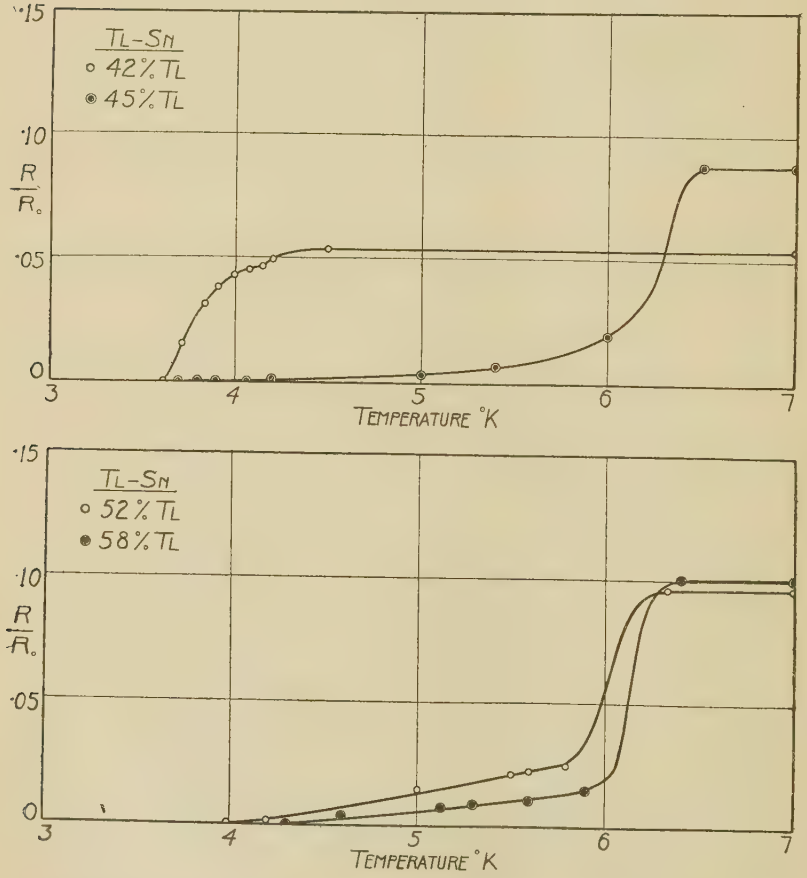

again taken off. Annealing was not attempted on the test pieces that had been worked, since it had been found that this procedure tended to disintegrate the alloy, even when heated in glycerine to a temperature considerably below the melting-point of the alloy. In order to test the effect of annealing, however, two alloys,

52 per cent. and 58 per cent. Tl, immediately after casting and while still under a vacuum in the pyrex tubes, were

Fig. 15.

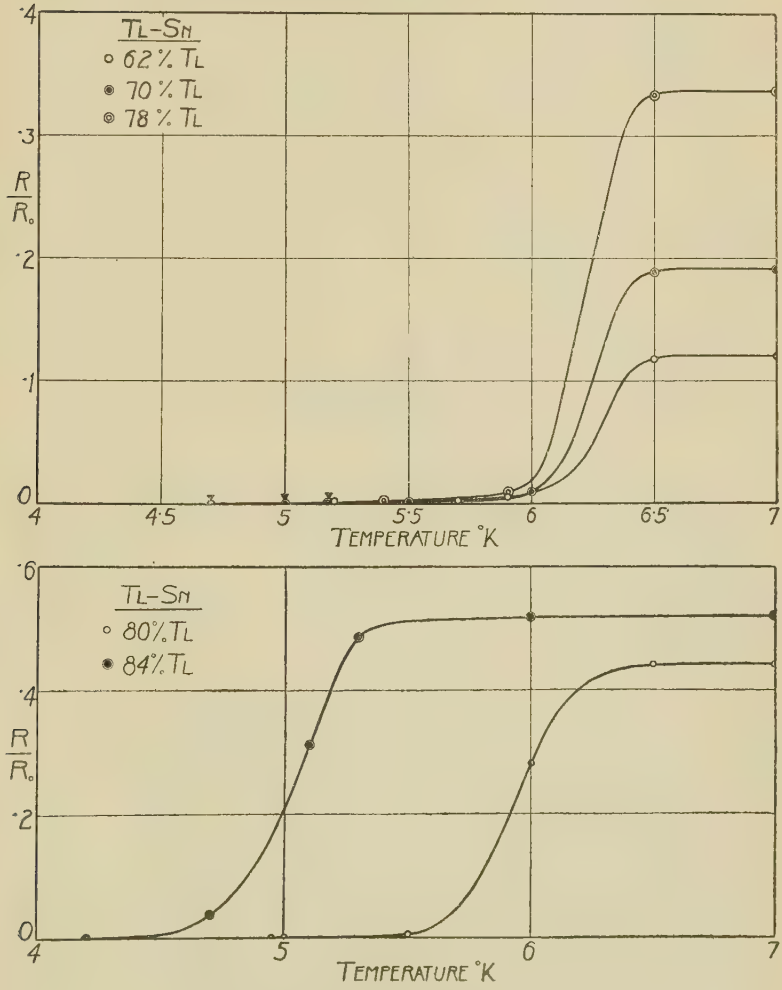

kept at a temperature slightly under the melting-point for twenty minutes. The measurements on these two alloys (fig. 14) show slightly elevated lower portions of the transition curves. In fig. 13 it is seen that the r-values

for these two alloys fall below the residual resistance curve.

Fig. 16.

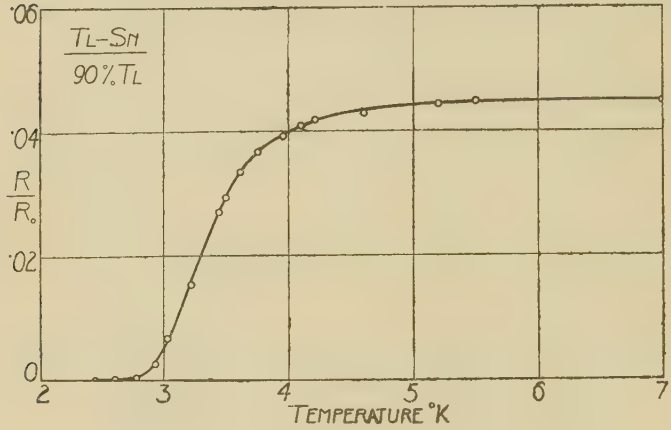

Fig. 17.

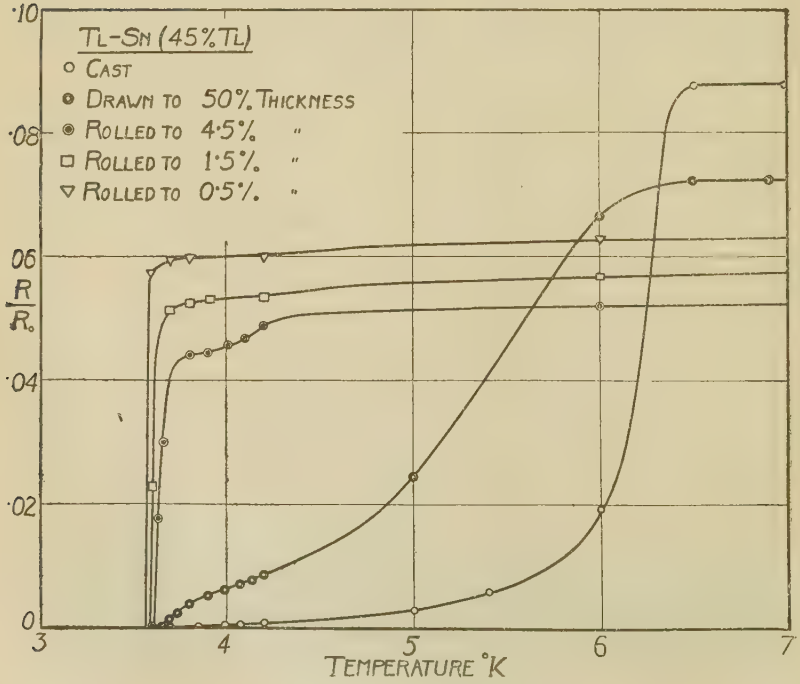

TABLE VII.

Tl–Sn.

Alloy.	Ta°K.	T°K.	*r*-value.
Pure Tin	3·72	3·71	·00079
5% Tl	4·5	4·06	·0518
15% Tl	5·5	4·4	·0890
22% Tl	5·6	4·4	·1130
35% Tl	5·4	3·98	·0885
38% Tl	4·3	3·75	·0740
42% Tl	4·0	3·61	·0535
45% Tl	6·4	3·69	·0877
52% Tl	6·5	3·99	·0965
58% Tl	6·6	4·3	·1002
62% Tl	6·5	4·7	·1192
70% Tl	6·5	5·0	·1880
78% Tl	6·5	5·2	·3365
80% Tl.	6·4	4·9	·4400
84% Tl	6·0	4·2	·5200
90% Tl	5·2	2·45	·4450
100% Tl	2·37	2·37	·00054

TABLE VIII.

Tl–Sn (45% Tl).

Treatment.	Ta°K.	T°K.	*r*-value.
Cast	6·4	3·69	·0877
Drawn to 50% diam.	6·4	3·655	·0723
Rolled to 4·5% „	4·5	3·605	·0500
„ „ 1·5 „	3·8	3·58	·0530
„ to 0·5 „	3·6	3·56	·0570

The measurements on the various test pieces of the cold-worked alloy containing 45 per cent. Tl are shown in fig. 17. Here the effect of working on the transition

curve is pronounced. The large transition interval is seen to disappear gradually on continued drawing and rolling of the metal, and the final transition curve observed for the alloy when rolled to ·005 per cent. diameter, strongly resembles that observed for a single crystal. During the cold-working process the residual resistance is also seen to vary, although irregularly, and the supraconducting point is slightly depressed.

The results of cold-working and annealing are slightly analogous in that they both tend to reduce the magnitude of the transition interval. The explanation of this phenomena has been given in previous papers, and instances of it have been noted by de Haas[11], who first explained it, and by the writer in collaboration with McLennan and Wilhelm. De Haas found that a tensional stress applied to a supraconductor raised its transition temperature. He also found that, as a piece of metal approached more and more closely the perfection of a single crystal, the transition interval from normal to supraconductivity became smaller and smaller until the transition itself appeared to be discontinuous. Thus he deduced that the real transition normally observed was caused by stresses between the unaligned faces of crystallites in the metal. The reason for the large transition interval observed in Tl–Sn alloys might be explained in some such way, and the effect of rolling or heat treatment may be to align the crystallites and thereby eliminate the stresses between them, or, in short, to simulate a single crystal.

Discussion.

Supraconductivity.

For purposes of generalization, the alloy systems examined in the present research were admirably suited. They were sufficiently varied in detail to present many different situations, and yet similar enough to lend coherence to the conclusions which were drawn.

It is clear from the results of this research, as well as from the investigation by Meissner and his collaborators, that one is no more justified in saying that an alloy system has a unique supraconducting point than that it has a particular hardness or specific resistance. It will be shown in the following discussion that the supraconductivity of an alloy depends on its structure.

From the standpoint of supraconductivity there are three general structural types in alloy systems. The first type comprises eutectic regions, which consist of simple mixtures of two components, and in which varying concentration causes no expansion or contraction of the component lattices. The second structural type is that of a solid solution or simple mixed crystal series, in which change in the concentration of the solute results is a change of the lattice constant. This second type is usually found as a narrow phase at the end of an alloy system, where it is bounded by the pure solvent and the saturation boundary of the solution. The third type is a combination of the first and second, in that it is usually a eutectic region of which both components form mixed crystal series, and in that the effect of change in concentration is to alter the lattice constants of both phases simultaneously.

Examples of structure of the first type are seen in six of the seven systems examined, namely :—

Alloy.	Eutectic Regeion.
Au–Sn	71 to 100 per cent. Cu.
Au–Pb.....	27 to 100 ,, ,, Sn.
Ag–Sn	27 to 100 ,, ,, Sn.
Ag–Pb	6 to 100 ,, ,, Pb.
Cu–Sn	38 to 100 ,, ,, Sn.
Cu–Pb	Entire system.

Eutectic regions were examined also by Meissner in the sustems Pb–Bi and Pb–Hg.

Characteristic of the eutectic region was a supraconducting point which, except in the neighbourhood of the boundaries, maintained a practically constant value. The supraconducting point was always observed to be close to that of the supraconductive component, although, in the case of Cu–Pb, the transition temperature for the eutectic region is half a degree higher than that for pure lead. A similar displacement was observed by Meissner[3] in the Pb–Bi system, in which the eutectic region had a supraconductive point of 8·8° K, or 1·6° higher than that of lead. The high value was attributed by Meissner to the fact that one component of the eutectic is a saturated solution of Bi in Pb. It might consequently be inferred that the eutectic in the Cu-Pb system is formed by a

saturated solution of 2 per cent. Cu in Pb. In the eutectic regions of Ag–Sn and Cu–Sn, a slight depression in the transition temperature was observed at the respective eutectic points. The depression in each case, however, was less than two-tenths of a degree.

Near the boundary of a eutectic region the supraconducting point changed rapidly. The example investigated most thoroughly was the region near the eutectic boundary Ag_3Sn in the Ag–Sn system. As the eutectic boundary was approached, the supraconducting point dropped over half a degree for each change of one per cent. in concentration. Transition curves were observed in other alloy systems for alloys near the eutectic boundary, namely Au–Pb (40 per cent. Pb), Ag–Pb (10 and 20 per cent. Pb), Cu–Sn (45 per cent. Sn), and Cu–Pb (10 per cent. Pb). Thus it is apparent that supraconductivity does not depend on the short circuit of a supraconductive component through a specimen, but that each concentration of the components in an alloy possesses a definite supraconducting point. In other words, supraconductivity is not a property of one component of an alloy, but is a property of the general structure of that alloy.

Regardless of variations in the supraconducting point in a eutectic region, the curve showing the commencement of transition throughout the region does not vary. The curve, moreover, appears to extend to the boundary of the region and then to break suddenly to a new value in another alloy phase, or else to disappear entirely at a non-supraconductive boundary. In the Au–Pb system the break is from 7·3° K to 4·2° K at the eutectic boundary Au_2Pb. A different condition is observed in the Ag–Sn system. Ag_3Sn forms a non-supraconductive boundary to the eutectic phase, but below 3·7° K its resistance drops about 50 per cent. in value. Since Ag_3Sn is present as a constituent in the mixture phase from 19 to 27 per cent. Sn, we were led to assume that resistance curves in this region would also exhibit changes below 3·7° K. Hence, although supraconductivity disappeared at about 29 per cent. Sn, the curve showing the commencement of the transition should extend to 19 per cent. Sn before breaking. In the case of the Cu–Sn eutectic region, the curve representing the commencement of transition is not quite constant. The deviation may be due either

to lack of internal equilibrium or to the nature of crystallization, both of which factors profoundly affect the magnitude of the transition interval. The Cu–Pb system is apparently a single eutectic phase, and therefore the curve showing the beginning of transition to supraconductivity extends to the pure copper and pure lead boundaries. The addition of even a trace of lead to copper should result in a drop in resistance commencing at 8·0° K.

Supraconductivity in the second structural type, *i. e.*, mixed crystal phases, differs completely in character from supraconductivity in eutectic phases. Most of the mixed crystal or solubility phases in the alloy systems examined occurred at the non-supraconductive end of the systems, and were found to be themselves non-supraconductive. Two supraconductive solubility phases did come under observation, namely, Tl–Sn (80 to 100 per cent. Tl), and Au–Sn (50 to 55 per cent. Sn). The latter, however, was not thoroughly examined. Meissner and his collaborators have investigated several solubility regions, notably the systems In–Tl, in which both components showed unlimited solubility. Meissner observed that, in a solid solution phase, the supraconducting point varied continuously between the phase boundaries. He found, moreover, that the curve showing the commencement of transition also varied continuously throughout the phase, and varied in such a way that the transition interval was least at the boundaries and greatest in the middle of the phase. This phenomenon he explained as due to slight irregularities in the statistical arrangement of the solute atoms in the solvent lattice, which irregularities naturally would be greatest in the middle of the phase, and theoretically zero at both the pure solvent and saturation boundaries. The irregularities would cause strains to be present, which would in turn, according to the theory of de Haas, cause localized supraconductivity to appear at a temperature slightly higher than that required for complete supraconductivity.

The solubility region from 80 to 100 per cent. Tl in the Tl–Sn system, showed a continuous change in supraconducting point from 2·3° K for pure thallium to 5·2° K at the saturation point (20 per cent. Sn). In two respects the present results differed from those of Meissner. In the first place, Meissner observed the peak in the

supraconductivity curve at the mixed crystal saturation point to be only 4·2° K. In his report, however, Meissner expressed the view that probably a slight eutectic disintegration caused the supraconductivity peak to be unexpectedly low, and that if a boundary alloy were quenched or supercooled from the melting-point it might exhibit a supraconducting point of 4·5° K or higher. Whether or not such is the case, our investigations of quickly cooled alloys showed that the peak in supraconductivity at the saturation point of the mixed crystal phase occurred at 5·2° K.

The second point of difference between the results of the present research and those of Meissner, appeared in the magnitude of the transition interval. The small interval observed by Meissner in alloys in the solubility region of Tl–Sn, has been explained already as the result of cold-working the alloys after casting. In the present research the transition interval was negligible for pure Tl, but grew to 2·5° at 10 per cent. Sn and then decreased to 1·2° in the saturated solution. Thus the variation of magnitude of the transition interval agreed with the general deductions of Meissner regarding this phenomenon.

The existence of a solubility phase between 50 and 55 per cent. Sn in the Au–Sn system (fig. 1), was considered the only possible explanation for the disappearance of supraconductivity within that region. From a consideration of the other alloy systems examined, the non-supraconductive boundary to a supraconductive region is always either a compound or a saturation boundary. We assumed, therefore, that a slight solubility of Au in $AuSn_2$ was possible, and that the saturation point of the solution formed the non-supraconductive boundary in the system.

The third type of alloy structure, is comparatively uncommon. As has been indicated above, it is usually a eutectic region in which the lattice dimensions of both components vary continuously with the concentration. Three examples of this type of structure were observed, namely: the eutectic region from 0 to 80 per cent. Tl in Tl–Sn, the region from 8 to 35 per cent. Pb in Au–Pb, and the phase between $AuSn_2$ and $AuSn_4$ in Au–Sn.

Although Vogel found three structural elements present in the region of Au–Pb under consideration, it is probable

that there are only two, Au_2Pb and lead saturated gold crystals.

The supraconductive characteristics observed in Au–Pb, 8 to 35 per cent. Pb, were similar to those observed in simple solubility phases. The supraconducting point varied continuously in the region and the transition interval reached a maximum in the middle of the phase. The change in position of the transition curve relative to change of concentration is shown in fig. 4.

The lattices of the two structures $AuSn_2$ and $AuSn_4$ are not known, but the region between them must contain both compounds in varying proportions. This phase must therefore come into the third structural category, since its supraconductivity curve (fig. 1) and transition interval varied in a fashion similar to that of the tin-rich half of the Tl–Sn eutectic region.

The eutectic region of the Tl–Sn system is possibly the most interesting case examined. Both halves of the region (fig. 13) exhibited the distinctive supraconductive characteristics of a simple mixed crystal phase. The transition interval increased from zero for pure tin to 1·3° for 22 per cent. Tl, and then decreased to 0·8° at the eutectic point. The interval grew to 2·5° again near 60 per cent. Tl, and again shrank to 1·2° at the eutectic boundary. The supraconductivity curve also varied continuously throughout the system, but with cusps at both the eutectic point and the phase boundary.

Meissner gives the following explanation of his unusual results in the eutectic region of Tl–Sn. He claims that the two components of the region possess different transition temperatures and that the component of lower transition point is a dominant phase which causes a slight eutectic disintegration in the weaker component of high transition point. The main transition therefore occurred near the transition point of the weaker phase, but due to its partial disintegration, complete supraconductivity appeared only at the lower transition temperature of the dominant phase.

Our observations on the Tl–Sn system did not substantiate the foregoing theory. The lattice structure of the system, which was given in the preceding description of Tl–Sn, showed that both the components possessed maximum lattice dimensions at the eutectic point, and that the lattice constant of the face-centred cubic thallium

solution dropped to a minimum at the eutectic boundary. Thus in the Tl–Sn system the supraconducting temperature varied with the magnitude of the lattice dimensions in inverse ratio, except in the tin-rich region. Preliminary X-ray measurements on alloys of the mixed crystal region 8 to 35 per cent. Pb in Au–Pb also indicate that the supraconducting point bears an inverse relation to the magnitude of the lattice constant. That the inverse relation between supraconductivity and lattice dimensions is not general is demonstrated both by the tin-rich alloys of the Tl–Sn system and by the Pb–Bi system. Comparison of results of supraconductivity measurements on the Pb–Bi system by Meissner[3] and his associates, and the X-ray measurements by Solomon and Morris-Jones[12] reveal that in the solubility region of Bi in pure Pb the supraconducting point rises from 7·2° to 8·0° K as the lattice constant grows larger. It is apparent therefore that changing lattice dimensions causes either a rise or fall in the supraconducting point and that supraconductivity is fundamentally a property concerned with the electrostatic field of the lattice.

We are now perhaps in a position to explain why the eutectics of such alloys as Ag–Pb, Zn–Pb and Cd–Pb possess essentially the same transition temperatures as does pure Pb, whereas the eutectics of the alloys Pb–Bi, Tl–Bi, and Sn–Bi possess much higher transition temperatures than do pure Pb, Tl, and Sn. In the former instance, the supraconductive components occur as pure crystals in the eutectics, from which it is evident that the presence of the non-supraconductive component has little effect on the supraconductivity of the eutectic. When we examine, however, the phase diagram of the alloys Pb–Bi, Tl–Bi, and Sn–Sb, we find, typically, that the supraconductive component does not appear in the eutectic as a pure metal, but as a mixed crystal. It is the solution of the non-supraconductive metal in the supraconductive lattice, as in the case of Cu–Pb, which produces the altered transition temperature observed in the eutectic region.

Residual Resistance.

When we examine the r-value curves of the various systems we find that residual resistance is more structure-sensitive than is supraconductivity. The former pheno-

menon is also more dependent on structure and structural change than is specific resistance at normal temperature.

Due to the extreme structure-sensitivity of residual resistance, the observed values are not to be considered absolute, since all processes such as working, ageing, and especially annealing and other heat treatments exert a profound influence on the r-value. In order, however, to obtain coherence in the results as far as was experimentally possible, all the alloys examined were allowed to cool immediately after casting, but not quenched in any way. Annealing was avoided, except in special cases where the effect of such treatment was being investigated.

Two inconsistencies occurred in the present results, namely, the r-values for 33 and 36 per cent. Sn in Ag–Sn, and 10 and 30 per cent. Pb in Cu–Pb. In these cases difficulty was encountered in preparing the alloys. The Ag–Sn alloys were re-melted several times before test pieces large enough to measure were obtained. The repeated melting resulted in low r-values, although the supraconductivity of the alloys was unaffected. The Cu–Pb, 10 and 30 per cent. Pb alloys were prepared by drawing out the metal while molten and enclosed in soft pyrex. It is possible that in these cases part of the melt solidified in the eutectic mixtures during the drawing process, which might cause inhomogeneity in the alloys. Since there is no phase boundary in the system which might cause an r-value maximum, the high r-values in both Cu–Pb alloys were unexpected.

In spite of the sensitivity to structure of residual resistance, we can formulate several general statements concerning its behaviour in various types of alloy structures. The general conclusions regarding r-values are not unlike those arrived at concerning supraconductivity. In simple eutectic regions, the residual resistance maintains a fairly constant value except in the neighbourhood of the boundaries. Near the boundaries, the r-value curve slopes upward toward a solubility boundary, or drops sharply to a pure metal boundary. Internal phase boundaries in an alloy system are usually indicated in the r-value curve by cusp-shaped minima or maxima. Particularly clear examples of these cusps are seen in Au–Sn and Au–Pb, in figs. 1 and 3.

It is in mixed crystal phases, however, that the variation

and magnitude of residual resistance were at their greatest. Phases of this type show as well the greatest variation in other physical properties such as hardness and tensile strength, which latter fact lends them industrial importance. The great variation in physical properties in solubility phases has been explained by the fact that the introduction of foreign atoms into a pure crystal induces lattice strains of considerable magnitude, which are responsible for greatly increased strength and electrical and thermal resistance.

Residual resistance peaks at solubility boundaries were found in six of the seven systems examined. The change in r-value relative to concentration is perhaps most strikingly shown in the Au–Sn system. The r-value for pure Au is ·00029, and the addition of 5 per cent. Sn raised the r-value to ·785. In other words, the solution of 5 per cent. tin in gold increased the residual resistance over four thousand times. In the Ag–Sn system an even higher peak was found. Silver, containing 19 per cent. tin in solid solution possessed an r-value of approximately ·95 which indicated that in this alloy the temperature coefficient of resistance was practically zero.

In the Tl–Sn system an unusual case was observed. The r-value curve was almost identical in shape to the supraconductivity curve, with a cusp at the eutectic point and a sharp maximum at the solubility boundary.

It was hoped that from the investigation of alloy systems, of which one component was a non-supraconductor, data might be obtained concerning the possible supraconductivity of these metals at temperatures below those which it is possible to attain. The results of our research, however, leave the question practically unchanged.

The boundaries to the supraconductive regions in the Au–Sn, Ag–Sn, and Cu–Sn systems have been proved by the work of de Haas to be non-supraconducting as low as 1° K. The breaks, however, that occur in the supraconductivity curves at the compounds $AuSn_1$ and Au_2Pb in their respective systems leave open the possibility that such breaks might occur also, for example, in the Au–Sn system below 50 per cent. Sn, and in the Ag–Sn system below 27 per cent. Sn., at temperatures below 1° K. It is also possible that from an examination of copper-rich Cu–Pb alloys down to 1° K, the supraconductivity curve

might be extrapolated to some point above absolute zero at pure copper.

It is possible that further research on copper-, silver-, and gold-rich alloys with tin and lead in the neighbourhood of one degree absolute might prove the ultimate supraconductivity or non-supraconductivity of these metals.

Summary.

The supraconductivity of seven alloy systems was examined, namely :—Au–Sn, Au–Pb, Ag–Sn, Ag–Pb, Cu–Sn, Cu–Pb, and Tl–Sn. From the analysis of these systems, different supraconductive characteristics were found for each of three structural types. The first type, simple eutectic mixtures, showed a constant supraconductivity point except in the neighbourhood of the boundaries. The second type, comprising simple mixed crystals or solubility phases, showed a continuously varying supraconducting point and transition interval. The latter was found to be least at the phase boundaries and greatest in the middle of the phase. The third type, which is composed of what might be termed a double series of mixed-crystals, showed similar supraconductive characteristics to the second type, namely, continuously changing supraconducting point and transition interval. From an X-ray examination of the third type of structure as found in the Tl–Sn system, it was observed that the transition temperature varied inversely with the magnitude of the lattice constants.

In all types of structure, the supraconductivity curve was found to be a continuous function of the concentration. It was deduced from this that supraconductivity is a property of the complete homogeneous structure of an alloy and not a property of any one of its components.

Residual resistance was found to be a structure-sensitive phenomenon that exhibited great variations in magnitude throughout alloy systems, especially in solubility phases.

From a general survey of all the results obtained it was impossible to say definitely whether gold, silver, or copper would be supraconductive or non-supraconductive at temperatures below 1° K.

In conclusion I should like to express my gratitude to Professor J. C. McLennan, and to Professor E. F.

Burton for the kind interest they have shown during the course of this research. I should like also to thank Mr. J. P. Blewett who supplied me with X-ray information on some of the alloys, and Mr. J. O. Wilhelm, whose constant collaboration in the production of liquid helium enabled me to carry out the research.

Bibliography.

(1) Kamerlingh Onnes, *Comm. Leiden*, no. 1206 (1911).
(2) J. C. McLennan, J. F. Allen, and J. O. Wilhelm, Phil. Mag. viii. p. 1196 (1932).
(3) W. Meissner, H. Franz and H. Westernhoff, *Ann. der Phys.* xiii. p. 505 (1932); xiii. p. 967 (1932).
(4) R. Vogel, *Zeits. f. Anorg. Chemie*, xlvi. p. 61 (1905).
(5) *Loc. cit.* xlv. p. 11 (1905).
(6) G. J. Petrenko, *Zeit. f. Anorg. Chemie*, liii. p. 200 (1907).
(7) W. J. de Haas, Van Aubel and Voogd, *Comm. Leiden*, no. 197 (1929).
(8) Haughton, Journ. Inst. of Metals, xxv. p. 309 (1921).
(9) Heycock and Neville, Phil. T.R.S. clxxxix A, p. 25 (1897).
(10) P. Fuchs, *Zeits. f. Anorg. Chemie*, cvii. p. 308 (1919).
(11) W. J. de Haas und Voogd, *Comm. Leiden*, no. 212 (1931).
(12) D. Solomon and W. Morris Jones, Phil. Mag. xi, p. 1091 (1931).

McLennan Laboratory,
University of Toronto,
Toronto, Canada.
January 1933.

LXXXVI. *Notices respecting New Books.*

The Expanding Universe. By Sir Arthur Eddington, F.R.S. [Pp. 128.] (Cambridge University Press. Price 3*s.* 6*d.* net.)

ANY book by Sir Athur Eddington, in his inimitable style, is welcome. The present little work will be particularly welcomed by the many who nowadays are interested in scientific discovery and advance but who have not the time—nor, perhaps, the equipment—to study deeply.

As the author explains admirably in his Preface, the subject lies at the meeting point of astronomy, relativity, and wave mechanics, and is, therefore, of special interest at the present time.

The first chapter deals in the main with the "facts" of the case—the recession of the galaxies; the next section introduces lightly, but effectively, the Einstein and de Sitter universes—and others; while the last chapter, most aptly, is on the "Universe and the Atom."

The book will be read with pleasure by many people who have the urge to explore within them but no way of satisfying it, for this is an attempt, in popular style, to give a simple account of our present knowledge of a little-known territory.

The Calculation of Heat Transmission. By MARGARET FISHENDEN and OWEN A. SAUNDERS. [Pp. 280.] (H.M. Stationery Office, 1932. Price 10*s.* net.)

THIS useful book has been produced under the ægis of the Department of Scientific and Industrial Research by authors actually engaged under the Fuel Research Board.

A Preface by Dr. Lander, Director of Fuel Research, and a Foreword by the late Sir Richard Threlfall make the object of the publication clear. It is there pointed out that reliable information in heat-transmission problems is exceptionally difficult to obtain with any ease in view of the scattered nature of the original papers and the time which must be necessarily spent in sifting and comparing data. From this point of view alone the book is bound to be of real value, more particularly as the excellent bibliography provides very full references for further information when wanted.

A clear and good account of the fundamental physics of conduction and radiation is given, but the authors have, in their wisdom, not included matter either too complicated theoretically or too specialized technically. The result is an eminently readable volume and a useful one.

While some of the diagrams are hardly up to the same standard as the really beautiful printing, they are adequate for the purpose, and the book is sure to be of the greatest interest to technologists and other students of applied science.

Experimental Atomic Physics. By G. P. HARNWELL and J. J. LIVINGWOOD. First Edition. [Pp. 472.] (McGraw-Hill Book Co. Inc., New York. Price $5.00.)

EMANATING from the Palmer Physical Laboratory, Princeton, this very useful book, as is to be expected, is written with vigour and ability.

It is a students' text-book. The particular feature which may commend itself—or otherwise—to the reader is the inclusion in the text of details in experimental procedure.

This makes the volume a little voluminous perhaps, and to some the alternative of a two-section volume in which parallel chapters dealt with the theoretical and practical aspects of the same topics might appear to be more attractive.

All the usual topics are dealt with in broad fashion: radiation, electrons, spectra, and radioactivity. Whenever there is an experiment capable of being performed by a student it finds a place often with very full experimental instructions.

There are two appendices—the first on instruments for measuring small currents—in which, by the way, no mention is made of that excellent modern instrument, the Lindemann electrometer—and the second on vacuum technique—both informative and useful sections.

This book—admittedly not covering the whole field of Atomic Physics—is admirably worked out and produced, and will be attractive to all senior students of the subject.

Les Transmutations Artificielles. By Louis Leprince Ringuet. (*Actualités Scientifiques et Industrielles, Exposés de Physique Atomique expérimentale.*—I.) Ed. Hermann et Cie. [45 pp., 10″×6″, 15 fr., stiff paper covers.]

This is a compact little booklet which gives a general account of the experimental side of nuclear disintegration, including experimental methods of observing the occurrences and the recent wide extensions of the field of research. The disintegration by neutrons and protons is described, but the more recent reactions involving H_2 are not included—otherwise it keeps abreast of the rapidly moving times. It forms an admirable introduction to the subject as well as a useful centre for reference to original papers, and should appeal to both unspecialized and specialized interests.

Notions de Mécanique Ondulatoire ; les méthodes d'approximation. By L. Brillouin. (*Actualités Scientifiques et Industrielles, Exposés sur la Théorie des Quanta.*—I.) Ed. Hermann et Cie. [34 pp., 10″×6″, 10 fr., stiff paper covers.]

This little pamphlet collects a few of the cases in which problems of wave mechanics yield solutions to approximate methods. It opens with a skeleton introduction and proceeds to consider the method of successive approximations applied to the problem of a point moving in a field of force ; a general discussion of perturbations follows, and the whole concludes with some examples of the application of the formulæ deduced. It should be useful to those interested in the detailed working out of wave mechanical problems.

Atom and Cosmos. By Hans Reichenbeck. English translation by E. S. Allen. [Pp. 300.] (George Allen & Unwin, Ltd. Price 8*s.* 6*d.*)

Written in 1930 as an outgrowth of lectures broadcast from Berlin this English edition "revised and brought up-to-date in collaboration with the author was first published in 1932."

Frankly a popular presentation of physical knowledge to non-physicists, the book is an attempt "to give an insight into the physicist's way of thinking and a general view of the results of his research ; and it wishes to show how the physical theories of to-day have united in a picture of the world."

The book is eminently readable and is admirably written in lucid style. Space and time, radiation, matter in its corpuscular and wave aspects all receive adequate attention.

There are extremely few misprints—but there is an especially obvious one on page 202, which will surely be corrected in the next edition !

Professor Reichenbeck's lucid style and closely reasoned phraseology loses nothing in Professor Allen's very good translation.

Sur l'absorption exponentielle des rayons beta du Radium E. By G. Fournier and M. Guillot. (*Actualités Scientifiques et Industrielles, Exposés de Physique Théorique.*—VII.) Ed. Hermann et Cie. [37 pp., 10″×6″, 10 fr., stiff paper covers.]

An account is given of experiments which show the absorption of Beta-rays from Radium E to be exponential, and values of the absorption coefficients are given for a range of substances. The exponential curve is explained in terms of a sum of homogeneous Beta-rays, using the results of Madgwick to deduce the curve actually found. The effects of solid angle and other experimental conditions are fully discussed, and suggestions made for the nature of the distribution of the Beta-rays with energy. It is clearly and thoroughly written, and should be a useful account for a worker in this somewhat narrow field.

The Kinetics of Reactions in Solution. By E. A. Moelwyn-Hughes, D.Sc. (Liverpool), D.Phil. (Oxford). [Pp. vi+313.] (Oxford, at the Clarendon Press, 1933. Price 15*s.* net.)

This book is written to show that reaction in solution—that is to say, the phenomena of chemical change in general—can profitably be examined in the light of the kinetic theory.

It may be laid down as fundamental that for a reaction to occur collision between the reacting particles must take place. The law of reaction found experimentally by Arrhenius can be represented by the equation $k = Ze^{-E/RT}$, where k denotes the velocity constant of a reaction, Z, for bimolecular reaction is the collision frequency as calculated by Maxwell, while E may be interpreted as a quantity of the same dimensions as energy which is such that the exponential term represents the fraction of the collisions which are effective in causing a chemical change. In modern days the expression "critical increment of energy" has been given to this term E, and it is taken as a measure of the activation which "is a necessary step in almost all chemical changes which proceed with measurable velocity." The student might very well ask how it comes about that E is necessary for a reaction, yet the bigger E is the smaller becomes the rate of reaction k, for if E has any value greater than zero the exponential term is less than unity. Something in the way of explanation seems to be required here.

And again, if a satisfactory answer is given, the student may ask, further, in what sense E is a "critical" value. Its presence may encourage or discourage reaction, but it does not appear to do so in any critical way.

Something seems to have been left out of the exposition near the beginning which may cause the thinking student to hesitate; but when once the author has started and got under way he has produced a most excellent summary of what is known concerning the subject of chemical change in its various aspects. Where real difficulties have arisen (as in the case of unimolecular reactions) the matter is dealt with in a detailed and masterly fashion in the endeavour to give a fair explanation of the manner in which the difficulties have been overcome.

The book is certain to take a leading place amongst expositions of the subject.

A Textbook of Physics.—Vol. III. *Electricity and Magnetism.* By E. Grimsehl. Edited by R. Tomaschek. Translated from the seventh German edition by L. A. Woodward, B.A. (Oxon.), Ph.D. (Leipzig). [Pp. xiv+685.] (Blackie & Son, Ltd., London and Glasgow, 1933. Price 25*s.* net.)

The first two volumes of this textbook in its English form have already appeared and been noticed. The German volume on Electricity and Magnetism from which this one has been translated has passed through seven editions. It deals with the more classic side of the subject. Its characteristic quality is the thoroughness with which all definitions and descriptions are put forward. Similarly the diagrams, which are very numerous, are thoroughly well thought out and reproduced. Throughout, the field standpoint of Faraday and Maxwell has been adopted.

A very full and satisfactory account is given of alternating currents (about 70 pages); and in a later chapter the subject of electromagnetic oscillations and waves is equally well presented.

Although the more modern developments (especially on the theoretic side) have been relegated to a later volume, the book contains a sufficient account of the discoveries made from 1890 onwards to call a student's attention to the developments which were then beginning to take place.

The chief drawback is the price. We can hardly expect a student for a pass degree, for which it is suitable, to purchase the five or more volumes necessary to cover the subject of physics; but it can be recommended heartily as suitable for any College Library.

[*The Editors do not hold themselves responsible for the views expressed by their correspondents.*]

Fig. 3.

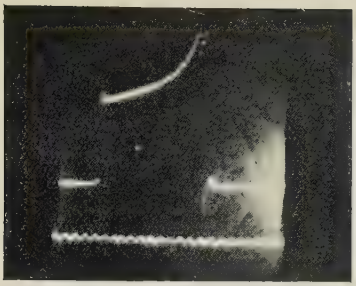

Fig. 4.

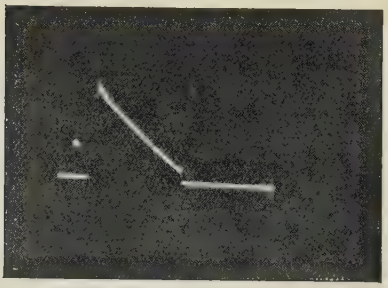

Fig. 5.

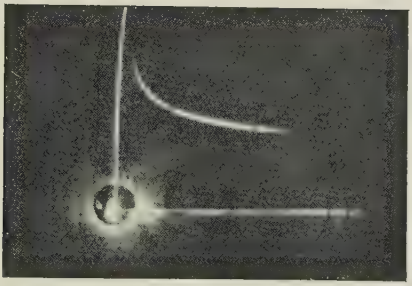

Fig. 6.

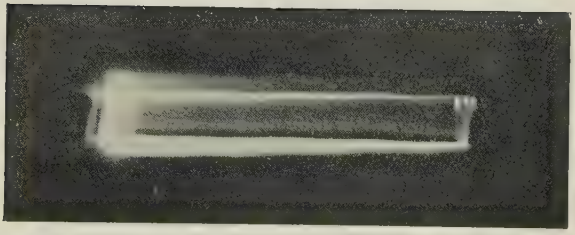

Fig. 7.

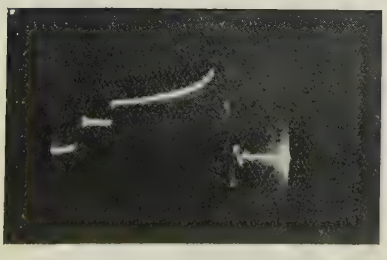

Fig. 8.

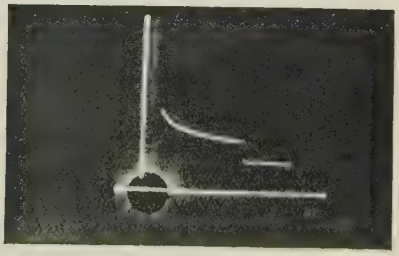

Fig. 9.

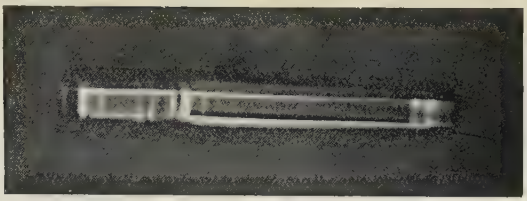

Fig. 10.

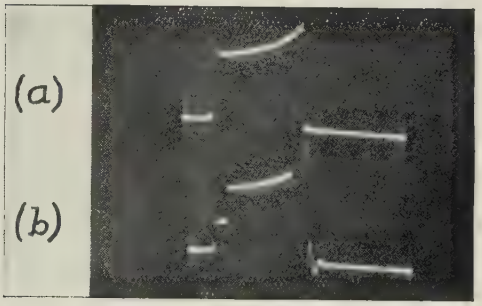

Fig. 15.

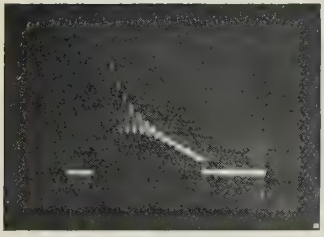

(a)

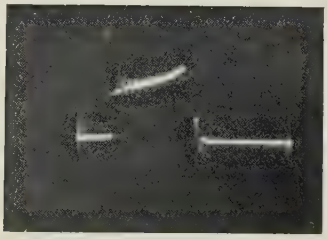

(b)

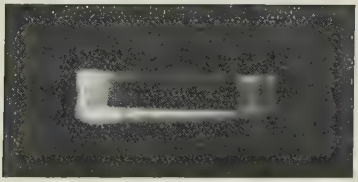

(c)

Fig. 16.

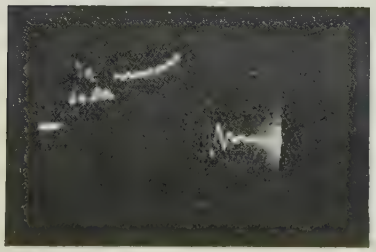

Fig. 17.

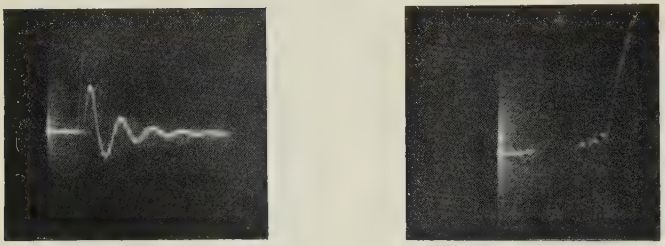

(*a*) (*b*)

Fig. 18.

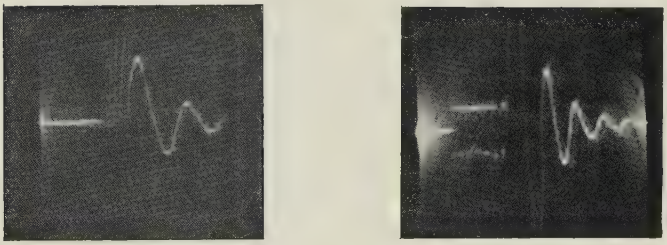

(*a*) (*b*)

Fig. 20.

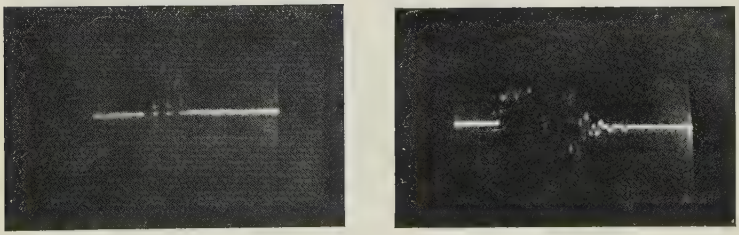

(*a*) (*b*)

(*c*)

Fig. 22.

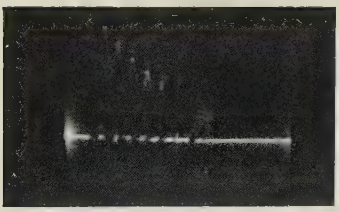

(*a*)

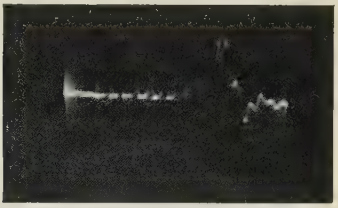

(*b*)

(*c*)

Fig. 23.

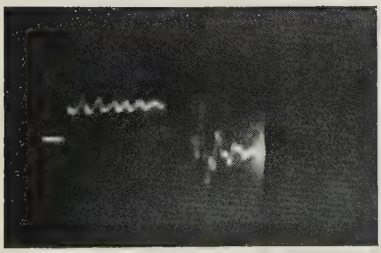

Fig. 24.

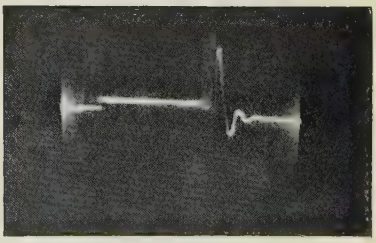

Fig. 19.

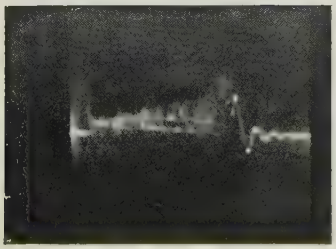

Fig. 3.

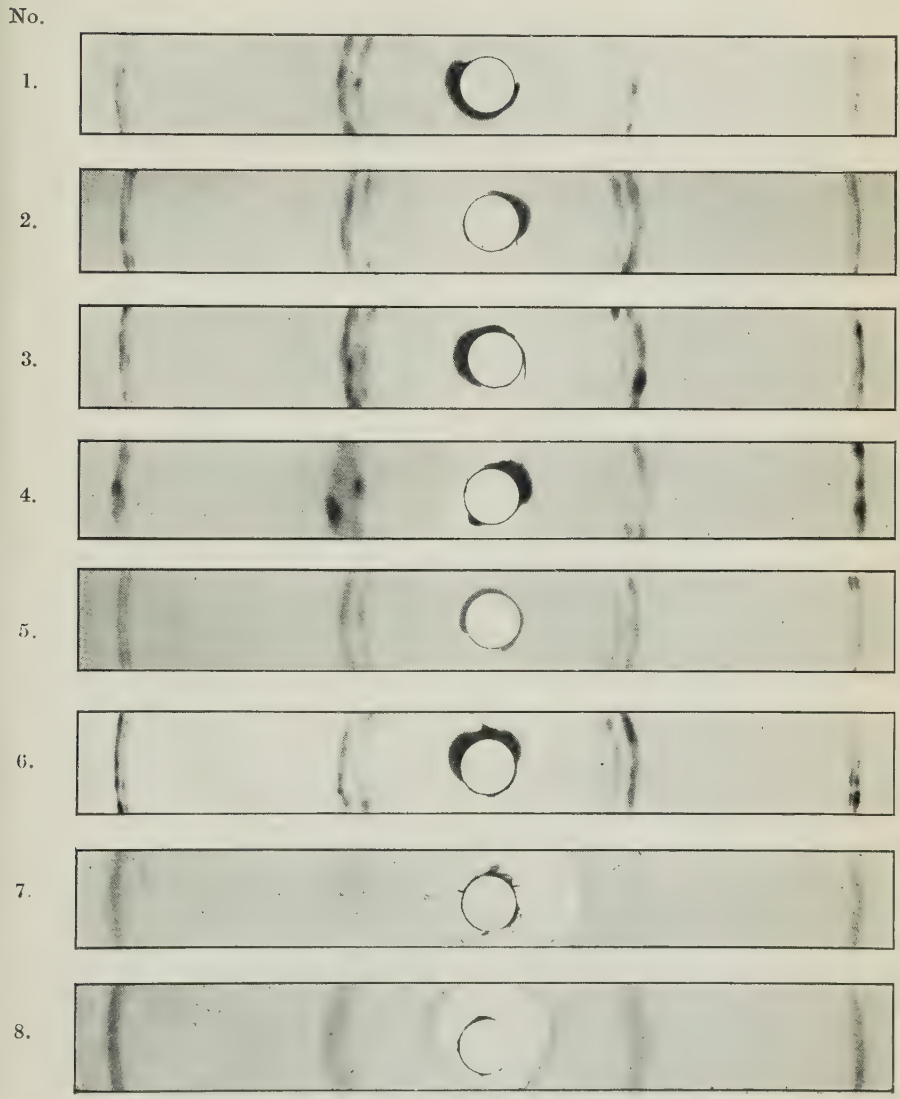

Fig. 1.

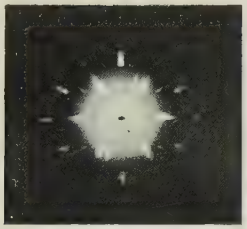

Celluloid. Triple pattern. Central portion.

Fig. 2.

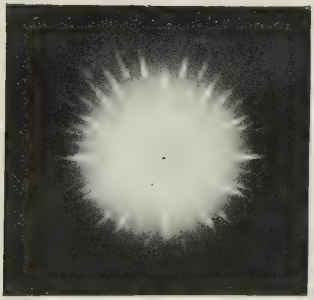

Celluloid. Triple pattern. Outer portion.

Fig. 6.

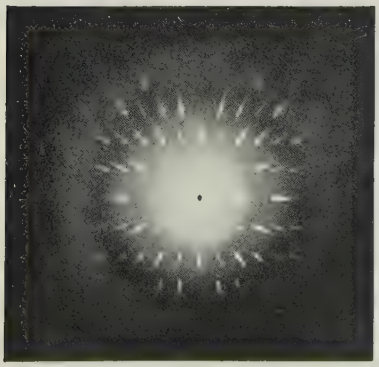

Celluloid. Double pattern.

Fig. 1.

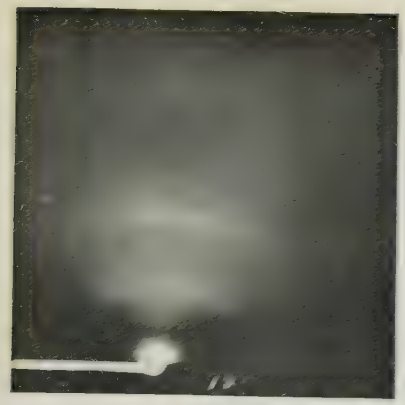

Fig. 2.

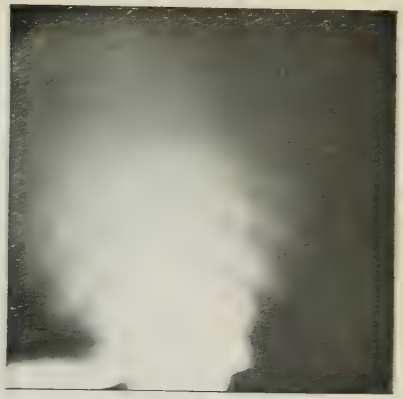

Fig. 3.

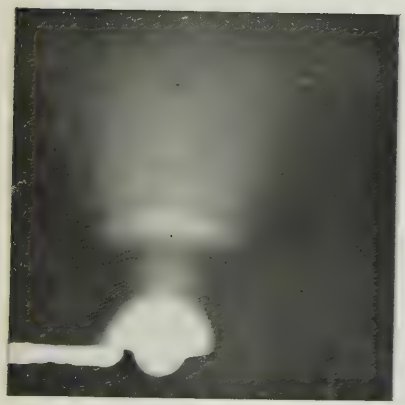

Fig. 4.

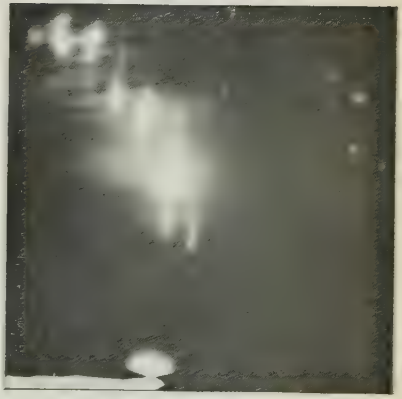

Fig. 5.

Fig. 6.

Nature of print lower

Fig. 2.

Galena, showing Kikuchi lines due to the cleavage face.

Fig. 3.

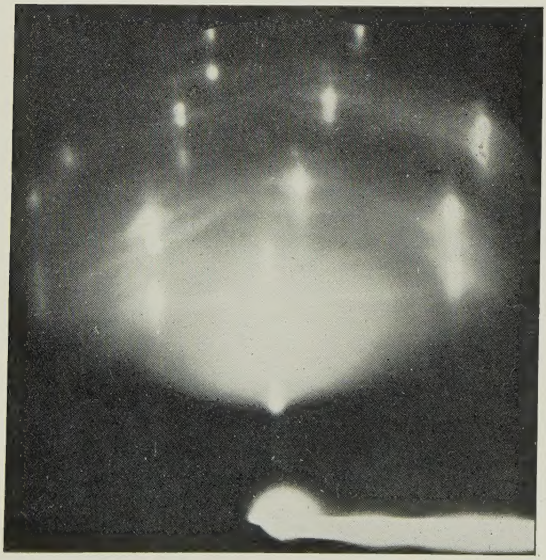

Iron pyrites, showing surface effect, but the spots are fairly sharp showing that more than one layer is taking part. Kikuchi lines due to the cleavage face are also seen.

Fig. 4.

Fe_2O_3 showing intersections of Kikuchi line.